Investigate Syntrophic Cross-feeding in *E. Coli* Co-culture via ^{13}C Metabolic Flux Analysis

by

Yu-Jun Hong

A dissertation submitted in partial fulfillment
of the requirements for the degree of
Doctor of Philosophy
(Chemical Engineering)
in the University of Michigan
2024

Doctoral Committee:

Professor Maciek R. Antoniewicz, Chair
Professor Xiaoxia Nina Lin
Professor Thomas Schmidt
Professor Peter M. Tessier

Yu-Jun Hong

yjhongum@umich.edu

ORCID iD: 0000-0002-1910-8797

Dedication

To Mom, Dad and Sister. Thank you for your unconditional love and support throughout this journey.

Acknowledgements

I am extremely lucky to have received so much support over the past five years. I would not have been able to accomplish my goal without you.

First, I want to thank my advisor, Dr. Maciek R. Antoniewicz. It is hard for me to express how grateful and lucky I am to be your PhD student. You are an amazing advisor, teacher, and mentor. Your knowledge and passion for this field have had a profound impact on me. I am truly happy and proud of my PhD thesis. I enjoyed every conversation with you, even when my project was not going well. You were always super helpful, supportive, and patient with any challenge we faced. There were times when I was so frustrated with the experiment results, but I never felt alone, knowing that you were always there to support us. Additionally, thank you for understanding the struggles of being an international student. I was able to visit my family for a couple of weeks every year, which meant a lot to me. I could not have asked for a better advisor. Thank you so much.

I would like to thank my thesis committee members, Dr. Xiaoxia (Nina) Lin, Dr. Thomas Schmidt, and Dr. Peter M. Tessier, for their valuable feedback and suggestions for my thesis. Thank you for the many insightful questions that helped me critically evaluate my thesis and conduct better research.

Next, I want to thank all my lab mates in the Antoniewicz lab. The former graduate students, Dr. Eleanor Oates, Dr. Michael Dahle and Dr. Gerald Har, helped me a lot when I first joined the group. I will forever be grateful for the automatic button on Metran created by

Michael. Gerald is my go-to person whenever I have a question, and he is always willing to help. And Dr. Harry Cai, who joined the lab with me in the same year, you are the best lab mate I could ever ask for. You were always on top of things and reminded me of all kinds of deadlines. Most importantly, thank you for teaching me all the CHO cell culture techniques. I greatly enjoyed my time working with you.

I would like to thank all my friends in Michigan. I had a great time in my first year with my cohort. Although COVID made it harder to maintain a social life, I still have these amazing friends who supported me throughout my PhD journey. First, my biggest thanks to Carolina Espinoza. We maintained our Coffee Tuesdays almost every single week for the past five years. I consider this to be one of my greatest achievements during my PhD. I cherished the time we spent together, updating each other on our research lives, sharing struggles, and being each other's biggest support. I feel so lucky to have you in my life. I would also like to thank Shiqi Zhao. I loved the times when we lived close to each other and took walks every week during COVID. We always had great conversations about research and personal life. I also want to thank Kristi Pepa, who is not only my "little brother" in DnD but also one of my close friends in Michigan. I always had a great time hanging out with you, and I am grateful that we both made time for each other despite our busy lives. Additionally, I want to thank my amazing friends Yi Dai, David Kitto, Shawn Lu, and Chris Kim. It was always nice to run into you in the hallway and catch up on our lives.

I would like to thank my Taiwanese friends who are currently in the US as well. I would definitely feel super lonely and homesick without you here. We share the same language and cultural background, so I always feel at home when hanging out with you. First, I want to thank Han-Ting Chen, who has been my best friend since undergrad. You are always there whenever I

need your suggestions or help. Thank you for being so supportive. I would also like to thank Shiuan-Bai Ann, who was my classmate in undergrad, though we never really spoke to each other then. I am glad we became friends after you joined UMich. Thank you for always being willing to help, and I really enjoy hanging out with you. I would like to thank Fan-Wei Wang, with whom I always had good conversations. We shared similar research struggles, and I always felt better after talking to you. I would also like to thank Ellen Chao for always telling me I am doing great. I miss the times when we used to hang out every day during undergrad. I am happy that we were able to take a couple of trips together, and thank you for visiting me so many times in the past few years.

I would like to thank my friend who is currently in Taiwan now. To Yi-Hua Liao and Yu-Wen Wang, thank you for always being there for me and make me feel welcome whenever I went back home.

I would like to thank my boyfriend, Kyle Glazier, for being my biggest support throughout this journey. You are truly my biggest cheerleader. I cannot imagine going through all these challenges without you by my side. You always believed in me when I doubted myself and cheered me up when I was down. Thank you for always being kind and understanding of my struggles and for being proud of my accomplishments.

Finally, I would like to give my biggest thanks to my dearest family. I want to thank my grandpa and grandma for their love and for thinking I am the best, even though they have no idea what I am doing. To my mom and dad, thank you for supporting me in pursuing my goals and for your unconditional love. I would not be where I am today without you. And to my dearest sister, Dr. Yu-Tong Hong, thank you for all your help and love. You are the best sister I could have ever asked for. I feel so lucky to have you here, especially when I first moved to the United

States. I am glad that we have family group calls almost every day and stay close even when we are physically far away from each other. I love you all.

Table of Contents

Dedication ii

Acknowledgements iii

List of Figures xi

Abstract xiv

Chapter 1 Introduction 1

1.1 Microbes in our life 1

1.2 Syntrophic interaction 2

1.3 Cell metabolism 3

1.3.1 Glycolysis 5

1.3.2 Pentose phosphate pathway 5

1.3.3 Tricarboxylic cycle 6

1.3.4 Anaplerosis 6

1.4 Metabolic flux analysis 7

1.4.1 ^{13}C Metabolic flux analysis 9

1.4.2 ^{13}C Metabolic flux analysis in co-culture 10

1.5 Fluorescent protein 11

1.6 Aim and outline of each chapter 13

Chapter 2 ^{13}C Metabolic Flux Analysis on *E. coli* Lethal Knockout Strains Reveal How Metabolism is Restored in Auxotrophic Strains Supplemented with Required Metabolites 15

2.1 Abstract 15

2.2 Introduction 16

2.3 Methods 17
2.3.1 Cell strain 17
2.3.2 Cell growth 18
2.3.3 Gas chromatography-mass spectrometry and chemical derivatization 18
2.3.4 ^{13}C metabolic flux analysis 21
2.3.5 Statistical analysis 22
2.4 Results 22
2.4.1 Cell growth 22
2.4.2 Labeling experiment 23
2.4.3 ^{13}C metabolic flux analysis 25
2.5 Discussion 30
2.6 Supplementary experiment 32
2.6.1 Glucose uptake rate 32
2.6.2 Acetate secretion rate 34
Chapter 3 ^{13}C Metabolic Flux Analysis Identifies Unexpected Metabolite Exchanges in *E. Coli* Co-Culture 36
3.1 Abstract 36
3.2 Introduction 37
3.3 Methods 39
3.3.1 Cell strain 39
3.3.2 Growth condition 40
3.3.3 Gas chromatography-mass spectrometry and chemical derivatization 40
3.3.4 ^{13}C metabolic flux analysis 40
3.4 Results 41
3.4.1 Syntrophic growth for two auxotrophic strains. 41
3.4.2 Parallel labeling experiment and new metabolic models for flux analysis 42

3.4.3 ^{13}C metabolic flux analysis with new co-culture metabolic models 43
3.4.4 Exchange flux map 47
3.4.5 Central carbon metabolism 49
3.5 Discussion 52
3.6 Supplementary experiment 57
3.6.1 Growth verification 57
3.6.2 Population composition 60
Chapter 4 Cross-feeding of Amino Acid Pathway Intermediates is Common in Co-culture of Auxotrophic *Escherichia coli* 63
4.1 Abstract 63
4.2 Resulting publication 64
4.3 Introduction 64
4.4 Methods 65
4.4.1 Strains and materials 65
4.4.2 Culture condition 65
4.5 Results 66
4.5.1 Arginine auxotroph 66
4.5.2 Histidine auxotroph 69
4.5.3 Isoleucine and proline auxotrophs 70
4.5.4 Tryptophan auxotroph 72
4.6 Discussion 75
Chapter 5 Overexpression of Fluorescent Proteins in *Escherichia Coli* Has Negligible Impact on Cell Physiology and Metabolism 78
5.1 Abstract 78
5.2 Introduction 79
5.3 Methods 81

5.3.1 Cell strains and plasmid 81
5.3.2 Competent cell preparation 81
5.3.3 Plasmid transformation 81
5.3.4 Growth condition 82
5.3.5 Fluorescent measurement 82
5.3.6 Gas chromatography-mass spectrometry 82
5.3.7 ^{13}C metabolic flux analysis 83
5.3.8 Biomass composition 83
5.4 Results 84
5.4.1 Cell growth and fluorescence 84
5.4.2 Biomass composition 88
5.4.3 ^{13}C metabolic flux analysis 90
5.5 Discussion 92
5.6 Supplementary experiment 97
5.6.1 IPTG induction 97
Chapter 6 The Future and Challenge for Co-culture ^{13}C Metabolic Flux Analysis 99
6.1 Case study for fluorescent co-culture by applying ^{13}C metabolic flux analysis 99
6.1.1 Cell strain and growth 99
6.1.2 ^{13}C metabolic flux analysis 101
6.1.3 ^{13}C metabolic flux analysis for different glucose uptake 106
6.2 Challenges for ^{13}C metabolic flux analysis 109
6.3 Future direction 110
Appendix 115
Bibliography 131

List of Figures

Figure 1.1 Central carbon metabolism in *Escherichia coli* (*E. coli*). 5

Figure 2.1 Gene knockout location of the two model strains *ΔilvC* and *Δicd*. 17

Figure 2.2 Growth of *ΔilvC* and *Δicd* with only minimal medium M9 or 1mM of required amino acid valine (Val), isoleucine (Ile) or glutamate (Glu). 23

Figure 2.3 Parallel labeling experiment of *ΔilvC* and *Δicd* supplemented with 2mM of required amino acid valine (Val), isoleucine (Ile) or glutamate (Glu). 24

Figure 2.4 The flux maps of central carbon metabolism in (A) Wild type *E. coli*. (B) Δ*ilvC* strain. (C) Δ*icd* strain. 29

Figure 2.5 Three possible scenarios for *Δicd* to replenish oxaloacetate (OAC). 31

Figure 2.6 Glucose specific uptake rate for *ΔilvC*. 33

Figure 2.7 Glucose specific uptake rate for *Δicd*. 34

Figure 2.8 Acetate secretion rate for *ΔilvC*. 34

Figure 2.9 Acetate secretion rate for *Δicd*. 35

Figure 3.1 Syntrophic growth of *ΔilvC* and *Δicd*. 42

Figure 3.2 Illustrations of models used in ^{13}C Metabolic Flux Analysis. 43

Figure 3.3 Sum of square residual (SSR) of co-culture models with different exchange metabolites. 46

Figure 3.4 Exchange flux map with co-culture model that include all possible exchanges. 47

Figure 3.5 Exchange flux map of *ΔilvC* and *Δicd* syntrophic co-culture. 48

Figure 3.6 Central carbon metabolism flux map of *ΔilvC* in co-culture. 50

Figure 3.7 Central carbon metabolism flux map of *Δicd* in co-culture. 51

Figure 3.8 Sum of square residual (SSR) for co-culture model with different exchange metabolites combination. 55

Figure 3.9 Exchange flux map of *ΔilvC* and *Δicd* with all amino acids, intermediates and pyruvate exchange fluxes included in the metabolic model. 56

Figure 3.10 Growth rate and final OD of *Δicd* growing on different concentration of glutamate and alpha-ketoglutarate. 58

Figure 3.11 Growth rate and final OD of *ΔilvC* growing on different concentration of valine and isoleucine and their keto-acid. 60

Figure 3.12 Population dynamic of the *ΔilvC*/*Δicd* co-culture with different inoculation ratio. .. 62

Figure 4.1 Growth of arginine auxotrophic co-culture and arginine biosynthetic pathway. 67

Figure 4.2 Growth of the arginine auxotrophic strains on arginine biosynthesis pathway intermediates. 68

Figure 4.3 Growth of histidine auxotrophic co-culture and histidine biosynthetic pathway. 69

Figure 4.4 Growth of the histidine auxotrophic strains on histidine biosynthesis pathway intermediates. 70

Figure 4.5 Growth of isoleucine auxotrophic co-culture proline auxotrophic co-culture and their biosynthetic pathway. 71

Figure 4.6 Growth of the isoleucine auxotrophic strains on isoleucine biosynthesis pathway intermediates. 72

Figure 4.7 Growth of tryptophan auxotrophic co-culture and tryptophan biosynthetic pathway. 74

Figure 4.8 Growth of the tryptophan auxotrophic strains on tryptophan biosynthesis pathway intermediates. 75

Figure 5.1 The growth and fluorescence signal of wild type and fluorescent strains CFP, Crimson, GFP, Tomato and YFP. 86

Figure 5.2 Growth rate of wild type and fluorescent strains CFP, Crimson, GFP, Tomato and YFP. 87

Figure 5.3 The contents of four major macromolecules: protein, lipid, RNA and glycogen of wild type and fluorescent strains. 89

Figure 5.4 Amino acid distribution of wild type and fluorescent strains. 90

Figure 5.5 Fatty acid distribution of wild type and fluorescent strains. 90

Figure 5.6 Central carbon metabolism of wild type and fluorescent strains. 91

Figure 5.7 Acetate secretion and glucose uptake of wild type and fluorescent strains. 92

Figure 5.8 The growth curve and growth rate of wild type and four GFP strains. 94

Figure 5.9 The GFP fluorescent signal of four GFP strains during cell growth. 95

Figure 5.10 Amino acid distribution of wild type *E. coli* biomass and fluorescent protein. 96

Figure 5.11 The growth and fluorescence signal with inducer IPTG. 98

Figure 6.1 *ΔilvC*-Crimson and *Δicd*-CFP co-culture under fluorescent microscopy. 100

Figure 6.2 Growth and population dynamic of *ΔilvC*-Crimson and *Δicd*-CFP co-culture. 101

Figure 6.3 Sum of square residual (SSR) of co-culture model with different exchange metabolites combination for the fluorescent co-culture *ΔilvC*-Crimson/ *Δicd*-CFP..... 104

Figure 6.4 Exchange flux map of co-culture model that include all possible exchanges. 105

Figure 6.5 Exchange flux map of *ΔilvC*-Crimson and *Δicd*-CFP co-culture. 106

Figure 6.6 Metabolic model for different glucose uptake..... 107

Figure 6.7 Exchange flux map of *ΔilvC*-Crimson and *Δicd*-CFP co-culture for different glucose uptake. 108

Figure 6.8 Workflow for evaluating how flux differences in two strains impact the mono-culture model and co-culture model performance. 112

Abstract

Auxotrophic microbes are widespread in nature. These organisms lack one or more genes required to synthesize essential metabolites and thus require nutrient cross-feeding for their growth, termed syntrophy. Currently, few methods exist to identify and quantify these metabolite exchanges. This thesis addresses this knowledge gap by applying ^{13}C metabolic flux analysis (^{13}C MFA) to elucidate cross-feeding interactions in auxotrophic microbial co-cultures.

To this end, two auxotrophic *Escherichia coli* single knockout strains, Δ*ilvC* and Δ*icd,* were selected as model strains. Both strains are deficient in synthesizing an essential amino acid. We first applied ^{13}C MFA on single strains to understand how they restore their metabolism when supplemented with required metabolites. Our results demonstrate how auxotrophic strains rewire their metabolic flux to overcome auxotrophy and that the location of the knockout impacts how they adjust their metabolism.

Next, we applied ^{13}C MFA on a syntrophic co-culture, consisting of Δ*ilvC* and Δ*icd*, to elucidate the cross-feeding metabolites. Several metabolic network models were constructed and tested. We showed that by applying ^{13}C MFA, we were capable of not only resolving individual intracellular fluxes with high precision but also identifying and quantifying the rates of exchanged metabolites. We discovered that in addition to amino acid exchange, metabolic pathway intermediates were also exchanged between the syntrophic partners. This unexpected exchange of intermediates demonstrates a more complicated exchange network than previously assumed.

Inspired by this finding, we further investigated how commonly pathway intermediates are exchanged. We selected 25 *E. coli* single-gene knockouts that are auxotrophic for five amino acids: arginine, histidine, isoleucine, proline, and tryptophan. In co-culture experiments pairing strains with the same amino acid auxotrophy, we observed growth in 23 out of 55 pairings, indicating the exchange of pathway intermediates. The results were further supported by culturing auxotrophic *E. coli* strains in media supplemented with metabolic pathway intermediates, which recovered cell growth as predicted. Taken together, these results demonstrate that the exchange of metabolic pathway intermediates is more common than has been assumed so far.

In studies of microbial interaction, another important aspect is how the interactions impact and shape population composition. Fluorescent proteins are commonly employed to track their relative abundances. However, the overexpression of these heterologous proteins can potentially impose a metabolic burden on the host cell. To address this concern, we characterized the impact of fluorescent protein overexpression in *E. coli*. We selected five common fluorescent proteins—CFP (cyan fluorescent protein), Crimson, GFP (green fluorescent protein), Tomato, and YFP (yellow fluorescent protein)—and overexpressed them in wild-type *E. coli*. We measured cell growth, biomass composition and the metabolic state, comparing the fluorescent protein overexpression strains to wild-type. Overall, we conclude that overexpression of fluorescent proteins in *E. coli* has a negligible impact on cell physiology and metabolism.

In conclusion, this thesis first demonstrates the application of ^{13}C MFA to uncover the metabolic fluxes in auxotrophic strains when supplemented with required metabolites. Furthermore, we expanded the application of ^{13}C MFA to a syntrophic co-culture to elucidate the cross-feeding metabolites between the auxotrophic strains. We discovered the exchanges of

metabolic pathway intermediates between auxotrophic strains. The impact of fluorescent protein overexpression on cells were investigated in this thesis as well. In the final chapter, we studied a fluorescent syntrophic co-culture and discussed some of the challenges in the field and potential future directions.

Chapter 1 Introduction

1.1 Microbes in our life

Microbes, or microorganisms, are tiny living cells of microscopic size that are too small to be seen with naked eyes. Microbes were first observed under a microscope and reported by Anton van Leeuwenhoek, who is also known as the father of microbiology (Leewenhoeck, 1676; Lane, 2015). To date, it is well established that microbes are ubiquitous on our planet and critical for the ecosystem, human health and even industrial manufacturing. In nature, microbes interact with their surroundings and thrive by collecting nutrients, generating energy and secreting waste. All of these processes are coupled with the elemental cycles in the environment including the carbon, nitrogen and phosphorus cycles, driving the biogeochemical cycles in the ecosystem (Burgin *et al.*, 2011). Microbes, as the main drivers of the biotransformation of organic chemicals, affect the stability of the entire ecosystem (Fester *et al.*, 2014). In the human body, trillions of microbes are present in different parts of the human body and serve a fundamental role in human metabolism and health (Kumar and Chordia, 2017). The diversity of microbes in the human body has been associated with a number of diseases including obesity, inflammatory bowel disease and even cancer (Huttenhower *et al.*, 2012; Petersen and Round, 2014; Garrett, 2015; Lloyd-Price, Abu-Ali and Huttenhower, 2016). Besides naturally existing microbial communities, synthetic microbial consortia have shown great potential for biosynthesis and biodegradation (Che and Men, 2019). For industrial production, recent advances in synthetic biology and metabolic engineering have allowed researchers to engineer microbes that can turn cheap feedstocks into fine chemicals (Jagmann and Philipp, 2014; Jullesson *et al.*, 2015; Johns *et*

al., 2016). Microbes are also used in degrading toxic products such as wastewater treatment and degrading crude oil to prevent oil pollution (Tang *et al.*, 2010; Rani *et al.*, 2019). Taken together, microbes play crucial roles in our lives. So far, various studies have focused on different aspects of microbes ranging from their fundamental functions to how they can be applied to improve our lives. In my thesis, I specifically look into how microbes interact with each other and how we can develop better tools to understand their interactions.

1.2 Syntrophic interaction

Unlike the single strains we culture in the lab, most microbes in nature do not exist in isolation. The complex interactions between various species within microbial communities can have positive, negative or no impact on individual species (Faust and Raes, 2012). Mutualism, where both species benefit from the relationship, is commonly observed in nature. One type of mutualism, termed syntrophy, describes the dependency on metabolite cross-feeding between two species and has become a popular topic for studying microbial cooperation (Morris *et al.*, 2013; Kouzuma, Kato and Watanabe, 2015). The reliance on the cross-feeding of growth factors has been identified as one of the main reasons for microbial unculturability in vitro (Klitgord and Segrè, 2010; Vartoukian, Palmer and Wade, 2010; Pande and Kost, 2017). It has been estimated that less than 1% of them can be cultivated under standard methods in the lab (Amann, Ludwig and Schleifer, 1995; Hugenholtz, Goebel and Pace, 1998; Torsvik, Øvreås and Thingstad, 2002). Analysis of the sequenced genome in bacteria, archaea and eukarya suggests that most microorganisms in nature are auxotrophs, lacking key gene(s) to synthesize essential molecule(s) for their own survival (Mee and Wang, 2012; D'Souza *et al.*, 2014; Mee *et al.*, 2014). These auxotrophic strains rely on the cross-feeding of essential growth factors to thrive in nature, and therefore cannot grow in synthetic media in the lab (Morris *et al.*, 2008; D'Onofrio *et al.*, 2010)

Thus, the cross-feeding of metabolites between microbes is commonly found in microbial communities. The exchanged molecules include electron donors, sugar, organic acid, amino acids, vitamins and other co-factors (Jones, 1967; Rodionova *et al.*, 2015; Zengler and Zaramela, 2018; Fritts, McCully and McKinlay, 2021). The exchanges of metabolites are not only common but also serve a critical role for supporting growth and shaping microbial communities (Nemergut *et al.*, 2013; Mee *et al.*, 2014; Kouzuma, Kato and Watanabe, 2015). To date, studies focusing on syntrophic interaction often assume the exchanging metabolites based on the genomic information i.e., the gene knockout. For example, if a microbe is deficient in producing a certain essential amino acid, it is often assumed that the cross-feeding metabolite is that particular amino acid (Mee *et al.*, 2014; Pande *et al.*, 2014; Germerodt *et al.*, 2016; Antoniewicz, 2020). Identifying metabolites exchange, however, remains challenging due to the inherently dynamic nature and system complexity (Ponomarova and Patil, 2015). In my thesis, one of the main goals is to develop new approaches to elucidating the exchanged metabolites by applying ^{13}C metabolic flux analysis.

1.3 Cell metabolism

Before introducing ^{13}C metabolic flux analysis, it is important to first understand the cellular metabolism. Metabolism is a series of interconnected chemical reactions within organisms. These chemical reactions can be categorized as catabolism and anabolism. Catabolism refers to the reactions that break down substrates to generate energy for cellular processes. Anabolism, on the other hand, uses energy to produce building blocks such as proteins, lipids and nucleic acids for cell proliferation (Mesquita and Rodrigues, 2018; Judge and Dodd, 2020). In my thesis, I mainly investigate central carbon metabolism of the cell. Central carbon metabolism consists of a complex series of enzymatic reactions that convert sugars into

energy and precursors that are used for cell growth and proliferation, as shown in Fig. 1.1 (Noor *et al.*, 2010). In this section, I will introduce the major metabolic pathways of central carbon metabolism in bacteria, specifically *Escherichia coli* (*E. coli*), to build a basic understanding for my thesis.

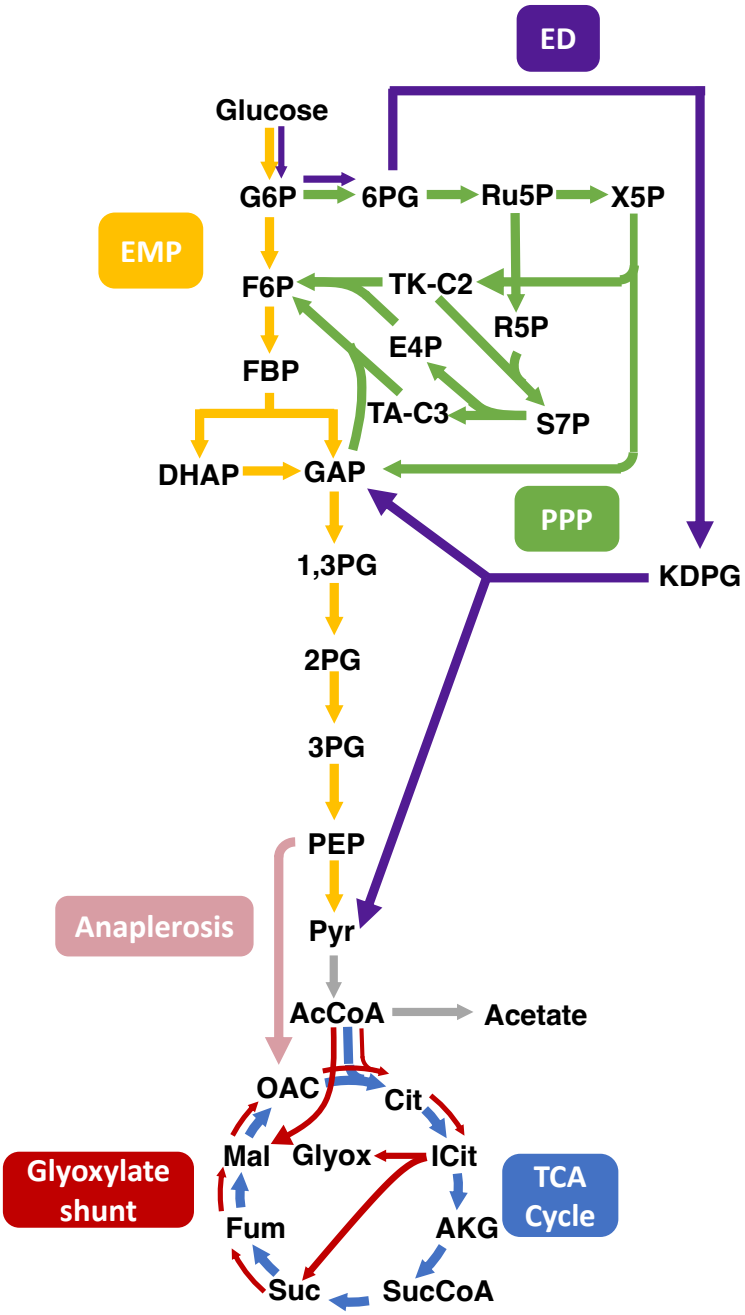

Figure 1.1 Central carbon metabolism in *Escherichia coli* (*E. coli*). The main metabolic pathway in central carbon metabolic pathway: Embden-Meyerhof-Parnas pathway (EMP), the main glycolytic pathway in *E. coli* that convert glucose to pyruvate. Entner-Doudoroff pathway (ED), alternative pathway for glycolysis, which is generally inactive in *E. coli* during the growth on glucose. Pentose phosphate pathway (PPP), which include oxidated and non-oxidated phases, is essential for the biosynthesis of nucleotide and several amino acids. Tricarboxylic cycle (TCA) not only produce reducing equivalent for energy generation, but also several precursors for amino acid biosynthesis. Anaplerosis is important for replenishing the intermediates that are removed for biosynthesis. The main anaplerotic reaction in *E. coli* growing on glucose is the conversion from phosphoenolpyruvate (PEP) to oxaloacetate (OAC), which is an important precursor for the biosynthesis of 6 amino acid. Glyoxylate is an alternative anaplerotic reaction that is critical for *E. coli* growing on acetate or fatty acid.

1.3.1 Glycolysis

Glycolysis is the pathway that converts glucose into pyruvate and has a net production of adenosine triphosphate (ATP) (Chaudhry and Varacallo, 2018). The most common type of glycolysis is the Embden-Meyerhof-Parnas pathway (EMP), which is named after the scientists in honor of their contribution to the discovery of this pathway (Akram, 2013). There are 10 steps in the EMP pathway that convert 1 glucose molecule into 2 pyruvates with a net production of 2 ATP, as shown in Fig. 1.1. An alternative glycolytic route, the Entner-Doudoroff (ED) pathway, requires fewer enzymatic steps and is more thermodynamically favorable, but is generally inactive in *E. coli* when grown on glucose (Conway, 1992; Hollinshead *et al.*, 2016). More and more evidence suggests that the ED pathway is essential to *E. coli* for the metabolism of sugar acids such as gluconate and for colonization in both intestinal and aquatic habitats (Peekhaus and Conway, 1998; Chang *et al.*, 2004).

1.3.2 Pentose phosphate pathway

The pentose phosphate pathway (PPP), a metabolic pathway parallel to glycolysis, is a fundamental component of cell metabolism. The pathway was first presented in 1955 (GUNSALUS, HORECKER and WOOD, 1955) after decades of effort by many biochemists (Stincone *et al.*, 2015). There are two phases in the pentose phosphate pathway: the oxidative phase and the non-oxidative phase. In the oxidative phase, the reducing equivalent nicotinamide

adenine dinucleotide phosphate (NADPH) is generated for reductive biosynthesis reactions (Kruger and Von Schaewen, 2003). In the non-oxidative phase, several precursors are generated for the synthesis of nucleic acids and amino acids. For instance, ribose 5-phosphate (R5P) is required for DNA and RNA synthesis and erythrose 4-phosphate (E4P) is a precursor for the aromatic acids tyrosine, phenylalanine, and tryptophan (Stincone *et al.*, 2015).

1.3.3 Tricarboxylic cycle

The tricarboxylic Acid (TCA) cycle, also known as the Krebs cycle or the citric acid cycle, is a crucial metabolic pathway that plays a central role in cellular respiration. The TCA cycle is the major energy generating pathway and produces several precursors for various biosynthetic processes (Vuoristo *et al.*, 2016). Acetyl-CoA derived from sugars or fatty acids is oxidized through a series of chemical reactions to release energy stored in the nutrients, which provides reducing equivalent nicotinamide adenine dinucleotide (NADH) (Guest and Russell, 1992). The TCA cycle not only provides energy for cellular processes, but also serves as a hub for the synthesis of amino acids (Kaleta *et al.*, 2013). Alpha-ketoglutarate (AKG) is the precursor for synthesizing glutamate, which can further be converted into proline, glutamine and arginine. Oxaloacetate is another important precursor for aspartate, which can then be utilized for the biosynthesis of methionine, asparagine, threonine and isoleucine (Akashi and Gojobori, 2002).

1.3.4 Anaplerosis

Anaplerotic reactions are essential metabolic processes that replenish the TCA cycle intermediates that are withdrawn for amino acid biosynthesis. The principal anaplerotic reactions in *E. coli* involve the enzyme phosphoenolpyruvate carboxylase (PPC) that catalyzes the conversion of phosphoenolpyruvate (PEP) to oxaloacetate (OAC), which is the precursor for 6

amino acids (Ashworth and Kornberg, 1966; March, Eiteman and Altman, 2002; Muñoz-Elías and McKinney, 2006). Another important anaplerotic pathway is the glyoxylate shunt, which allows the bypassing of the decarboxylation steps of the TCA cycle, facilitating the net synthesis of four-carbon dicarboxylic acids from two-carbon acetyl-CoA (Dolan and Welch, 2018). The glyoxylate shunt is generally inactive in *E. coli* growing on glucose, but can be induced during growth on acetate and fatty acids (Kornberg, 1966; Farmer and Liao, 1997). Anaplerotic reactions are crucial for maintaining the balance of TCA cycle intermediates, thereby supporting both energy production and the biosynthesis of various cellular components.

1.4 Metabolic flux analysis

Metabolic flux analysis (MFA) is a quantitative approach that provides critical insights into cellular metabolism, identifies bottlenecks in the metabolic network and reveals regulatory mechanisms within the cells (Stephanopoulos and Vallino, 1991; Vallino and Stephanopoulos, 2000). To date, MFA has been applied not only to native strains to understand the regulation of in vivo metabolism, but also to optimize the performance of metabolically engineered strains (Tang *et al.*, 2009). Applications on native organisms range from investigating microbial responses to environmental perturbations (Yang, Hua and Shimizu, 2002; Shastri and Morgan, 2005; Young *et al.*, 2011) to studying mammalian cells, such as cancer cells, for therapeutic targets (Dai and Locasale, 2017; Antoniewicz, 2018). In the field of metabolic engineering, which focuses on modifying metabolic pathways within an organism to enhance the production of desired products or to endow the organism with new capabilities, metabolic flux analysis and metabolic engineering are closely intertwined, collectively driving advancements in biotechnology (Stephanopoulos, 1999; Toya and Shimizu, 2013). Metabolic engineering techniques enable scientists to introduce new metabolic pathways, alter the expression levels of

enzymes or remove competing pathways to drive the production of desired products (Bailey, 1991). A key aspect in this process is understanding and manipulating metabolic fluxes, in which metabolic flux analysis serves as a powerful tool by providing critical quantitative information (Stephanopoulos, 1999). Overall, MFA is an indispensable tool for elucidating cellular metabolic processes, identifying regulatory mechanisms, and enhancing our ability to investigate and manipulate metabolic networks.

Over the past three decades, three main stoichiometry based approaches have been developed to quantify metabolic fluxes: flux balance analysis (FBA), metabolic flux analysis (MFA) and ^{13}C metabolic flux analysis (^{13}C MFA) (Antoniewicz, 2021). Flux balance analysis (FBA) leverages stoichiometric models that represent the biochemical reactions in a cell to calculate optimal flux distributions that maximize or minimize specific objective functions, such as biomass production or the synthesis of a particular metabolite (Orth, Thiele and Palsson, 2010). Although much progress has been made in FBA through the integration of additional constraints and regulatory information, the accuracy of metabolic fluxes predicted by FBA remains limited due to the challenge of identifying a proper objective function (Lee, Gianchandani and Papin, 2006; Raman and Chandra, 2009). Metabolic flux analysis (MFA), on the other hand, estimates fluxes based on experimentally measured rates such as nutrient uptake rate, growth rate and production rate. Fluxes are determined by fitting the metabolic network model predictions to the measured rates, which do not require an objective function as in FBA, therefore having broader applications on engineered strains under various growth conditions (Antoniewicz, 2021). MFA, however, often requires a simplified network model due to limited constraints, which sometimes causes MFA to fail to predict accurate fluxes when new pathways are activated under different growth conditions (Antoniewicz, 2015). ^{13}C metabolic flux analysis

(^{13}C MFA) is the gold standard for determining fluxes by model-based analysis and the isotope labeling pattern. This technique does not require optimality assumptions or model simplification, therefore providing precise flux results (Sauer, 2006; Zamboni, 2011; Crown and Antoniewicz, 2013)

1.4.1 ^{13}C Metabolic flux analysis

^{13}C MFA quantifies metabolic fluxes by fitting the experimental measurements, including external rates and isotopic labeling, to the metabolic network model. The isotopic labeling patterns, which provide additional constraints, are generated by culturing the organism with a labeled substrate, known as a tracer, in the culture medium. Tracer selection can largely impact the precision of flux estimation (Crown and Antoniewicz, 2012; Antoniewicz, 2013). Recent literature (Crown, Long and Antoniewicz, 2016) has provided a comprehensive guidance on selecting proper tracers for elucidating fluxes in central carbon metabolism. Overall, [1,6-^{13}C] glucose and [1,2-^{13}C] glucose are the optimal choices for parallel tracer experiments, which are also utilized in my thesis work. The isotopic distributions can be measured by gas chromatography mass spectrometry (GC-MS) (Fischer and Sauer, 2003; Zhao and Shimizu, 2003), liquid chromatography mass spectrometry (LC-MS) (Nöh *et al.*, 2007) or NMR (Goudar *et al.*, 2010). Isotopic labeling measurements are extremely useful for elucidating relative flux distributions in the metabolic network. However, at least one external rate measurement is required to obtain the absolute metabolic fluxes. In my thesis work, isotopic labeling distributions and glucose uptake rate, which serves as the external rate measurement, are both measured by GC-MS.

The metabolic network used for fitting the experimental measurements is the core of ^{13}C metabolic flux analysis. The network can be constructed from databases such as KEGG (Feng *et*

al., 2012; Kanehisa *et al.*, 2012). It is critical to include all the reactions that are related to the transition of labeled atoms in order to obtain accurate estimates. Flux estimation requires solving a non-linear regression problem with a set of fluxes so that the derived labeling pattern best matches with the experimental measured isotopic labeling distributions (Gopalakrishnan and Maranas, 2015; Antoniewicz, 2021). The mathematical framework to predict the labeling patterns from a given set of fluxes is critical for flux estimation efficiency. Various frameworks have been developed to allow more efficient calculation including isotopomers (Schmidt *et al.*, 1997), cumomers (Wiechert *et al.*, 1999) and elementary metabolite units (EMU) (Antoniewicz, Kelleher and Stephanopoulos, 2007b). The development of the EMU framework has significantly reduced the computational calculation. It has been extensively applied in several commonly used ^{13}C metabolic flux analysis tools such as Metran (Yoo *et al.*, 2008), INCA (Young, 2014), OpenFLUX2 (Shupletsov *et al.*, 2014) and 13CFLUX2 (Weitzel *et al.*, 2013). These software tools apply different optimized strategies to estimate fluxes that minimize the difference between experimental measurements and the simulated results. The estimated fluxes should be assessed for goodness of fit to ensure the fit is statistically acceptable (Antoniewicz, Kelleher and Stephanopoulos, 2006).

1.4.2 ^{13}C Metabolic flux analysis in co-culture

In most studies using applying ^{13}C MFA, it was applied in mono-culture, which provides the intracellular fluxes for a single strain (Crown and Antoniewicz, 2013). In a few cases where ^{13}C MFA was applied in a co-culture system, it required physical separation of cells in order to estimate individual fluxes. The separation of cells was usually accomplished through overexpressing heterologous reporter protein such as fluorescent protein for cell sorting, which raises the concern of altering cell metabolism (Shaikh *et al.*, 2008; Rühl, Hardt and Sauer, 2011).

An alternative approach based on labeled peptides was proposed in 2014 (Ghosh *et al.*, 2014) and further tested experimentally in recent work to elucidate cross-feeding metabolites (Gabrielli *et al.*, 2023). However, the peptide approach can only be applied to two species with distinct protein sequences in order to assign the measured labeled peptides to corresponding strains. Furthermore, this approach requires different preferences in carbon source for the two strains as well.

In 2015, a new approach, which only requires the measurement of total biomass and does not require any physical separation of cells or protein. was developed (Gebreselassie and Antoniewicz, 2015). It demonstrated that with proper tracer design and by employing a new co-culture model framework, fluxes within a co-culture system could be resolved. This new approach was tested with both simulated data and a co-culture experiment, in which two *Escherichia coli* single knockout strain Δ*pgi* and Δ*zwf* were cultured together. The fluxes were successfully predicted for individual strains. In this thesis, I take a step further to apply ^{13}C MFA to a co-culture system with interactions. Specifically, I aim to study syntrophic interactions and elucidate cross-feeding of metabolites.

1.5 Fluorescent protein

Green fluorescent protein (GFP) was first discovered in 1962 by Shimomura et al (Shimomura, Johnson and Saiga, 1962). After 30 years, the heterologous expression of GFP in prokaryotic and eukaryotic cells (Chalfie *et al.*, 1994) was recognized as a major breakthrough in cellular biology and the beginning of the GFP revolution (Ward, 2005; Remington, 2011). To date, fluorescent proteins have broad applications including protein localization, organism visualization and transcriptional reporter (Gerdes and Kaether, 1996; Misteli and Spector, 1997; March, Rao and Bentley, 2003).

In the field of metabolic engineering, fluorescent proteins allow us to expand our understanding of engineered organisms. Throughout the Design-Build-Test (DBT) cycle for strain engineering, the limiting step has always been product detection and selection due to the low throughput of traditional measurement approaches such as gas chromatography (GC) and mass spectrometry (MS) (Dietrich, McKee and Keasling, 2010; Lin, Wagner and Alper, 2017). Various types of specific biosensors were developed to provide high throughput screening. These biosensors are designed to target different molecules and often utilize fluorescent protein as a reporter to transduce the response of biosensors into an easily measurable transcriptional output (March, Rao and Bentley, 2003). These outputs can be further sorted and isolated through screening methods such as Fluorescence-Activated Cell Sorting (FACS) or a microdroplet system, providing an efficient tool for strain engineering (Morgan *et al.*, 2016; Bowman and Alper, 2020). Moreover, fluorescence coupled with advanced techniques such as Multiparametric Flow Cytometry (MPF) can be applied to bioprocess development. Applications include monitoring fermentation processes, analyzing metabolism and stress physiology and identifying productive cellular states (Tracy, Gaida and Papoutsakis, 2010).

Despite the broad application of fluorescent proteins, the metabolic stress caused by overexpressing heterologous proteins can be undesired for the host cells. The expression of foreign proteins often utilizes significant amount of energy and resources and places metabolic burden on the host cells (Glick, 1995). Altered cell physiology, especially growth reduction in recombinant cells has been widely reported in much literature (Peretti and Bailey, 1987; Neubauer, Lin and Mathiszik, 2003; Rozkov *et al.*, 2004). More detailed analysis such as transcriptomic analysis or even metabolic flux analysis has provided insights to how cells respond to metabolic stress (Rozkov *et al.*, 2004; Haddadin and Harcum, 2005; Wang *et al.*,

2006). Computational approaches have also been developed for predicting resource allocation and the trade of between growth and heterologous protein production (Weiße *et al.*, 2015; Zeng and Yang, 2019; Oftadeh and Hatzimanikatis, 2024). Despite extensive studies on recombinant proteins, there are only a handful of papers focusing on quantifying the impact of fluorescent proteins themselves. Therefore, in the second part of my thesis, I will focus on analyzing the impact of fluorescence protein production on cell metabolism. Furthermore, I will study how the overexpression of heterologous proteins might impact the interaction between microbes.

1.6 Aim and outline of each chapter

In my thesis, I aim to accomplish two goals: In the first part, I aim to develop reliable method to elucidate cross-feeding of metabolites. In the second part, I aim to provide detailed analysis of how fluorescent proteins impact cells. Toward these goals:

Chapter 2 introduces the two *Escherichia coli* single knockout strains Δ*ilvc* and Δ*icd* I selected for this work. These are both amino acid auxotrophic strains that have been previously shown to grow when cultured together. In this chapter, strains were cultured alone with the supplementation of corresponding amino acids they required. This is the first work applying ^{13}C MFA on auxotrophic strains to uncover how their metabolism is affected.

Chapter 3 demonstrates how ^{13}C MFA was applied to syntrophic partners to elucidate the cross-feeding interaction. We verified the growth of Δ*ilvc* and Δ*icd* co-culture and conduct labeling experiments. Several metabolic networks were constructed for flux estimation. I carefully evaluated the performance of each network model to identify the exchanging metabolites. In this work, I found that out not only the deficient amino acids are being cross-fed, but some intermediates are also being exchanged at significant rates. This unexpected finding leads to the next chapter where I investigated the cross-feeding of amino acid intermediates.

Chapter 4 further investigates if metabolic pathway intermediates could be exchanged and to what extent this exchange is common between auxotrophic strains. For this purpose, I selected 37 *Escherichia coli* single gene knockout strains that are auxotrophic for 9 different amino acids. Strains that share the same amino acid deficiency were paired and their growth were monitored. Growth of the co-culture would indicate the exchange of amino acid intermediates. I also verified the growth on intermediates for these auxotrophic strains.

Chapter 5 investigates five commonly used fluorescent proteins CFP, Crimson, GFP, Tomato and YFP and how they impact the cell when overexpressed in wild type *E. coli*. I evaluated the impact of fluorescent protein overexpression including cell physiology and metabolism. I analyzed cell growth, biomass composition and most importantly, metabolic states.

Chapter 6 starts with a case study of applying ^{13}C MFA on fluorescent syntrophic co-culture consisting of Δ*ilvc*-Crimson and Δ*icd*-CFP. I will highlight some of the challenges for co-culture MFA. Future directions with respect to ^{13}C MFA are also discussed in this chapter.

Chapter 2 ^{13}C Metabolic Flux Analysis on *E. coli* Lethal Knockout Strains Reveal How Metabolism is Restored in Auxotrophic Strains Supplemented with Required Metabolites

2.1 Abstract

Amino acid auxotrophy, i.e., the inability to synthesize one or more essential amino acids, is commonly found in nature. To date, amino acid auxotrophic strains have widely been used as model strains in various fields. In this work, by applying ^{13}C Metabolic Flux Analysis (^{13}C MFA), we aim to understand how auxotrophic strains restore their metabolism when supplemented with required metabolites. Specifically, we selected two auxotrophic *Escherichia coli* single knockout strains, Δ*ilvc* and Δ*icd,* as our model strains. The two strains were grown under supplementation of the required amino acid based on the knockout phenotypes. The restored metabolism was analyzed by conducting parallel labeling experiments with [1,2-^{13}C] glucose and [1,6-^{13}C] glucose. The isotopic labeling of intracellular metabolites was analyzed by GC-MS and used to perform flux analysis. We found that Δ*ilvc*, which has a knockout further away from central carbon metabolism, shows similar flux distribution to wild type *E. coli*. On the other hand, Δ*icd* shows significant flux rewiring with its knockout located in the TCA cycle. In conclusion, we visualized the restored metabolism of the auxotroph strains growing on the required amino acid and discovered that the location of the gene knockout could impact how the cells restore their metabolism.

2.2 Introduction

Auxotrophy, i.e., the inability to synthesize essential compound for growth, is prevalent in nature (D'Souza *et al.*, 2014; Mee *et al.*, 2014). In scientific studies, auxotrophic strains, especially auxotrophs for amino acid biosynthesis, are wildly applied for different purposes. For example, they are commonly used to study fundamental microbial interaction (Wintermute and Silver, 2010; Mee *et al.*, 2014; Noto Guillen *et al.*, 2021), engineered for applications such as biosensors (Bertels, Merker and Kost, 2012) or producing valuable chemicals through synthetic cultures (Liu *et al.*, 2018; Müller *et al.*, 2023) .

The inability to synthesize essential amino acids indicates that the auxotrophic strains require the lacking amino acid to be cross-fed from another strain or directly provided in the culture medium. In this work, we aim to understand how auxotrophic strains restore their growth when the required essential metabolites are provided and how the knockout impacts the recovered metabolism. Specifically, we will apply ^{13}C Metabolic Flux Analysis (^{13}C MFA) to obtain detailed metabolic fluxes. ^{13}C MFA is a powerful and widely used tool that determines fluxes by isotopic labeling patterns and model-based analysis (Antoniewicz, 2021). Previous studies have applied ^{13}C MFA on different knockout strains to understand the metabolic rewiring in response to genetic perturbation (Li *et al.*, 2006; Toya *et al.*, 2010; Long *et al.*, 2018; Long and Antoniewicz, 2019b). In this work, it is the first time that ^{13}C MFA is applied on auxotroph strains to uncover their metabolism. Here, we selected two *E. coli* single knockout strains, Δ*ilvc* and Δ*icd*, which are both auxotrophic for essential amino acids, and demonstrated their restored metabolism fluxes when the required amino acid is provided. We found that the location of the knockout can determine how the metabolism is impacted. We also discussed some other possible

metabolic rewiring scenarios that emphasize the importance of conducting ^{13}C MFA to elucidate cell metabolism.

2.3 Methods

2.3.1 Cell strain

The two model strains, Δ*ilvC* and Δ*icd*, are *Escherichia coli* (*E. coli*) single knockout strains obtained from the Keio knockout collection (GE Healthcare Dharmacon), which were generated by one-step gene inactivation in *E. coli* K-12 BW25113. They are both auxotrophic strain that are unable to synthesize essential amino acid(s). As shown in Figure 2.1, the ilvC gene encodes ketol-acid reductoisomerase, which is involved in the biosynthesis of valine, leucine and isoleucine. The icd gene encodes isocitrate dehydrogenase that catalyzes the reaction from isocitrate to alpha ketoglutarate, which is required to synthesize glutamate. Both strains have resistance to antibiotic kanamycin.

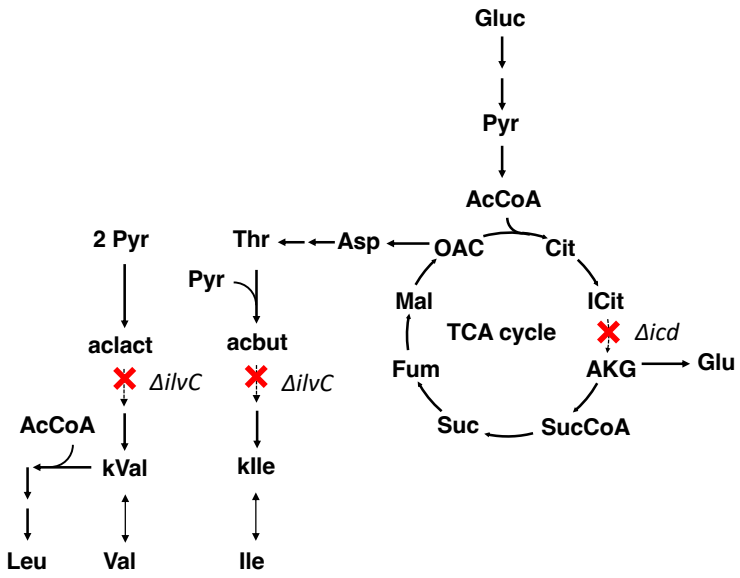

Figure 2.1 Gene knockout location of the two model strains Δ*ilvC* and Δ*icd*. The location of the knockout gene in the two selected strains Δ*ilvc* and Δ*icd* are marked with red crosses. Δ*ilvc* has knockout further away from central carbon metabolism and is not able to produce valine and isoleucine; while Δ*icd* has knockout in the TCA cycle and is not able to produce glutamate.

2.3.2 Cell growth

Both strains are precultured in 3% of LB Broth Miller, 1mM of glucose and 50µg/L of kanamycin in M9 minimal medium overnight before inoculation. For growth test, 100µL of cells from preculture are inoculated in 10 mL of minimal medium (M9) with 10mM of glucose and 50µg/L of kanamycin in shake flask. The optical density (OD) at 600nm is measured by spectrophotometer to obtain the cell growth.

For parallel labeling experiments, cells are precultured and inoculated as above. Cells are cultured with either 10mM of [1,2-^{13}C] glucose or 10mM of [1,6-^{13}C] glucose. Additional 2mM of valine and isoleucine are added in Δ*ilvC* culture. Likewise, 2mM of glutamate is supplemented for the Δ*icd* culture. Medium smaples from the cultures were taken at different time points during the growth for medium analysis. Cell samples are collected at mid-exponential growth phase when the OD_{600} is around 0.7 and stored in -20°C before further analysis.

2.3.3 Gas chromatography-mass spectrometry and chemical derivatization

All the biomass and medium samples were derivatized for gas chromatography-mass spectrometry (GC-MS) detection to obtain isotopic distributions. We followed the standard protocol for sample derivatization as previously described (Long and Antoniewicz, 2019a).

2.3.3.1 Biomass amino acid

For proteinogenic amino acids, the cell samples were derivatized by tert-butyldimethylsilyl (TBDMS) before GC-MS measurement. The collected cell pellets were resuspended in 500µL of 6N HCl and heated on 110°C for 12-18 hours. The heated samples were cooled under room temperature before centrifuging for 5 minutes at maximum speed.

400µL of the supernatants were transferred to new Eppendorf and dried at 65°C under air. 35µL of pyridine and 50µL of TBDMS were added to the dried samples and mixed by pipetting, followed by incubation at 60°C for 30 minutes. After cooling, the samples were centrifuged for 1 minutes at maximum speed and transfer to GC-MS vials for analysis.

2.3.3.2 Intracellular metabolites

For intracellular metabolites, we prepared 70% of ethanol that was heated to 70°C and mixed 1mL with the cell pellets by vortexing. The samples were incubated for 5 minutes at 95°C for extraction. After cooling on ice for 5 minutes, the samples were centrifuged for 5 minutes at the maximum speed and dried in lyophilizer (Labconco) overnight. The dried samples were resuspended with 50µL of 2% methoxyamine (MOX) in pyridine and incubated for 90 minutes at 37°C, followed by the derivatization of TBDMS at 60°C for 30 minutes. The samples were cooled and then centrifuged for 1 minute at maximum speed before transferring to GC-MS vials for analysis.

2.3.3.3 Biomass RNA and glycogen

For biomass RNA and glycogen, which provide the labeling of ribose and glucose in the biomass, were derivatized by propionic anhydride. The cell pellets were first washed with 500µL of glucose free medium twice. 50µL of 6N HCl was added to the pellets and incubated at 30°C for 30 minutes. After incubation, the samples were diluted with 250µL of DI water and incubated for 1 hour at 110°C. After cooling, the samples were briefly centrifuged before adding 40µL of 5N NaOH to neutralize the reaction, followed by drying at 65°C under air. The dried samples were resuspended in 50µL of 2% hydroxylamine in pyridine and incubate at 90°C for 1 hour. After cooling, the samples were centrifuged briefly before adding 100µL of propionic anhydride

and incubating at 60°C for 30 minutes. The samples were centrifuged for 1 minutes at maximum speed before transferring to GC-MS vials for analysis.

2.3.3.4 Biomass fatty acid

For biomass fatty acid analysis, which provide labeling information for acetyl Coenzyme A (AcCoA), it was measured by fatty acid methyl ester (FAME) derivatization. The cell pellets were resuspended by 50µL of DI water and transferred to glass tubes, followed by drying at 65°C under air. The dried samples were dissolved in 1mL of methanol and 50µL of sulfuric acid. The glass tubes were tightly sealed with caps and the samples were incubated at 100°C for 2 hours. After cooling, 1.5mL of DI water and 3mL of hexane were added to the sample and vortexed for 1minute for extraction. The mixtures were centrifuged for 5 minutes at 2500 rpm for phase separation, followed by transferring the upper organic to new tubes. The samples were dried at 40°C under nitrogen. Dried samples were redissolved with 100µL of hexane and transferred to GC-MS vials for analysis.

2.3.3.5 Glucose from medium

In order to obtain the glucose uptake rate, the supernatants from the cultures were taken at different time points. 20µL of medium samples were mixed with 20µL of 10mM of [U]-glucose which served as standard before derivatization. The mixtures were dried at 65°C under air before adding 50µL of 2% hydroxylamine in pyridine and incubating at 90°C for 1 hour. After cooling, the samples were centrifuged briefly. 100µL of propionic anhydride was added to the samples and incubated at 60°C for 30 minutes. The samples were centrifuged for 1 minute at maximum speed before transferring to GC-MS vials for analysis.

2.3.3.6 Acetate from medium

The acetate secretion rate was calculated by measuring the acetate concentration in the supernatant through TBDMS derivatization. 50µL of supernatants were mixed with 50µL of D-acetate, followed by adding 20µL of 6N HCl and 100µL of methyl propionate. The mixtures were vortex for over 30 seconds and centrifuged for 5 minutes at maximum speed. 50µL of the top layer were transferred to new Eppendorf and added with 20µL of TBDMS. The samples were incubated for 30 minutes at 60°C for 30 minutes and cooled at room temperature for over 15 minutes. The cooled samples were centrifuged for 2 minutes at maximum speed and transfered to GC-MS vials for further analysis.

2.3.3.7 Data processing

All the GC-MS measurements were integrated by mstool to obtain mass isotopomer distributions and corrected for natural abundance (Fernandez *et al.*, 1996) for ^{13}C metabolic flux analysis.

2.3.4 ^{13}C metabolic flux analysis

The full metabolic network model for ^{13}C MFA is provided in Appendix A.1. In short, the model contains central carbon metabolism including glycolysis, pentose phosphate pathway, ED pathway, TCA cycle and glyoxylate shunt; lumped amino acid biosynthesis and biomass formation reaction. ^{13}C MFA are performed by using Metran (Yoo *et al.*, 2008), which is based on elementary metabolite units (EMU) framework (Antoniewicz, Kelleher and Stephanopoulos, 2007b). Fluxes were estimated by minimizing the sum of squared residual (SSR) between the experimental measured isotopomer distributions and the simulation results. To ensure global minimum, each estimation started with random values, and reiterated based on the previous

result for at least 20 times or until no improvement in SSR. This process is repeated at least 10 times to find the global solution.

2.3.5 Statistical analysis

The final flux result was subjected to χ^2 statistical analysis for goodness-of-fit as described in previous literature (Antoniewicz, Kelleher and Stephanopoulos, 2006). In short, assuming the model is correct and the experimental data are without gross measurement errors, the SSR should be a stochastic variable with χ^2 distribution with degree of freedom equal fitted measurements n minus independent parameter p. The minimized SSR is considered acceptable within the range of $\chi^2_{\alpha/2}(n-p)$ and $\chi^2_{1-\alpha/2}(n-p)$, with α being a chosen threshold value, for example 0.05 for 95% confidence intervals. For each flux, we calculated 95% confidence intervals by evaluating the sensitivities of the minimized SSR to flux variations.

2.4 Results

2.4.1 Cell growth

Δ*ilvC* and Δ*icd* were both grown in 96 well plates and the growth was monitored by BioTek Cytation 5. Figure 2.2A shows the growth of Δ*ilvC* in minimal medium (M9) with or without additional 1mM valine and isoleucine. Similarly, Figure 2.2B shows the growth of Δ*icd* with or without 1mM glutamate. Both strains show no growth in M9 and their growth is restored when supplemented with amino acid supplementation. The growth rate of Δ*ilvC* with 1mM of valine and isoleucine is 0.52 1/h, and 0.58 1/h for Δ*icd* with 1mM of glutamate. This result confirms the auxotrophic phenotypes of the strains.

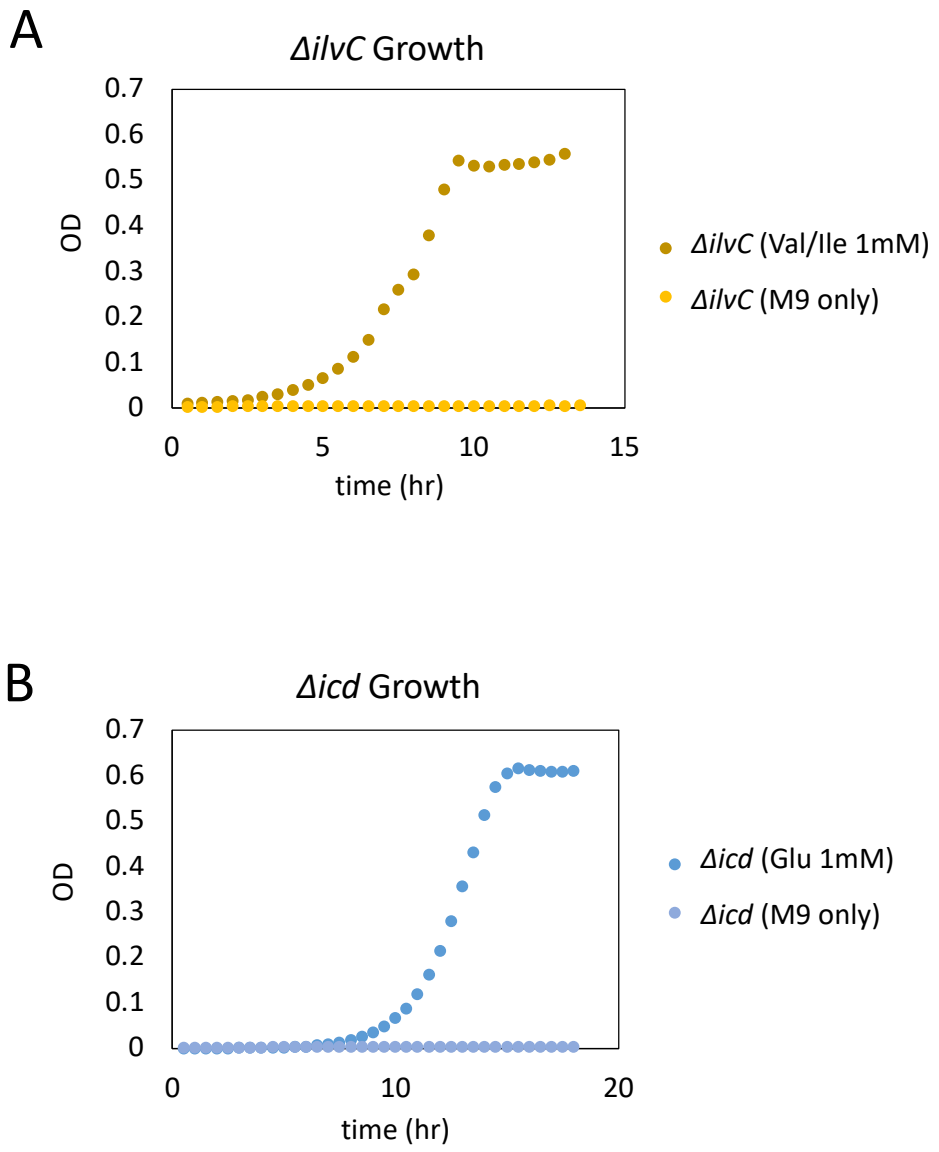

Figure 2.2 Growth of Δ*ilvC* and Δ*icd* with only minimal medium M9 or 1mM of required amino acid valine (Val), isoleucine (Ile) or glutamate (Glu). Δ*ilvc* and Δ*icd* are both lethal knockout strains that no growth is observed when culture in M9 only. Growth is restored when culture with corresponding lacking amino acid. Val: valine; Ile: isoleucine; Glu: glutamate; OD: optical density.

2.4.2 Labeling experiment

For parallel labeling experiments, cells were culture with either 10mM of [1,2-^{13}C] glucose or [1,6-^{13}C] glucose in flask. Both strains were supplemented with 2mM of required amino acids. The growth of Δ*ilvC* and Δ*icd* with labeled glucose are shown in Fig. 2.3. The

growth rate of different tracers showed similar trend for both strains. The average growth rate of Δ*ilvc* and Δ*icd* is 0.53 1/h and 0.47 1/h, respectively.

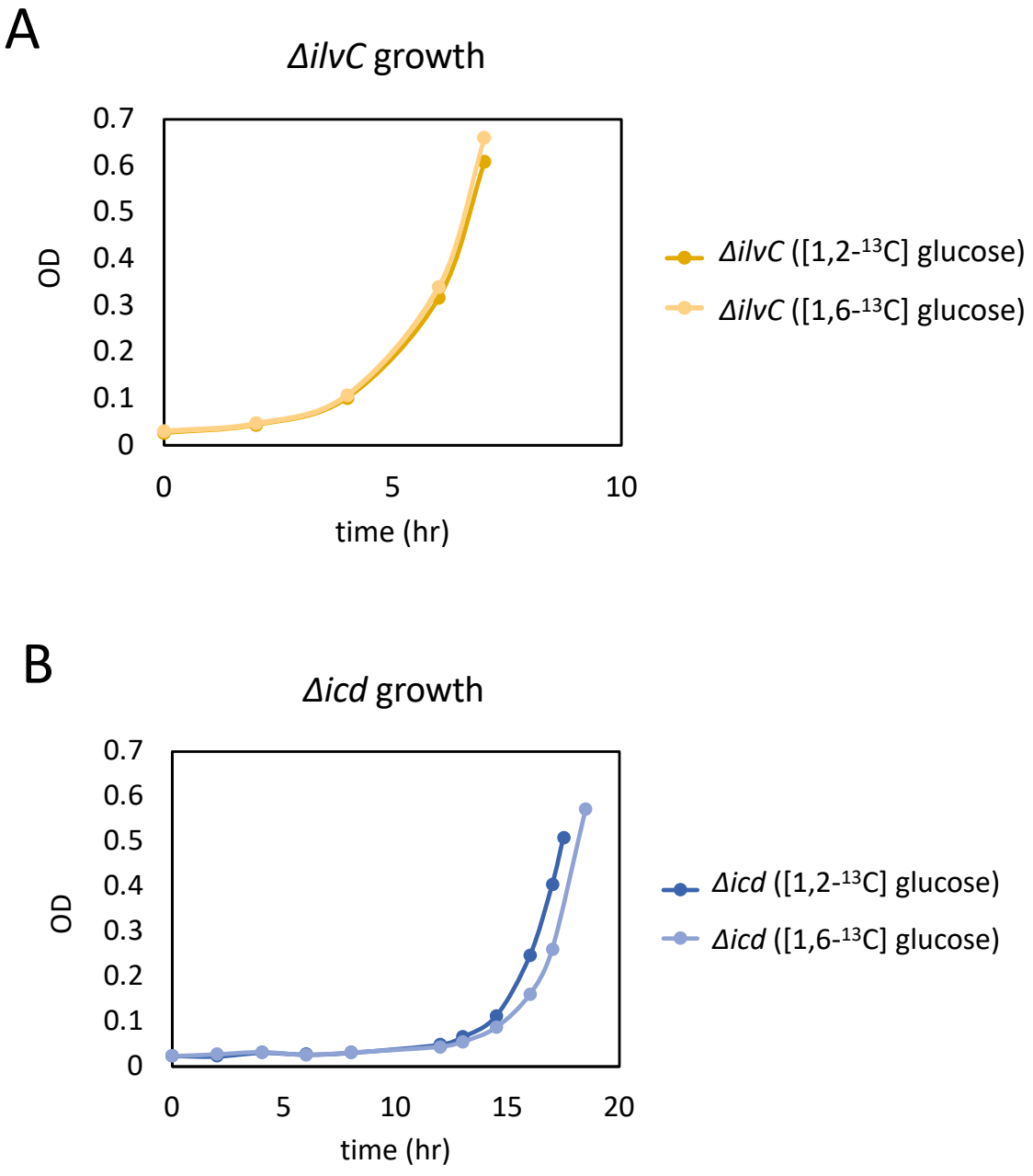

Figure 2.3 Parallel labeling experiment of Δ*ilvC* and Δ*icd* supplemented with 2mM of required amino acid valine (Val), isoleucine (Ile) or glutamate (Glu). The growth of Δ*ilvC* and Δ*icd* with labeled glucose as tracer. The OD was measured by spectrophotometer at 600nm.

2.4.3 ^{13}C metabolic flux analysis

We performed ^{13}C metabolic flux analysis on the lethal knockout strains, Δ*ilvc* and Δ*icd,* to better understand how the metabolism was restored when supplemented with corresponding amino acids. Flux analysis was also conducted on wild type (WT) *Escherichia coli* (*E. coli*) to serve as a base comparison.

Figure 2.4 demonstrates the estimated metabolic fluxes in central carbon metabolism for wildtype *E. coli*, Δ*ilvC* and Δ*icd*. The flux values are normalized to 100 glucose uptake. The specific glucose uptake rate estimated from flux analysis are noted on the top of the flux maps. Specifically, it was estimated by dividing biomass formation flux value, whose unit is kg_{DW}/100 mol glucose uptake, by growth rate. The knockout strains have similar growth rate and specific glucose uptake rate as wild type when supplemented with amino acid.

The flux distribution of the wildtype agreed well with previous report (Long and Antoniewicz, 2019b). In the knockout strains, the fluxes of the knockout reactions are all estimated to be zero (Δ*ilvc* not shown), confirming the knockout phenotype of the two lethal strains. Overall, Δ*ilvc* strain shows very similar flux distribution as wildtype. We only observed a slightly lower flux value from pyruvate (Pyr) to acetyl CoA (AcCoA) in Δ*ilvC* despite similar flux value from phosphoenolpyruvic acid (PEP) to pyruvate as wildtype. This could result from the fact that Δ*ilvc* is not able to produce valine, leucine and isoleucine, which use pyruvate as the main precursor. Therefore, more pyruvate is converted to acetyl CoA. On the other hand, Δ*icd* shows several differences from WT. We observed a lower TCA flux and an active glyoxylate shunt, which is likely due to the knockout located in the TCA cycle. In addition, the replenishing flux for oxaloacetate (OAC) from phosphoenolpyruvic acid (PEP), which is the main anaplerotic reaction in *E. coli* metabolism, in Δ*icd* is lower compared to WT. This might be due to the

activation of glyoxylate shunt, which serve as another source of oxaloacetate replenishment. In additional to these metabolic flux rewiring, we also observed a higher flux from malate to pyruvate.

Taken together, in this work, we visualize how the knockout strains restore their metabolism. We conclude that the location of the knockout could determine how much the central carbon metabolism is impacted. We found out that Δ*ilvc,* having knockout located further away from the central carbon metabolism, has very similar flux distribution as WT; and Δ*icd*, having knockout located in the TCA cycle, shows several differences.

A

^{13}C Metabolic Flux Analysis of wild type *E. coli*

μ: 0.47 1/h; q_{gluc}: 5.1 mmol/g_{DW}/h

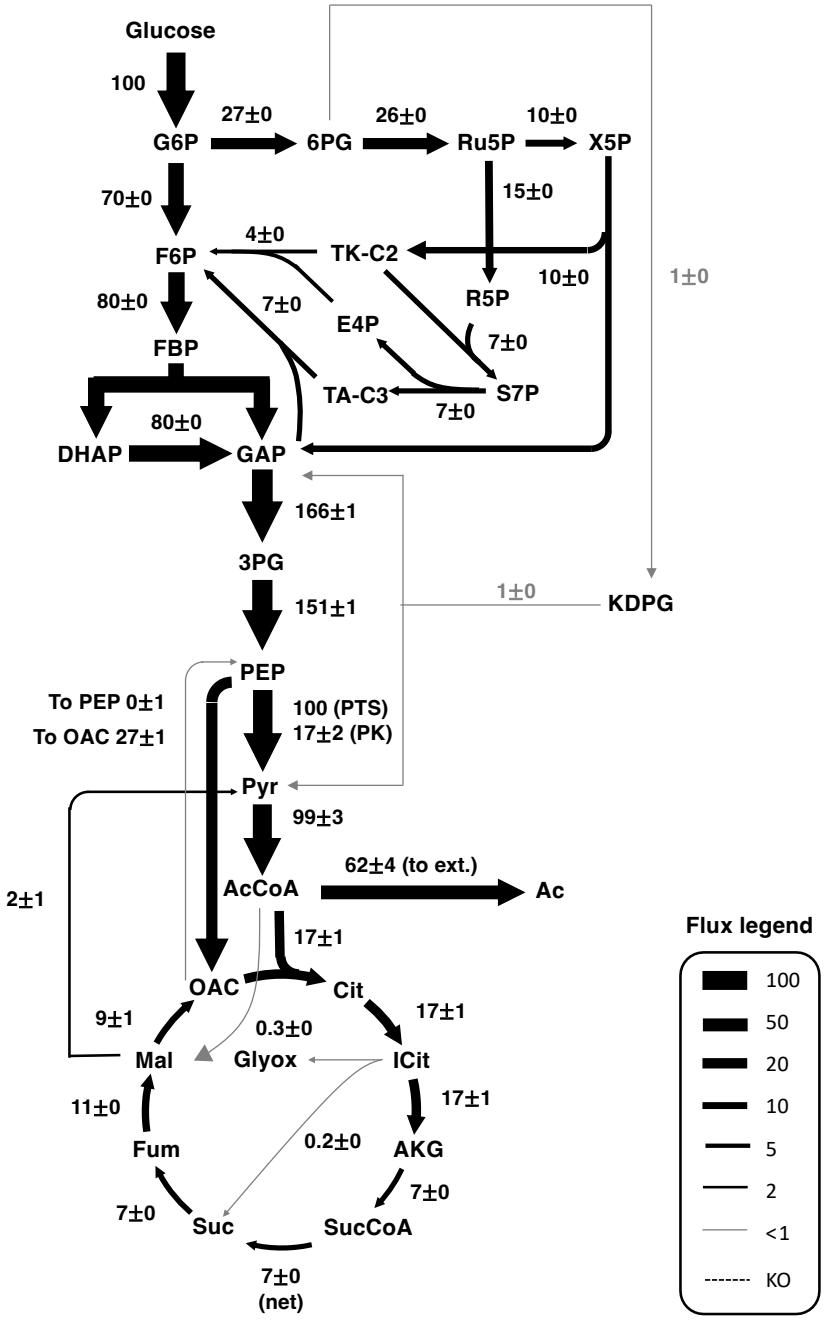

B

^{13}C Metabolic Flux Analysis of *Δilvc*

μ: 0.53 1/h; q_{gluc}: 5.2 mmol/g_{DW}/h

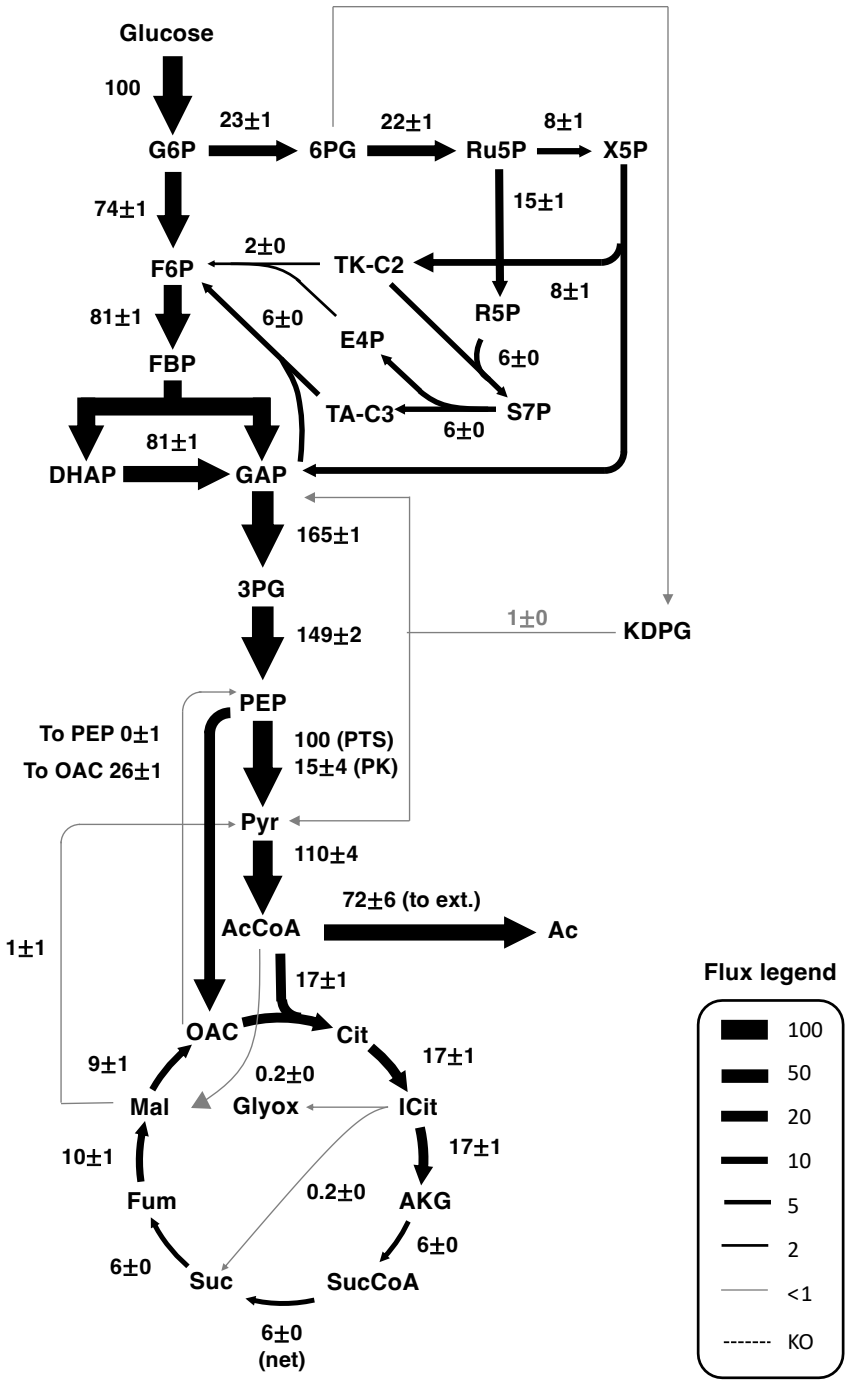

C

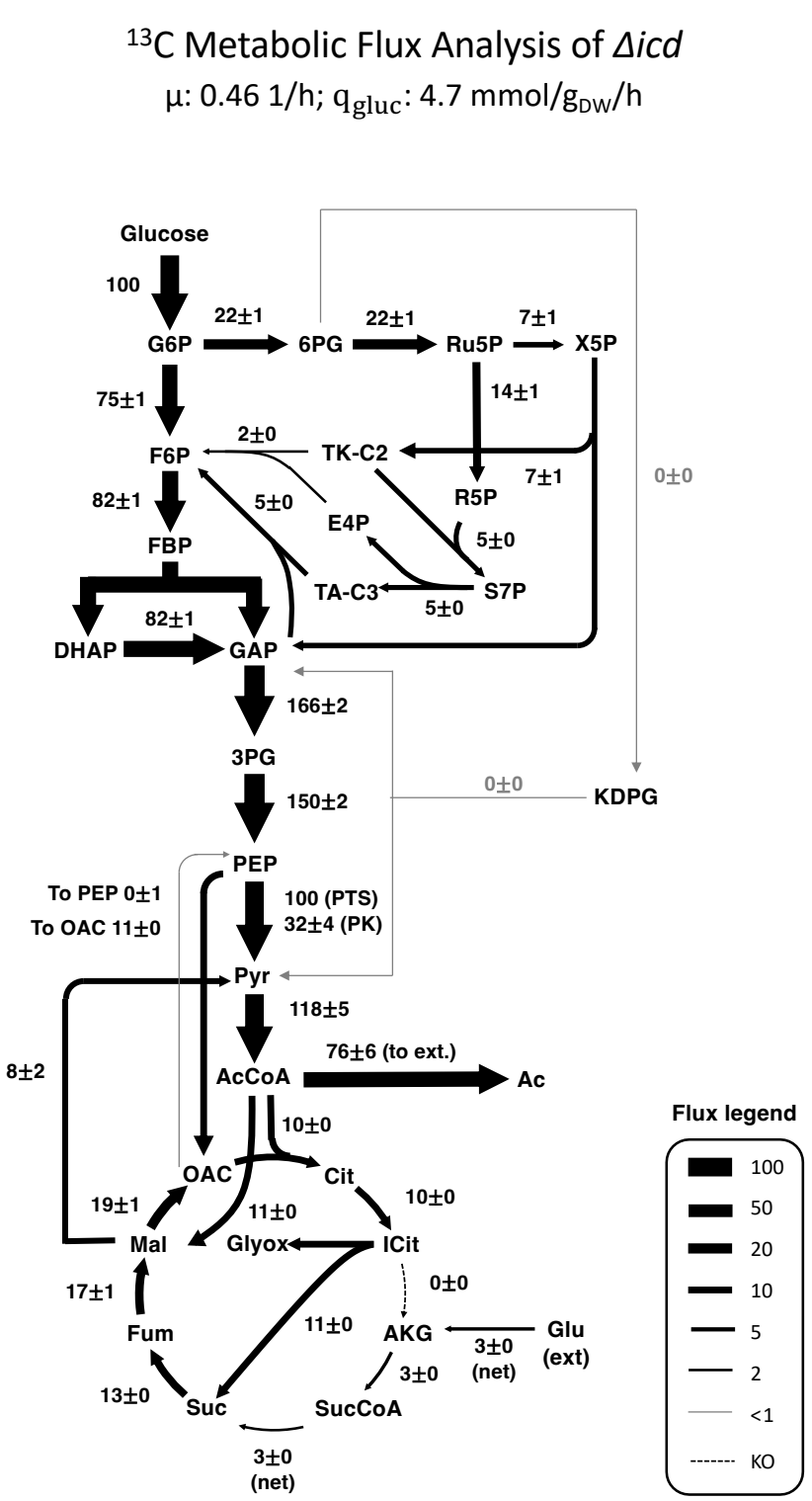

Figure 2.4 The flux maps of central carbon metabolism in (A) Wild type *E. coli*. (B) Δ*ilvC* strain. (C) Δ*icd* strain. The growth rate and specific glucose uptake rate are shown on the top of each flux map. Flux values are normalized to per 100 glucose uptake and are shown with standard deviation.

2.5 Discussion

In central carbon metabolism, TCA cycle is critical for producing precursors such as oxaloacetate (OAC) and alpha ketoglutarate (AKG) for amino acid biosynthesis. The loss of these intermediates in TCA cycle is replenished by anaplerotic reactions in order to remain stable TCA fluxes. In *E. coli* metabolism, the reaction from phosphoenolpyruvic acid (PEP) to oxaloacetate is the main anaplerotic reaction, converting C3 metabolites to replenish oxaloacetate extracted for biosynthesis. Glyoxylate shunt is another anaplerotic reaction that could generate oxaloacetate, but is typically inactive for *E. coli* when growing on glucose.

For Δ*ilvc* strain, we observed similar anaplerotic reaction as wildtype *E. coli*, i.e., active flux from PEP to OAC but inactive glyoxylate shunt. However, in the Δ*icd* strain, due to the knockout in TCA cycle, the cells rewired their metabolism to produce required precursors for growth. In this discussion, we will focus on some possible ways of how Δ*icd* strain can produce oxaloacetate.

Three possible scenarios for cells to produce oxaloacetate are shown in Fig 2.5. The first possible way in Fig 2.5A is to completely rely on the original anaplerotic reaction to produce OAC from PEP. In this case, since we supplemented additional glutamate to the culture, all the important precursors for amino acid can be produced/supported without TCA cycle being active. Another possible way to produce oxaloacetate is through the activation of glyoxylate shunt, as shown in Fig 2.5B. In *E. coli*, glyoxylate shunt is usually inactive during growth on glucose (Kornberg, 1966)(Farmer and Liao, 1997). However, it has been previously reported that the glyoxylate shunt could be activated in *E. coli* knockout strains (Long and Antoniewicz, 2019b), suggesting that this is a possible metabolic flux rewiring. The third possible scenario shown in Fig 2.5C is that the cell could simply convert the supplemented glutamate (Glu) into alpha

ketoglutarate (AKG) and restore the TCA cycle to produce oxaloacetate. In this hypothetical scenario, since no Acetyl CoA (AcCoA) enters the TCA or glyoxylate cycle, more acetate will be secreted.

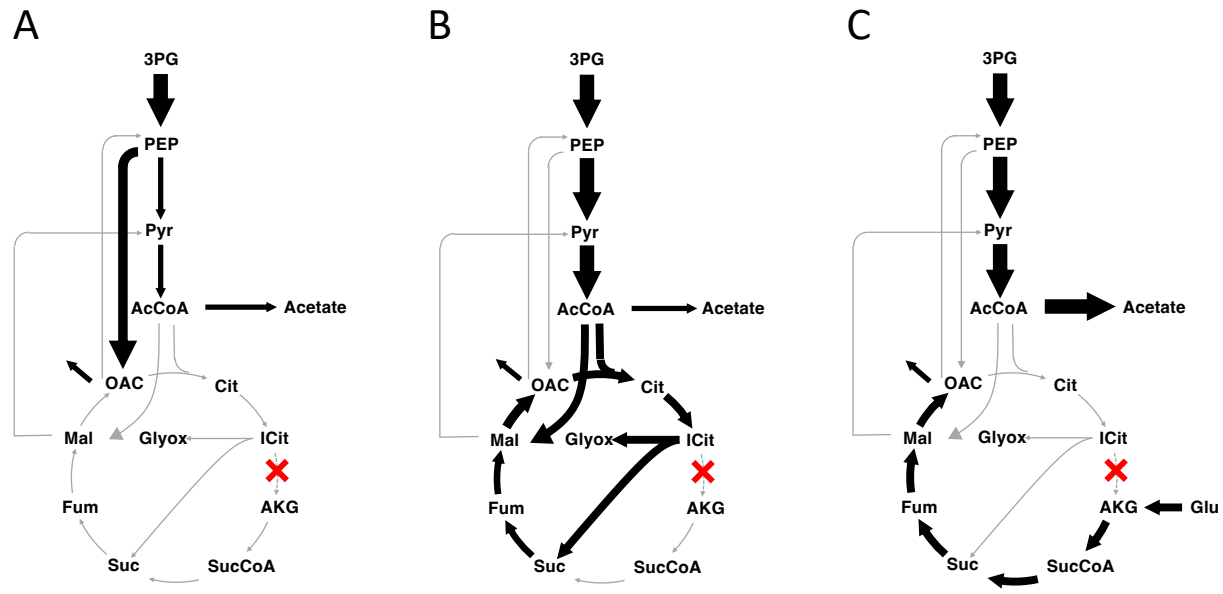

Figure 2.5 Three possible scenarios for Δ*icd* to replenish oxaloacetate (OAC). A) The first possible scenario for Δ*icd* to produce oxaloacetate (OAC) for amino acid biosynthesis. The cell could rely solely on anaplerotic reaction that converts phosphoenolpyruvic acid (PEP) to OAC to produce enough OAC. B) Another possible way to produce OAC is through the activation of glyoxylate shunt. C) The cell could also simply convert the external glutamate (Glu) into alpha ketoglutarate (AKG) and restore the lower half of the TCA cycle.

In our flux result, we observed a combination of all these scenarios (Fig 2.3C). The main production of oxaloacetate (OAC) is from the two anaplerotic reaction, PEP to OAC and the activation of glyoxylate shunt. When we compare the flux results between the wildtype and Δ*icd*, the anaplerotic reaction from PEP to OAC is slighting lower in Δ*icd*, but the influx of OAC could still maintain similar value through the activation of glyoxylate shunt. Besides the two anaplerotic reaction, we also observed a net flux of glutamate (Glu) converted into alpha ketoglutarate (AKG) and enter TCA cycle, which is another important source to produce these important precursors.

This observation serves as a good example of how difficult it is to predict the outcome of genetic perturbations. It also emphasizes the importance of conducting accurate flux analysis to elucidate rewired metabolism. In the future, a more comprehensive study of different auxotrophic strains could be valuable that provides a boarder understanding of how cells respond when the required metabolites are presented in the environment.

2.6 Supplementary experiment

2.6.1 Glucose uptake rate

Glucose concentration for the cultures were measured as described in the method section. Glucose specific uptake rate was obtained by plotting OD to glucose concentration for the slope and then divided by growth rate. Fig 2.6 and Fig 2.7 show the slope of labeling experiments and the calculation for glucose specific uptake rate for Δ*ilvC* and Δ*icd*, respectively. Here we convert 1 OD to 0.4 g_{DW}/L. For both strains, the measured glucose specific uptake rates are comparable with the rates estimated from MFA.

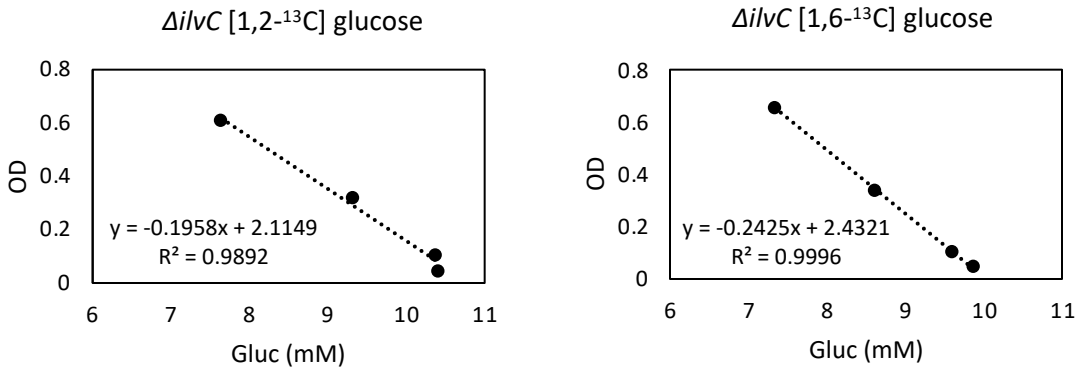

	μ (1/h)	slope (OD/mM)	gluc uptake rate (mM/OD/h)	gluc uptake rate (mmol/g_{DW}/h)
ΔilvC [1,2-^{13}C] glucose	0.53	0.20	2.7	6.7
ΔilvC [1,6-^{13}C] glucose	0.53	0.24	2.2	5.4

Figure 2.6 Glucose specific uptake rate for Δ*ilvC*. The plots show OD to glucose concentration. The slopes were shown on the plots and the table. The growth rates were calculated from the growth curve in Fig 2.3. Glucose specific uptake rate is the slope divided by growth rate. The last column in the table is for unit conversion.

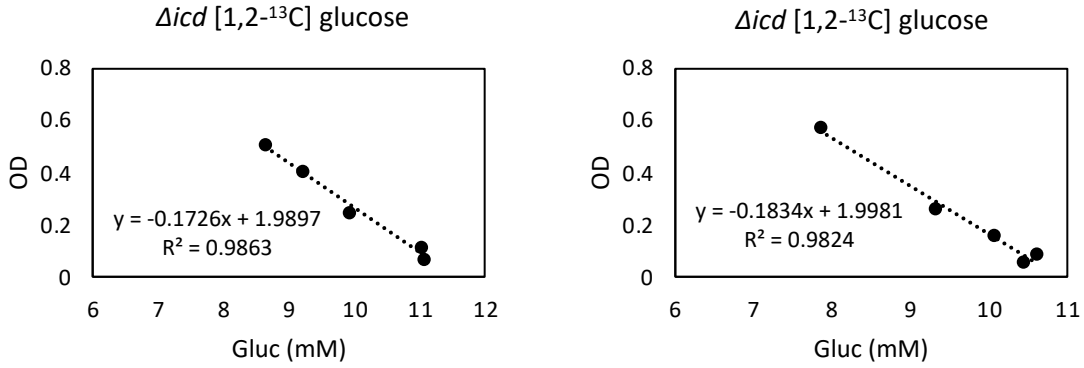

	μ (1/h)	slope (OD/mM)	gluc uptake rate (mM/OD/h)	gluc uptake rate (mmol/g_{DW}/h)
Δicd [1,2-^{13}C] glucose	0.46	0.17	2.7	6.7
Δicd [1,6-^{13}C] glucose	0.47	0.18	2.6	6.4

Figure 2.7 Glucose specific uptake rate for Δ*icd*. The plots show OD to glucose concentration. The slopes were shown on the plots and the table. The growth rates were calculated from the growth curve in Fig 2.3. Glucose specific uptake rate is the slope divided by growth rate. The last column in the table is for unit conversion.

2.6.2 Acetate secretion rate

Acetate concentration for the cultures were measured as described in the method section. Acetate concentration was plotted against glucose concentration, as shown in Fig. 2.8 and Fig. 2.9 for Δ*ilvC* and Δ*icd*, respectively. The slope of each plot times the glucose specific uptake rate calculated from section 2.6.1 will be the acetate secretion rate, as shown in the table in Fig 2.8 and Fig. 2.9.

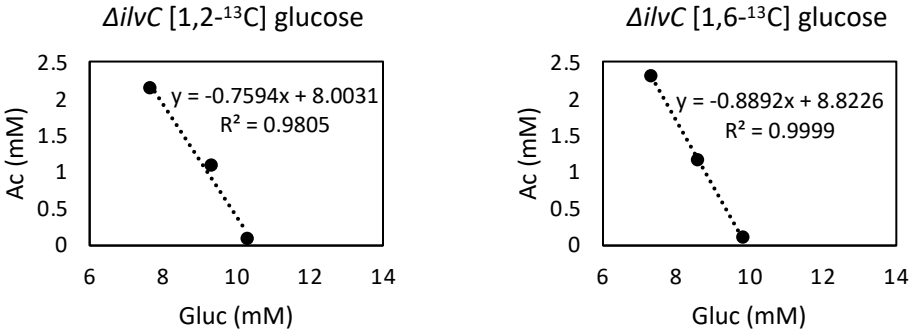

	Slope (mol/mol)	gluc uptake rate (mmol/g_{DW}/h)	acetate secretion (mmol/g_{DW}/h)
Δ*ilvC* [1,2-^{13}C] glucose	-0.8	6.7	5.1
Δ*ilvC* [1,6-^{13}C] glucose	-0.9	5.4	4.8

Figure 2.8 Acetate secretion rate for Δ*ilvC*. The plots show acetate concentration to glucose concentration. The slopes were shown on the plots and the table. The glucose uptake rate was calculated from the previous section. The acetate secretion was the slope times glucose uptake rate.

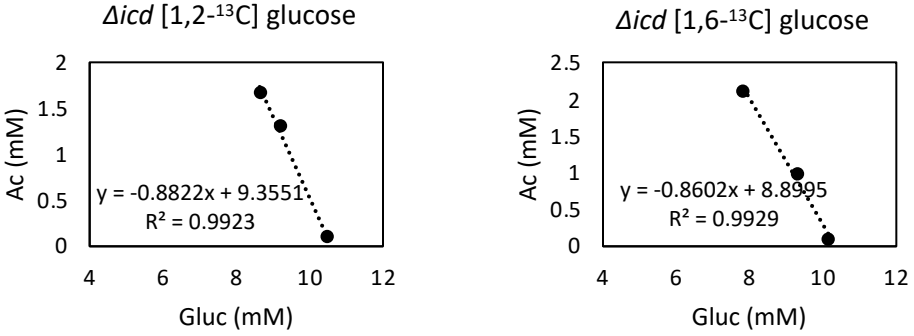

	Slope (mol/mol)	gluc uptake rate (mmol/g_{DW}/h)	acetate secretion (mmol/g_{DW}/h)
Δicd [1,2-^{13}C] glucose	-0.9	6.7	5.9
Δicd [1,6-^{13}C] glucose	-0.9	5.4	4.7

Figure 2.9 Acetate secretion rate for Δ*icd*. The plots show acetate concentration to glucose concentration. The slopes were shown on the plots and the table. The glucose uptake rate was calculated from the previous section. The acetate secretion was the slope times glucose uptake rate.

Chapter 3 ^{13}C Metabolic Flux Analysis Identifies Unexpected Metabolite Exchanges in *E. Coli* Co-Culture

3.1 Abstract

A key characteristic of microbial communities is the cross-feeding of nutrients, termed syntrophy. However, currently there are few methods to identify and quantify such metabolite exchanges. In most studies to date, the exchanging metabolites were assumed based on genomic or transcriptomic information. In this work, we show that by applying ^{13}C metabolic flux analysis (^{13}C MFA) on a syntrophic *E. coli* co-culture, we are capable of not only resolving the individual intracellular fluxes with high precision, but also elucidating and quantifying the rates of exchanged metabolites. Specifically, we have analyzed metabolite exchange in the co-culture of two auxotrophic *E. coli* strains, *Δicd* and *ΔilvC*, using parallel labeling experiments with [1,2-^{13}C] glucose and [1,6-^{13}C] glucose combined with isotopic labeling analysis by GC-MS. We have discovered that the interaction between the syntrophic partners was more complicated than was previously assumed. In addition to amino acid exchange, we show that metabolic pathway intermediates are also exchanged at significant rates. The results from this study provide a more comprehensive view of syntrophic interactions in co-cultures. Moreover, the methods developed in this study can be applied to other types of interactions, or even in multi-culture systems to improve our understanding of microbial communities.

3.2 Introduction

The coexistence of microbes as communities is critical for regulating body functions, coupling element cycle such as carbon (C), nitrogen (N), and phosphorus (P) cycle in the ecosystem (Burgin *et al.*, 2011; Kumar and Chordia, 2017). It is estimated that only 1% of the identified archaea and bacteria can be cultivated and studied under laboratory condition (Pande and Kost, 2017). Most microorganisms in nature are auxotrophs, which means that they lack the key gene(s) to synthesize essential molecule(s) for growth (D'Souza *et al.*, 2014; Mee *et al.*, 2014). Therefore, the cross-feeding of metabolites *i.e.,* syntrophic interactions between microbes is commonly found in microbial communities. The exchanging molecules include electron donors, sugar, organic acid, amino acids, vitamins and other co-factors (Jones, 1967; Rodionova *et al.*, 2015; Zengler and Zaramela, 2018; Fritts, McCully and McKinlay, 2021). In this study, we focus on deciphering syntrophic interactions and tackle the challenge that we currently face.

The exchange of metabolites is a critical part for supporting growth and shaping microbial communities (Mee *et al.*, 2014), but it remains challenging to elucidate the cross-feeding of metabolites due to the dynamic interaction and system complexity (Ponomarova and Patil, 2015). Studies that focus on syntrophic interactions often assume the exchanging metabolites based on the genomic information *i.e.,* the gene knockout. For example, if a microbe has a gene knockout that encodes an enzyme that catalyzed the reaction for the biosynthesis of essential amino acid, it is often assumed that the cross-feeding metabolite is that amino acid (Mee *et al.*, 2014; Pande *et al.*, 2014; Germerodt *et al.*, 2016; Antoniewicz, 2020). In the past decade, genomic, transcriptomic and proteomic information combined with computational models has been developed to provide a more comprehensive analysis (Zuñiga, Zaramela and Zengler, 2017). For examples, flux balance analysis (FBA), dynamic flux balance analysis

(DFBA), community flux balance analysis (cFBA) and other related constraint-based reconstruction and analysis (COBRA) are approaches that combined omic information with a model to predict exchanging metabolites (Khandelwal *et al.*, 2013; Henson and Hanly, 2014; Embree *et al.*, 2015; Zelezniak *et al.*, 2015; Sarkar *et al.*, 2021) However, although flux balance analysis (FBA) serves as one of the most common way so far to decipher microbial interactions (Basile *et al.*, 2020), there are some limitations. First, the accuracy of FBA is limited due to some assumptions such as maximum growth rate (Long *et al.*, 2017; Antoniewicz, 2021) and this could appear even more challenging in a complex system since it requires finding community objective function (Gottstein *et al.*, 2016). Second, FBA usually produces multiple flux solutions when calculating large metabolic network (Antoniewicz, 2021). Therefore, in some examples it can only determine a sets of possible cross-feeding metabolites rather than uncover the actual interactions (Khandelwal *et al.*, 2013; Sarkar *et al.*, 2021). A promising approach to resolve this is by tracing metabolic flow by isotope labeling, which is the most conclusive way to show metabolite exchange (Ponomarova and Patil, 2015; Zuñiga, Zaramela and Zengler, 2017). The major challenge of isotope labeling, however, is to resolve the labeling pattern for a complex system. Therefore, most examples that utilize isotopic analysis are under simplify assumptions (Ponomarova and Patil, 2015; Gottstein *et al.*, 2016). These challenges lead to the goal of this study: develop an effective and reliable method to elucidate syntrophic interactions, specifically on the cross-feeding of metabolites between syntrophic partners.

In this study, I apply ^{13}C metabolic flux analysis (^{13}C MFA) on a syntrophic co-culture to obtain detailed metabolic fluxes and identify exchanging metabolites between syntrophic partners. ^{13}C MFA is a powerful and widely used tool to determine fluxes by model-based analysis and the isotope labeling pattern. This technique does not require optimality assumptions

or model simplification, therefore providing precise flux results (Long and Antoniewicz, 2019a; Antoniewicz, 2020). In the past, ^{13}C MFA was mostly applied in mono-culture, which only provides the intracellular fluxes for a single strain (Crown and Antoniewicz, 2013). In 2015, a new approach was developed for utilizing ^{13}C MFA in a co-culture system. This is the only method so far that does not require physical separation of cells or proteins. It was demonstrated that with proper tracer design and by employing a co-culture model, fluxes within the co-culture system could be resolved (Gebreselassie and Antoniewicz, 2015). In this study, we take a step further to apply ^{13}C MFA to a co-culture system with interactions, specifically syntrophic interactions. We select two *E. coli* knockout strain Δ*ilvC* (valine and isoleucine auxotroph) and Δ*icd* (glutamate auxotroph), which have been previously reported to be syntrophic partners (Wintermute and Silver, 2010), as our model system for this study. We show that ^{13}C MFA is not only capable for predicting fluxes of individual strain in a co-culture system, but also distinguish metabolites that are being exchanged. Interestingly, the result shows that the syntrophic partners are exchanging not only the intuitive metabolites predicted from genomic information, which in our case are amino acids, but also the intermediates along the synthetic pathway. This new finding suggests that syntrophic interaction may be more complicated than we thought: instead of exchanging single metabolite for essential growth, microbes form a more convoluted network for better cooperation.

3.3 Methods

3.3.1 Cell strain

The two strains, Δ*ilvC* and Δ*icd* are knockout strains in amino acid metabolism. The ilvC gene encodes ketol-acid reductoisomerase, which is involved in the biosynthesis of valine and isoleucine. Ketol-acid reductoisomerase catalyzes the reaction of (S)-2-acetolactate (aclact) to 3-

methyl-2-oxobutanoate (kVal) and (S)-2-aceto-2-hydroxybutanoate (acbut) to (3S)-3-methyl-2-oxopentanoate (kIle) for valine and isoleucine biosynthesis, repectively. The icd gene encodes isocitrate dehydrogenase, it catalyzes the reaction of isocitrate to alpha ketoglutarate, which is a precursor for glutamate biosynthesis. Both strains have antibiotic resistance for kanamycin.

3.3.2 Growth condition

The two auxotrophic strains were precultured in 3% of LB Broth Miller, 1mM of glucose and 50µg/L of kanamycin in 10 mL of M9 minimal medium separately overnight before inoculation. For mono-culture, 100µL of cells are inoculated into separate flasks and cultured in 10mL of minimal medium (M9) with 10mM of glucose and 50µg/L of kanamycin in shake flask. For co-culture, we took 100µL from each pre-culture and inoculate into the same shake flask. The optical density (OD) at 600nm was measured by spectrophotometer to obtain the cell growth. For parallel labeling experiments, cells were precultured and inoculated as above. Cells were cultured with either 10mM of [1,2-^{13}C] glucose or 10mM of [1,6-^{13}C] glucose. Cells pellets were collected during mid-exponential growth when the OD_{600} was around 0.7 for further analysis.

3.3.3 Gas chromatography-mass spectrometry and chemical derivatization

Tert-Butyldimethylsilyl ethers (TBDMS) derivatized amino acids sample are prepared and analyzed as previously described. Fatty acid labeling data was determined from acetyl coenzyme A (AcCoA) as described (Long and Antoniewicz, 2019a). The results are integrated by mstool to obtain mass isotopomer distributions (Antoniewicz, Kelleher and Stephanopoulos, 2007a) and corrected for natural abundance (Fernandez *et al.*, 1996)for further analysis

3.3.4 ^{13}C metabolic flux analysis

In order to perform ^{13}C MFA on co-culture, we construct a co-culture metabolic network model. The full metabolic network is provided in Appendix A.2. In brief, for mono-culture model, the model is same as the previous chapter that contains the central metabolism pathway, lumped amino acid biosynthesis and biomass formation for cell growth. Co-culture model includes two compartments that represent individual species. Each compartment has identical metabolic pathways as described in the mono-culture model. The pathway reactions that Δ*ilvC* and Δ*icd* are not able to catalyze are deselected for the first and second compartment, respectively. The exchanging flux(es) is(are) added manually for each test run.

^{13}C MFA is performed by Metran software as previous paper (Gebreselassie and Antoniewicz, 2015). Metran calculations are based on elementary metabolite units (EMU) framework (Antoniewicz, Kelleher and Stephanopoulos, 2007b). Fluxes are estimated by minimizing the sum of squared residual (SSR) between the experimental measured isotopomer distributions and the predicted result. For each model (without/with exchange(s)), we start with a random value for each flux, and reiterate based on the previous result for at least 20 times until no improvement in SSR. This process is repeated at least 15 times to find the global solution. For the result that gives the lowest SSR, we calculate 95% confidence interval for each flux by evaluating the sensitivities of the minimized SSR to flux variation. The flux result is subjected to χ^2 statistical analysis for goodness-of-fit, as described in previous literature (Antoniewicz, Kelleher and Stephanopoulos, 2006).

3.4 Results

3.4.1 Syntrophic growth for two auxotrophic strains.

The growth of Δ*ilvC* and Δ*icd* are shown in Fig 3.1. When cultured alone, both strains show no growth in minimal medium over 48 hours culture, confirming their auxotrophic

phenotype. When we co-culture the two strains together, they show an apparent grow rate 0.062 1/h. This suggests that the two are syntrophic partners, i.e., they secret essential nutrients to support each other.

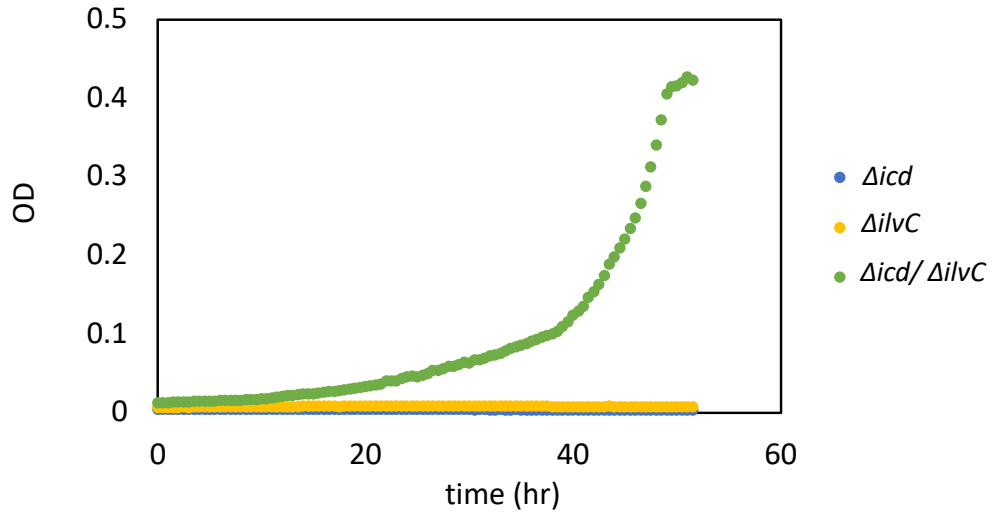

Figure 3.1 Syntrophic growth of Δ*ilvC* and Δ*icd*. Figure shows the growth curve of Δ*ilvC* and Δ*icd* mono-culture and co-culture. Neither auxotrophic strain grows when culture alone in minimal medium M9. Growth is only seen in coculture with growth rate 0.062 1/h.

3.4.2 Parallel labeling experiment and new metabolic models for flux analysis

Parallel labeling experiments for ^{13}C MFA were conducted by replacing non-labeled glucose with [1,2-^{13}C] glucose and [1,6-^{13}C] glucose for cell culture. Cell pellets were collected in mid growth phase when OD value was around 0.7. Metabolites including amino acid, fatty acid, glycogen and RNA were derivatized by corresponding methods (Long and Antoniewicz, 2019a). Isotopic distributions of these metabolites were measured by GC-MS for metabolic flux analysis.

Flux analysis was performed by Metran. Metabolic models with increased complexity were tested for best fit. The initial base model to start with is the mono-culture model, which has only one set of metabolic path way as shown in Fig 3.2 left box. The model includes lumped amino acid synthetic pathway, biomass formation reaction and central carbon metabolism. A

coculture model is shown in Fig 3.2 middle box, which includes another set of identical metabolic path way added to the original model to create a co-culture model. This allows two different metabolisms exist, but no exchange fluxes are present in this model. In the third model shown in Fig 3.2 right box, metabolites exchanges would be added between the co-culture partners. Different combinations of exchanging fluxes were tested to find out the best model that predicts accurate flux distribution to fit the experimental measurement.

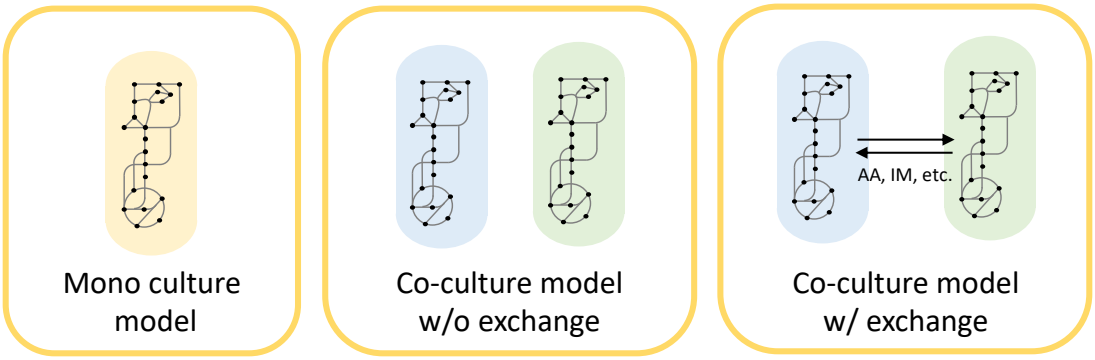

Figure 3.2 Illustrations of models used in ^{13}C Metabolic Flux Analysis. Mono culture model (left): contain one set of metabolic pathways in *E. coli*, including lumped amino acid synthetic pathway, biomass formation reaction and central carbon metabolism such as glycolysis, Entner-Doudoroff pathway, pentose phosphate pathway, TCA cycle and glyoxylate shunt. Co-culture model w/o exchange (middle): contain two identical sets of metabolic pathways same as described in mono-culture. Identical reactions are name with number 1 and 2 to distinguish the two strains. Co-culture model w/ exchange (right): different exchanging flux(es) is(are) added between microbe 1 and 2 with no boundary to allow either direction of cross-feeding. The pathways are deselected for individual strain based on their knockout gene.

3.4.3 ^{13}C metabolic flux analysis with new co-culture metabolic models

The first attempt using mono-culture model resulted in high SSR (Sum of Squared Residuals) around 1.6×10^5, which indicates that one set of metabolisms is not sufficient enough to describe this co-culture system. This result leads to testing the co-culture model with different exchanges. In Fig 3.3, the bars represent the SSR value of different models, which indicate how well each model is able to fit the experimental data. The red dotted line marks the statistically acceptable value calculated as described in previous section which is about 210 in our case. The first attempt with no exchange flux added, as shown in the first bar in Fig 3.3, resulted in SSR

1.25×10^5. The co-culture model fitted better than the mono-culture model, but the poor fit suggested that the model was lacking important interactions. Therefore, metabolite exchanging fluxes were included in the model and tested. We begin with the amino acids that individual strain cannot produce: glutamate, valine and isoleucine. Noted here that in the simulation, the model is not able to distinguish the exchange between glutamate (Glu) and alpha ketoglutarate (AKG); valine (Val) and keto-valine (kVal); isoleucine (Ile) and keto-isoleucine (kIle) since there is no carbon rearrangement. The three additional exchanges lead to a significant improvement in SSR to about 2×10^3. This result shows that adding the direct auxotroph amino acid did not give an acceptable SSR, which indicates that these intuitive amino acids might not be the only exchanging metabolites.

Moving forward, we included additional leucine (Leu), aspartate (Asp) and threonine (Thr) exchanging fluxes, which are the amino acids related to the biosynthesis pathway of the auxotroph amino acids, into the model. We find out that this expanded model did not improve the result as shown in the third bar in Fig 3.3. Therefore, instead of including the related amino acids, we try including the intermediates in the biosynthetic pathway, acetolactate (aclact) and 2-aceto-hydroxybutanoate (acbut) into the model. This attempt significantly improved the SSR value to the magnitude of acceptable range. This suggests that the intermediates are likely to be involved in the exchanging network.

If all the relevant metabolites are included as shown in the fifth bar in Fig 3.3, we are able to obtain the minimal SSR, which is the best fit so far. However, the result does not imply that all the metabolites exchange in this model are valid. In order to determine the exchanging metabolites, we apply two verification steps to eliminate the exchanging flux that is unlikely to be involved. First, we evaluate the flux value and the confidence interval of the predicted

exchange flux. If the predicted flux value is close to 0 with the standard deviation suggest that this flux could be either negative or positive, this exchanging flux could potentially be excluded from the exchanging map. We then took this exchanging flux out of the model and see how that impact SSR value. If there is no significant increase in the SSR value, we conclude that this additional flux is likely not the major exchanging metabolite. Following this principle and the exchange flux map shown in Fig 3.4, threonine (Thr) exchange flux is eliminated. New models without threonine exchange fluxes were testes and confirmed that there is almost no impact when it is removed from the model as shown in the last bar in Fig 3.3. Noted here that aspartate and 2-aceto-hydroxybutanoate exchange fluxes, which both had relatively low exchange fluxes, were tested as well and resulted in unacceptable fit. Taken together, our final exchanging metabolites include the essential amino acid that the cell required: glutamate, valine and isoleucine; the amino acid that are related: leucine and aspartate; and most importantly, the intermediates: acetolactate and 2-aceto-hydroxybutanoate.

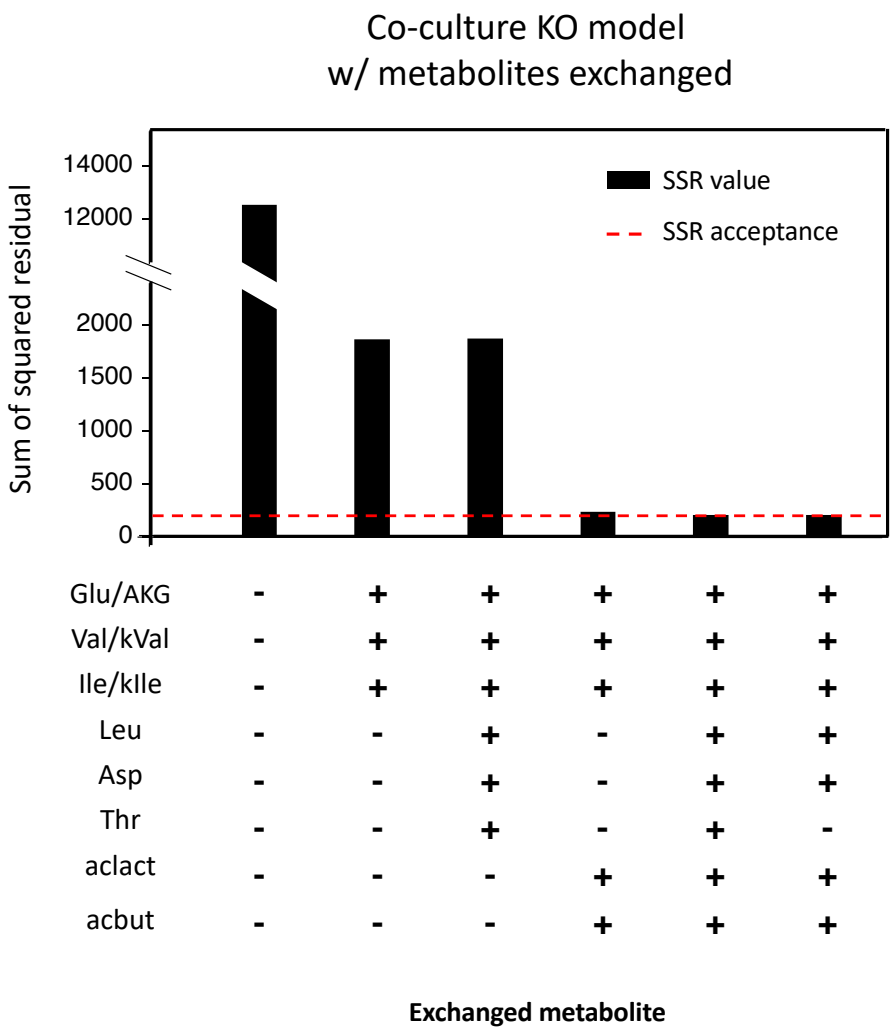

Figure 3.3 Sum of square residual (SSR) of co-culture models with different exchange metabolites. The bars represent the SSR values of each metabolic model, with the red dashed line indicating the threshold for an acceptable SSR. The chart below the bar graph displays the metabolite exchange fluxes included in the metabolic network model for each fit. Glu/AKG: glutamate/alpha-ketoglutarate; Val/kVal: valine/keto-valine; Ile/kIle: isoleucine/keto-isoleucine; Leu: leucine; Asp: aspartate; Thr: threonine; aclact: acetolactate; acbut: 2-aceto-hydroxybutanoate.

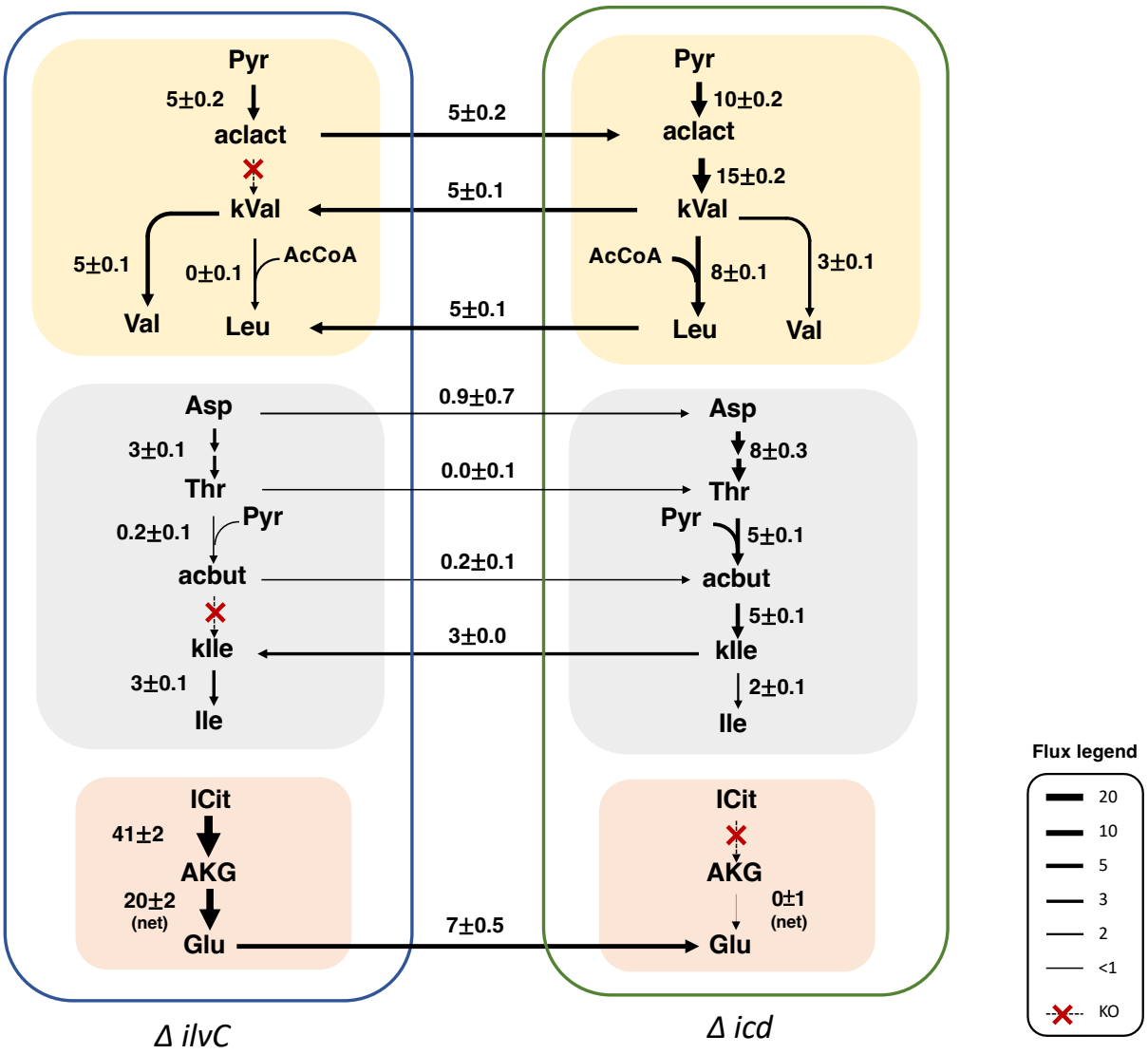

Figure 3.4 Exchange flux map with co-culture model that include all possible exchanges. The exchange flux map when all exchange fluxes are included in the model. Fluxes values are shown with standard deviation. Yellow box (top): Valine/Leucine biosynthesis pathway. Gray box (middle): Isoleucine biosynthesis pathway. Orange box (bottom): Glutamate biosynthesis pathway.

3.4.4 Exchange flux map

The final exchange flux map in Fig 3.5 demonstrates how the two strains overcome the auxotrophy by cross-feeding not only amino acid that they are incapable of synthesizing, but other amino acids and intermediates. For Δ*ilvC* strain, acbut and aclact are cross-fed to Δ*icd*, where the kVal/Val and kIle/Ile are produced and fed back to Δ*ilvC*. The Δ*icd* strain is supported

with Glu cross-fed from Δ*ilvC*. The flux map also shows the exchange of leucine between the two strains, which are unexpected since Δ*icd* is capable of synthesizing leucine and so does Δ*ilvC* with Val/kVal being cross-fed. The exchange of intermediates and metabolites other than the required amino acid glutamate, valine and isoleucine shows that there is a complex metabolic network formed even in a simple co-culture system, suggesting a higher degree of cooperation between microbes than previously expected.

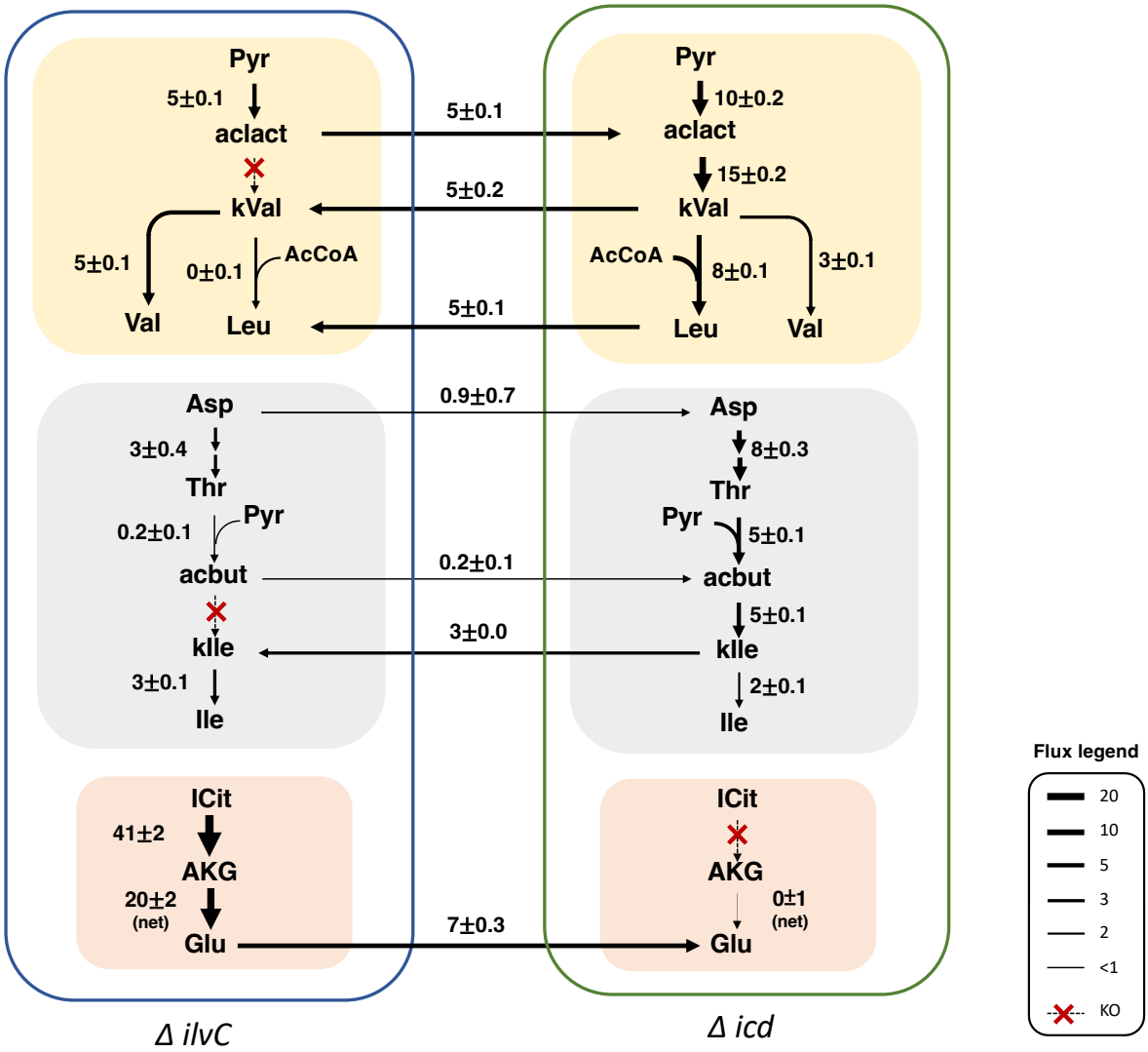

Figure 3.5 Exchange flux map of Δ*ilvC* and Δ*icd* syntrophic co-culture. Fluxes values are shown with standard deviation. Yellow box (top): Valine/Leucine biosynthesis pathway. Gray box (middle: Isoleucine biosynthesis pathway. Orange box (bottom): Glutamate biosynthesis pathway. The exchanging flux map demonstrates how two auxotroph strains form a complicated exchanging cycle to overcome the auxotroph.

3.4.5 Central carbon metabolism

Central carbon metabolism of the two strains is shown in Fig. 3.6 and Fig. 3.7. The Δ*ilvC* strain has a roughly similar flux distribution as the wild type *E. coli* shown in the previous chapter. The main difference is that the TCA cycle flux is significantly higher in Δ*ilvC* due to low acetate secretion. Typically, we observe overflow metabolism for fast growing *E. coli*, which means that the cell use fermentation instead of respiration to generate energy (Basan *et al.*, 2015). Both of our strains were growing slow in co-culture, which is likely the reason that both strains have low acetate secretion. For Δ*icd*, instead of TCA cycle, where the gene knockout is located, the glyoxylate cycle has very high flux. The high flux seems to provide enough oxaloacetate that the reaction from phosphoenolpyruvic acid (PEP) to oxaloacetate (OAC), which is originally the main anaplerotic reaction for replenishing oxaloacetate, is nearly shut down in Δ*icd*. We also observe a high flux from malate (Mal) to pyruvate (Pyr), which might be an overflow from the glyoxylate cycle.

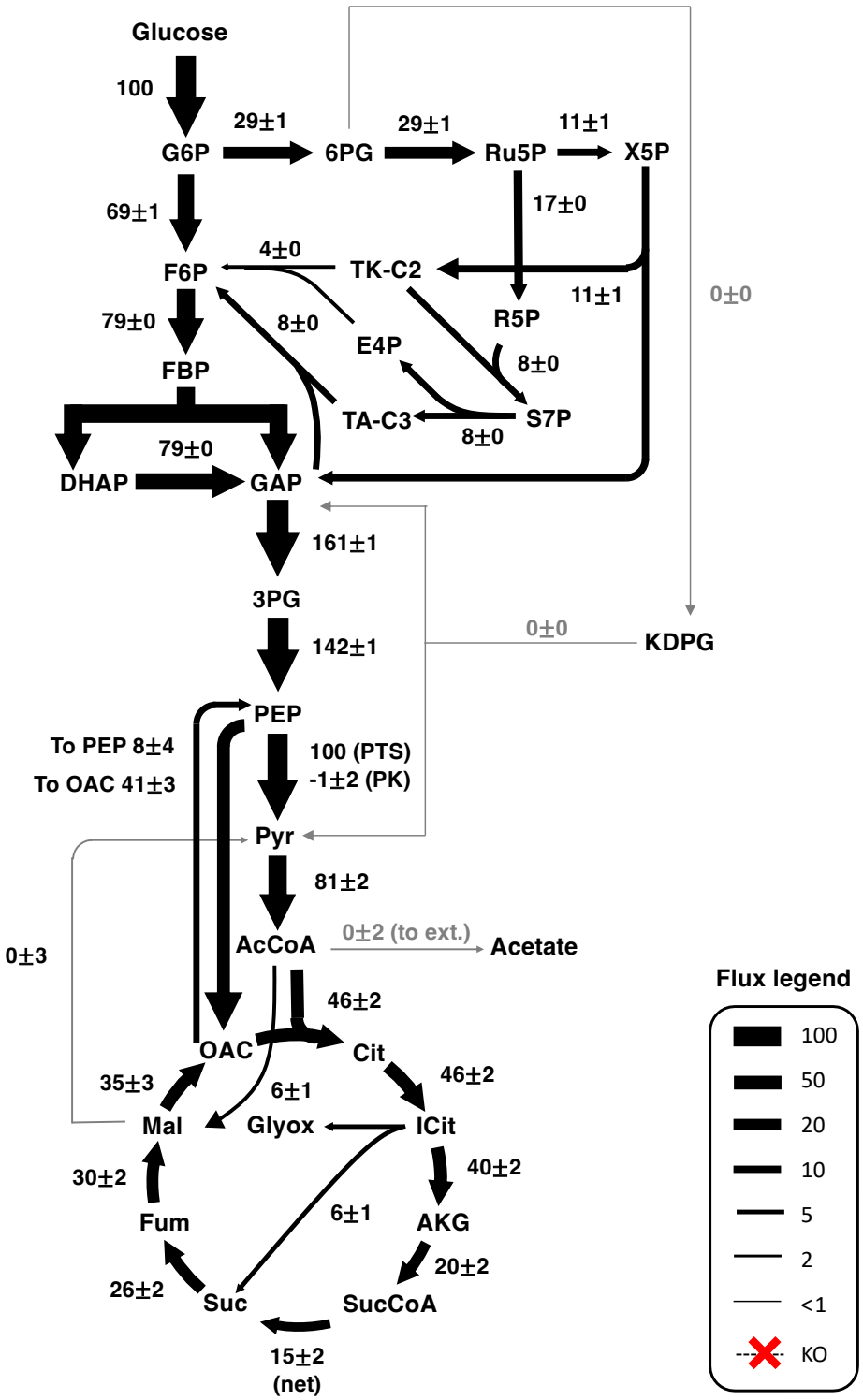

Figure 3.6 Central carbon metabolism flux map of Δ*ilvC* in co-culture. Fluxes are normalized to 100 unit of glucose uptake. Estimated fluxes value are shown with standard deviation. Red cross represents the knockout pathway (Δ*ilvC* knockout not shown). Width of arrows represent the relative value of fluxes.

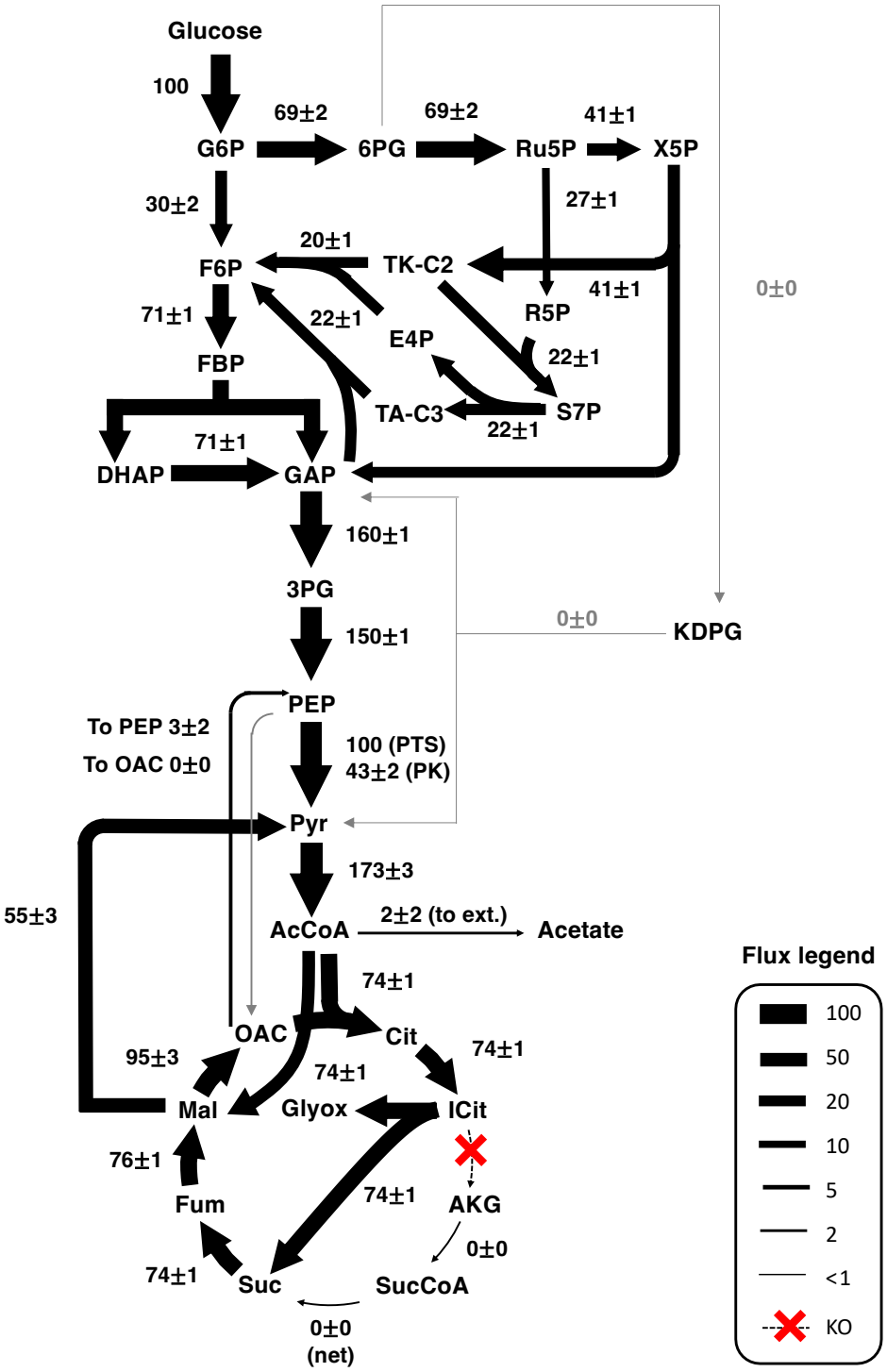

Figure 3.7 Central carbon metabolism flux map of Δ*icd* in co-culture. Fluxes are normalized to 100 unit of glucose uptake. Estimated fluxes value are shown with standard deviation. Red cross represents the knockout pathway. Width of arrows represent the relative value of fluxes.

3.5 Discussion

In this work, we demonstrated how we can apply ^{13}C metabolic flux analysis on an interacting co-culture system to elucidate the cross-feeding metabolites. In this approach, total biomass measurement from the co-culture is sufficient enough to estimate the metabolic fluxes. Co-culture metabolic models with different metabolite exchanges were constructed and tested. We applied statistical analysis to evaluate the performance of each model and which exchange fluxes were critical. We discovered that not only the "expected" amino acids are being exchanged, other amino acid and pathway intermediates also play important part in the exchange flux map. This finding is critical as it sheds light on our understanding of microbial communities. Beside exchanging the required metabolites for survival, the interactions between microbes were found to be more complex than we previously thought.

Although ^{13}C metabolic flux analysis can be a powerful tool to elucidate exchanging metabolites, there are still limitations and challenges that it could face when applying on a more complex system. In our co-culture metabolic flux analysis, statistical analysis provides valuable guidance in identifying which exchange fluxes are critical for fitting our experimental measurements. Specifically, the goodness of fit is quantified by calculating the sum of squared residuals (SSR). However, the SSR value only represents how well the overall model fits the measured data. Therefore, in some cases, we could achieve a statistically acceptable fit with different exchange fluxes combination, even if we removed exchange fluxes from the model that estimated to be present at significant rates.

Taking our co-culture as an example, in Fig. 3.8, the SSR value of more metabolic models with different exchange fluxes combination were shown. The first bar represents the best fit with all the amino acids and intermediates exchange fluxes in the model. We found that

including pyruvate (Pyr) can further reduce the SSR to around 170, as shown in the second bar. Fig. 3.9 demonstrates the exchange flux map when pyruvate exchange flux was included. Followed the same principle described above, we removed threonine and aspartate exchange flux due to both fluxes exhibiting extremely low values, with their standard deviations indicating that they could be zero. When both exchange fluxes were removed from the model, the fit was nearly as good as when they were included, as shown in the third bar. This result shows that addition of pyruvate exchange flux allowed us to further eliminate the aspartate exchange flux with acceptable fit.

Moving forward, we removed more exchange fluxes alongside threonine and aspartate to evaluate the impact of each elimination on the model fit. A rational choice was to remove the 2-aceto-hydroxybutanoate exchange flux, which also had a low exchange flux value similar to threonine and aspartate. This resulted in a statistically acceptable fit, with the SSR increasing by 20, as shown in the fourth bar of Fig. 3.8. However, removing the leucine exchange flux instead of the 2-aceto-hydroxybutanoate exchange flux also yielded an acceptable fit, with the SSR increasing by 35, as shown in the fifth bar. It was unexpected that the model without the leucine exchange could still be statistically acceptable, considering it was always predicted to be exchanged at a significant rate, as shown in Fig. 3.4, 3.5 and 3.9. This serves as a good example that statistical analysis alone is sometimes insufficient to definitively determine which metabolites are being exchanged, as the SSR can only evaluate the overall fitness of the model.

In this case, when pyruvate exchange fluxes were included, we were able to obtain acceptable fit without leucine being exchanged. It is important to keep in mind that there might be some other combination of exchange fluxes that could yield acceptable fit. For these exchange fluxes that could improve the SSR mildly, we do not have a statistically strong argument to keep

or eliminate either exchange fluxes. Therefore, even though pyruvate exchange flux was not included in the main part of this chapter, this does not imply that it was not being exchanged. In the future, collecting additional experimental measurements could potentially resolve the issue by providing more constraints to the simulation. Alternatively, designing new experiments to verify the exchange of metabolites predicted by the flux analysis could also be effective.

On the other hand, in some cases, statistical analysis can provide strong evidence that metabolites are being exchange. For example, the elimination of the acetolactate exchange flux from the model led to a significant increase in SSR, as shown in the sixth bar in Fig. 3.8, which is a solid proof that this intermediate was being exchanged. This also illustrates that the flux value itself does not solely determine its impact on the fit, as the acetolactate exchange flux, having similar value as leucine exchange flux, had a much greater impact on the fit. Taken together, currently, ^{13}C metabolic flux analysis can provide sufficient evidence of critical exchange fluxes through statistical analysis. More experimental works will be required to support the minor exchanging flux between microbes.

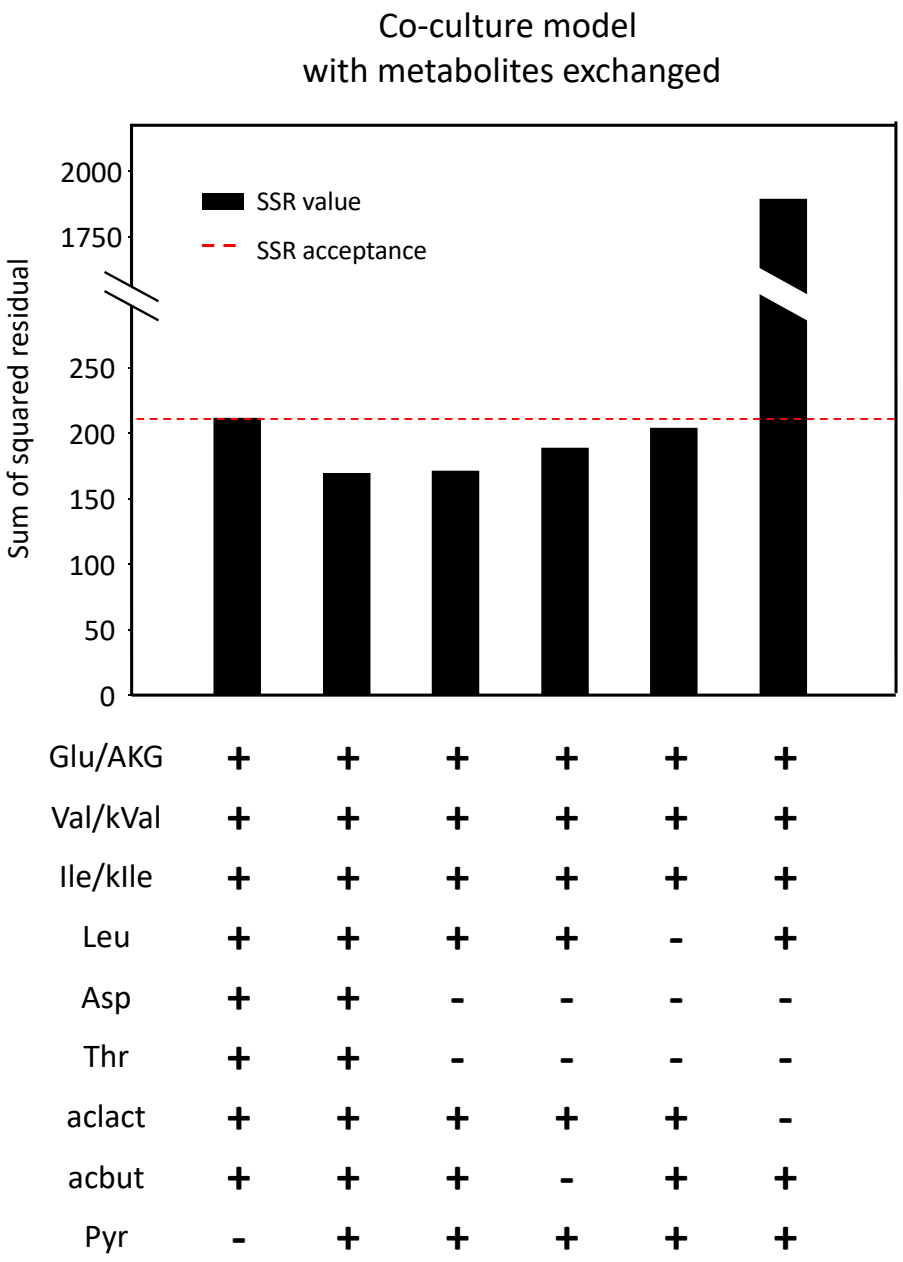

Figure 3.8 Sum of square residual (SSR) for co-culture model with different exchange metabolites combination. The bars represent the SSR values of each metabolic model, with the red dashed line indicating the threshold for acceptable SSR. The chart below the bar graph displays the metabolite exchange fluxes included in the metabolic network model for each fit. Glu/AKG: glutamate/alpha-ketoglutarate; Val/kVal: valine/keto-valine; Ile/kIle: isoleucine/keto-isoleucine; Leu: leucine; Asp: aspartate; Thr: threonine; aclact: acetolactate; acbut: 2-aceto-hydroxybutanoate; Pyr: pyruvate.

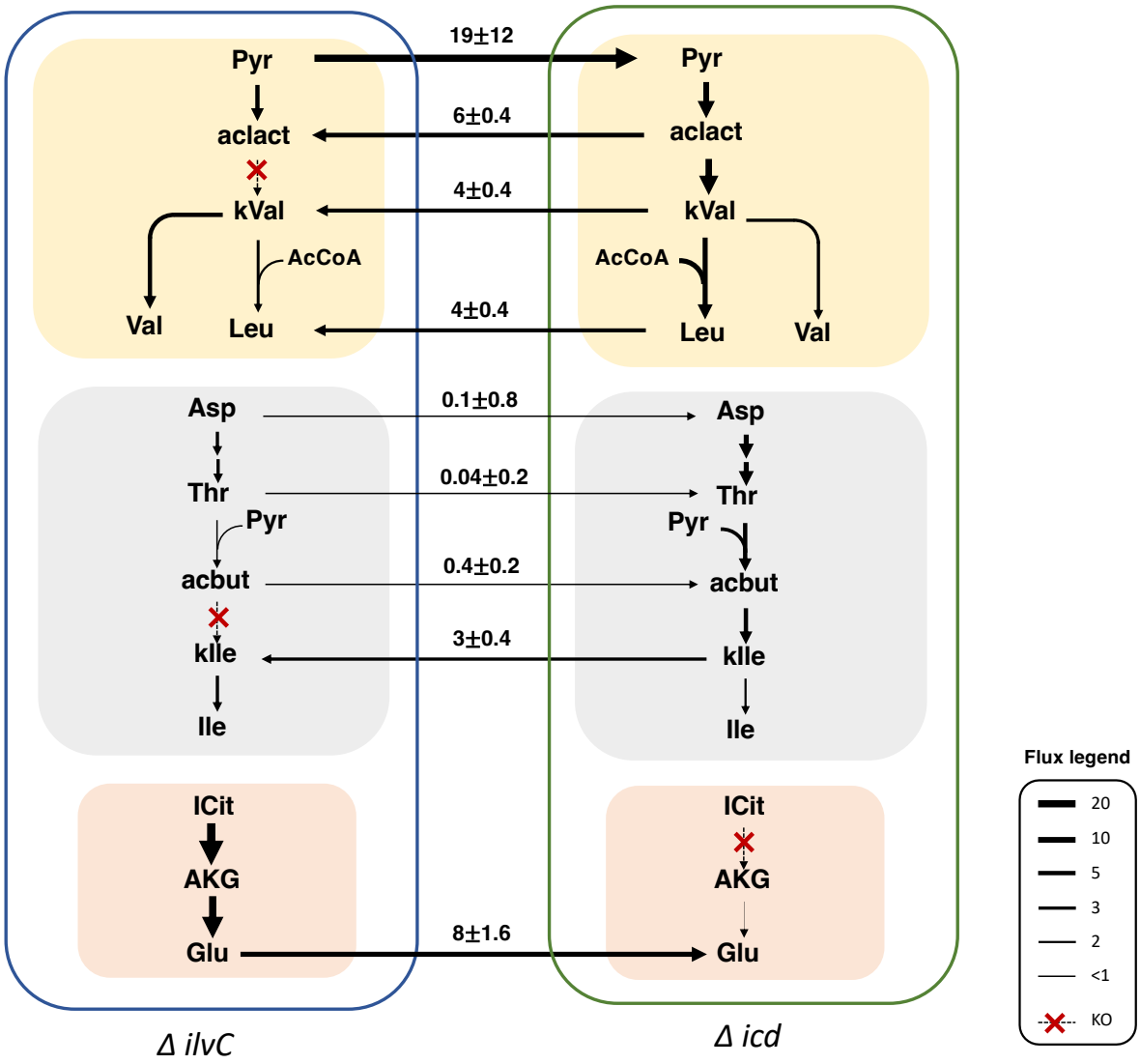

Figure 3.9 Exchange flux map of Δ*ilvC* and Δ*icd* with all amino acids, intermediates and pyruvate exchange fluxes included in the metabolic model. Fluxes values are shown with standard deviation. Yellow box (top): Valine/Leucine biosynthesis pathway. Gray box (middle: Isoleucine biosynthesis pathway. Orange box (bottom): Glutamate biosynthesis pathway.

Another limitation could arise from increased inefficiency as the system becomes more complex. In a typical parallel labeling experiment, where we apply [1,2-^{13}C] glucose and [1,6-^{13}C] glucose, we could obtain 50-100 measurements that are utilized for flux analysis. In an *E. coli* mono-culture metabolic model, which comprises 10-20 independent fluxes, these measurements provide sufficient redundancy to accurately determine the fluxes. In the co-culture model presented in this chapter, the number of measurements remain ample. Theoretically, ^{13}C

metabolic flux analysis could be extended to tri-culture systems or even more complex systems with currently collected measurements. The true challenges, however, lie in the intricate interactions between microbial species. In the co-culture model, we can elucidate the exchanging metabolites by manually incorporating exchange fluxes into the model. However, in more complex systems, the number of possible combinations of exchanging metabolites between each species increases exponentially with the addition of more species. Consequently, numerous models with different exchange combinations must be tested, which can become highly inefficient as the system complexity increases. As a result, a more efficient model network will be required in the future to overcome this limitation.

In summary, in this work, we demonstrate the power of ^{13}C metabolic flux analysis to elucidate the exchanging metabolites in syntrophic co-culture. We discover a more complex exchange network than previously assumed. In most cases where researchers investigated syntrophic interactions, they constructed the community metabolic model based on genomic information. We show that genomic information can be valid, but not comprehensive. Our work improves our understanding for syntrophic partner and can help build more accurate models for future applications.

3.6 Supplementary experiment

3.6.1 Growth verification

In our simulation, we are unable to distinguish the difference between valine and keto-valine exchange flux; isoleucine and keto-isoleucine exchange flux; and glutamate and alpha-ketoglutarate exchange flux. Here we demonstrate that the auxotrophic strain Δ*icd* can grow on either glutamate or alpha-ketoglutarate and Δ*ilvC* can utilize either the amino acid or the keto-forms of them. In Fig. 3.8, the growth rate and final OD of Δ*icd* cultured with glutamate and

alpha-ketoglutarate at different concentration are shown. The growth rate across all conditions is similar, and the final OD is limited by the total concentration of the two metabolites. Δ*icd* appears to have a slight preference for utilizing glutamate, as the group with a higher glutamate concentration grows better under the same total concentration.

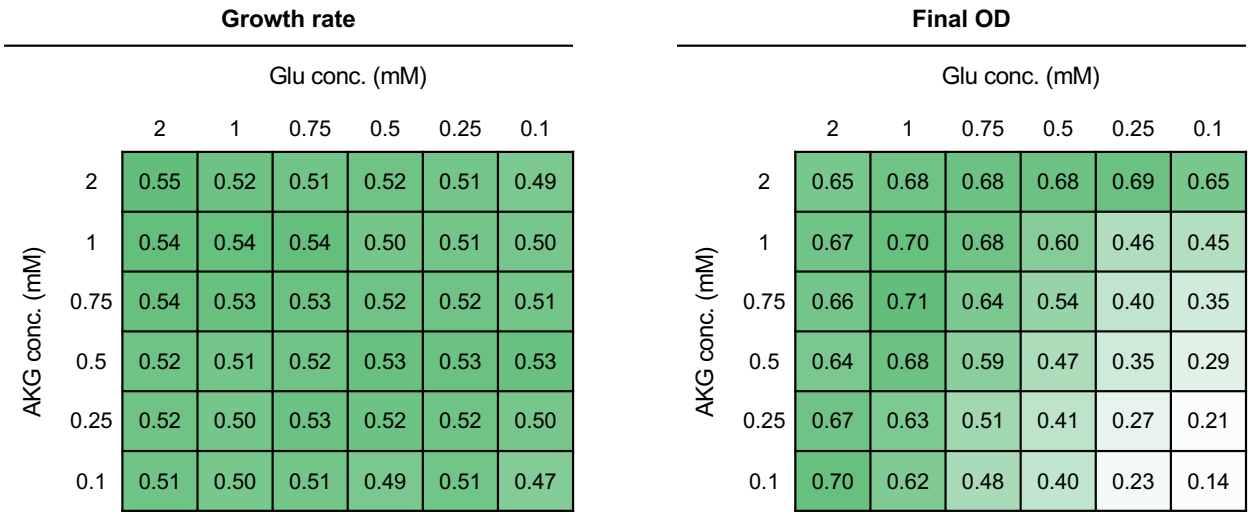

Figure 3.10 Growth rate and final OD of Δ*icd* growing on different concentration of glutamate and alpha-ketoglutarate. The Δ*icd* strains are cultured with glutamate (Glu) and alpha-ketoglutarate (AKG) in 96 well plate and monitored by BioTek Cytation 5. The growth rate and final OD of each condition are shown.

For Δ*ilvC* strain, we supplemented the cells with either valine and isoleucine or their keto-form, resulting in 4 different combinations. In Fig. 3.9, we show the growth rate and final OD of each condition. Overall, the strain can grow on all combinations and does not discriminate between the amino acid and the keto-acid. However, we notice some growth inhibition in the Ile/Val group when isoleucine is at a high concentration and valine is at a low concentration. Such inhibitory interrelationship between branch chain amino acid has been reported in previous literature (Dien, Ravel and Shive, 1954). The inhibition is likely due to the competition of the shared transporter (Guardiola *et al.*, 1974). Similar inhibition effect is observed in the kVal/kIle group as well but not the combination of amino acid/keto-acid group. Currently, there is no known transporter for keto-acid although it was demonstrated here that the cells could indeed

utilize the keto-acid. If the growth inhibition in the kVal/kIle was also due to transporter competition, it is likely that the keto-acids do not share the same transporter with the branch chain amino acids since no inhibition was observed in amino acid/keto-acid group.

Growth rate

Ile conc. (mM) \ Val conc. (mM)	2	1	0.75	0.5	0.25	0.1
2	0.53	0.51	0.40	0.21	0.09	0.04
1	0.52	0.51	0.47	0.41	0.21	0.03
0.75	0.53	0.52	0.50	0.44	0.30	0.07
0.5	0.52	0.54	0.53	0.49	0.28	0.11
0.25	0.53	0.54	0.56	0.56	0.45	0.26
0.1	0.54	0.55	0.55	0.54	0.59	0.38

Ile conc. (mM) \ kVal conc. (mM)	2	1	0.75	0.5	0.25	0.1
2	0.59	0.58	0.57	0.58	0.58	0.53
1	0.58	0.57	0.57	0.61	0.55	0.54
0.75	0.59	0.57	0.59	0.58	0.58	0.47
0.5	0.59	0.57	0.58	0.57	0.56	0.53
0.25	0.61	0.59	0.59	0.60	0.57	0.53
0.1	0.62	0.61	0.59	0.57	0.59	0.54

kIle conc. (mM) \ Val conc. (mM)	2	1	0.75	0.5	0.25	0.1
2	0.57	0.62	0.60	0.59	0.60	0.54
1	0.60	0.63	0.61	0.61	0.61	0.61
0.75	0.60	0.63	0.63	0.63	0.64	0.56
0.5	0.59	0.58	0.62	0.60	0.62	0.59
0.25	0.46	0.48	0.52	0.53	0.53	0.50
0.1	0.49	0.49	0.49	0.43	0.48	0.48

kIle conc. (mM) \ kVal conc. (mM)	2	1	0.75	0.5	0.25	0.1
2	0.56	0.58	0.55	0.52	0.47	0.27
1	0.58	0.58	0.55	0.55	0.56	0.34
0.75	0.60	0.61	0.61	0.60	0.57	0.36
0.5	0.54	0.60	0.61	0.57	0.54	0.44
0.25	0.24	0.43	0.56	0.60	0.55	0.57
0.1	0.10	0.20	0.25	0.32	0.56	0.56

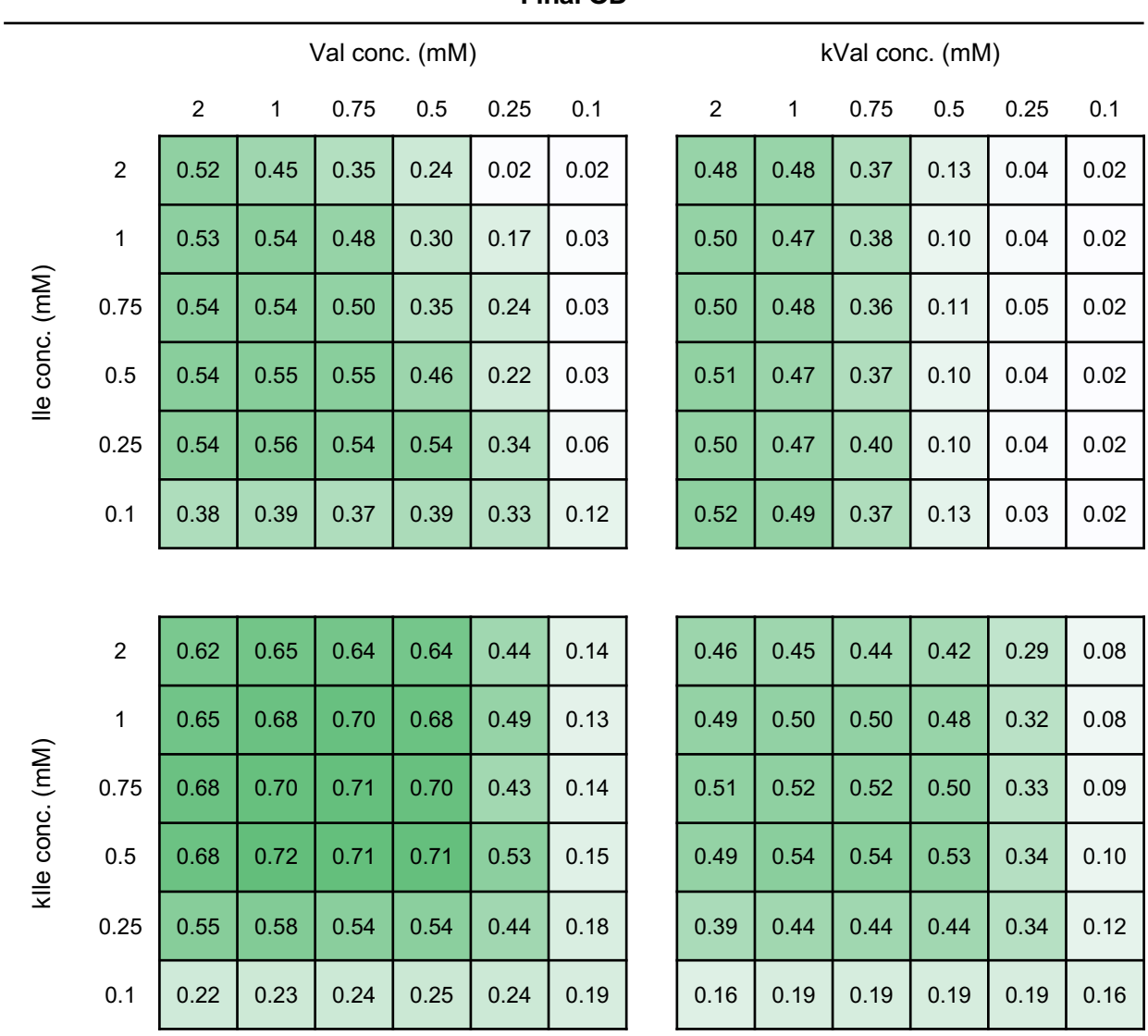

Figure 3.11 Growth rate and final OD of Δ*ilvC* growing on different concentration of valine and isoleucine and their keto-acid. The Δ*ilvC* strains are cultured with either valine (Val) and isoleucine (Ile) or their keto-acid in 96 well plate and monitored by BioTek Cytation 5. The growth rate and final OD of each condition are shown.

3.6.2 Population composition

In this chapter, we demonstrate the ability of ^{13}C metabolic flux analysis to resolve intracellular fluxes in cells and the intercellular fluxes between them. In the co-culture model, we included two sets of metabolic networks in the model. Since total biomass was measured and provided to the simulation, a mixing reaction in the metabolic model network wass required.

Normally, there is no cross-feeding between the two strains in the co-culture, as shown in previous case (Gebreselassie and Antoniewicz, 2015), the two sets of metabolism were calculated independently and combined with an estimated fraction for overall predicted labeling. The overall labeling simulated from the calculation is then fitted to the total biomass measured in the experiment. The estimated fluxes for both strains are normalized to 100 glucose uptake, which represent their relative flux distributions. In our case, however, the two strains are linked with the cross-feeding fluxes. When both strains are normalized to 100 glucose uptake, the inherent assumption is that they have the same total glucose uptake. Noted that the total glucose uptake here represents the glucose uptake of individual cell times their population. If we assume both strains have similar glucose uptake, since there is no mutant in the transporter, the population of the two strains should be roughly 50%: 50% for accurate simulation when we set both uptake to 100 in the model.

To test this, we grew the co-culture at different initial ratio and monitored their population dynamic over time. Three initial ratios were selected: 25%: 75%, 50%: 50% and 75%: 25%. The population was measured by selective plating. In brief, we prepared two different conditioned agar plate: M9 with 2mM of valine and isoleucine, M9 with 2mM of glutamate. The cultures were sampled at different timing on the three plates, where the conditioned plates should only allow one auxotrophic strain to grow and a LB plate can support both strains. Fig. 3.10 demonstrate the population dynamic over time at different inoculation ratio. Noted that the time points are not equally distributed. The three co-cultures, although starts at a different inoculation ratio, eventually stabilized to roughly Δ*ilvC*: Δ*icd* = 40%: 60%. Interestingly, in all cases, Δ*icd* seems to grow a lot faster initially compare to Δ*ilvC*, especially when the initial ratio of Δ*ilvC*: Δ*icd* = 75%: 25%. Based on this result, we confirmed that the

population is overall stable when the inoculation ration is 50%: 50% and the culture can roughly maintain similar population ratio overtime.

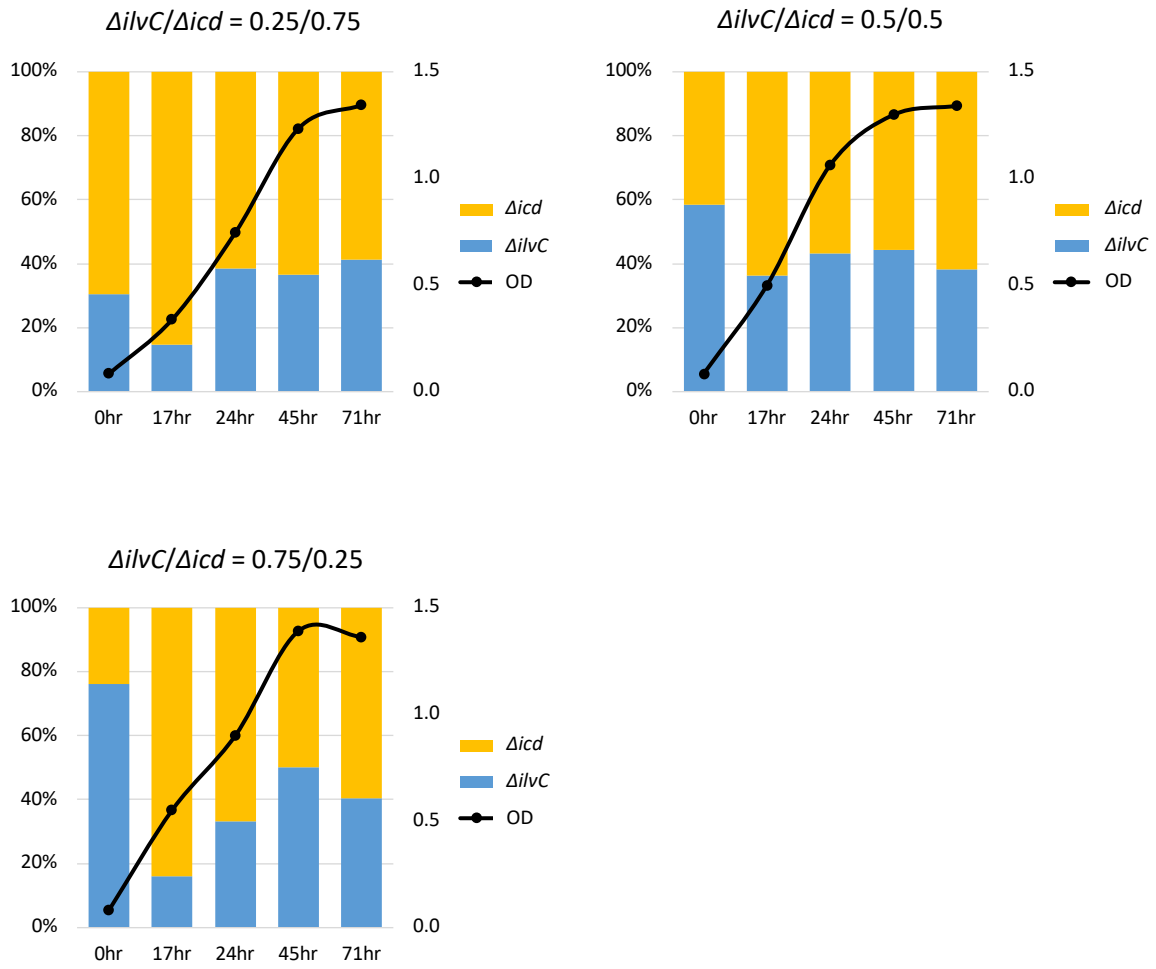

Figure 3.12 Population dynamic of the Δ*ilvC*/Δ*icd* co-culture with different inoculation ratio. The bar graphs show the percentage of each strain, where yellow represent Δ*icd* and blue represent Δ*ilvC*. The OD of the co-cultures are also shown in this graph. Noted that the time points are not equally distributed.

Chapter 4 Cross-feeding of Amino Acid Pathway Intermediates is Common in Co-culture of Auxotrophic *Escherichia coli*

4.1 Abstract

Amino acid auxotrophy refers to an organism's inability to synthesize one or more amino acids that are required for cell growth. In microbiome research, co-cultures of amino acid auxotrophs are often used to investigate metabolite cross-feeding interactions and model community dynamics. Thus far, it has been implicitly assumed that amino acids are cross-fed between these auxotrophs. However, this assumption has not been fully verified. For example, it could be that intermediates of amino acid biosynthesis pathways are exchanged instead, or in addition to amino acids. If true, this would significantly increase the complexity of metabolic interactions that needs to be considered. Here, we show that metabolic pathway intermediates are indeed exchanged in many co-cultures of amino acid auxotrophs. To demonstrate this, we selected 25 *E. coli* single gene knockouts that are auxotrophic for five different amino acids: arginine, histidine, isoleucine, proline, and tryptophan. In co-culture experiments, we paired strains that shared the same amino acid auxotrophy and monitored cell growth. We observed growth in 23 out of 55 strain pairings, indicating that pathway intermediates were exchanged between the strains. To provide further support for cross-feeding of pathway intermediates, auxotrophic *E. coli* strains were cultured in media supplemented with commercially available metabolic pathway intermediates. Supplementing media with many of these metabolites recovered cell growth as was predicted from the co-culture experiments. Taken together, this work demonstrates that exchange of metabolic pathway intermediates is more common than has

been assumed so far. In future, these exchanges must be explicitly considered when constructing models of metabolite cross-feeding interactions in microbial communities and when interpreting results from microbiome studies involving auxotrophic strains.

4.2 Resulting publication

This manuscript is currently submitted to the journal Metabolic Engineering.

4.3 Introduction

Auxotrophy is defined as the inability of an organism to synthesize one or more metabolites that are essential for cell growth. Amino acid auxotrophs are widespread in nature (Mee and Wang, 2012; D'Souza *et al.*, 2014), and have been extensively used in academic research as model systems to study microbial interactions and community dynamics (Wintermute and Silver, 2010; Mee *et al.*, 2014; Germerodt *et al.*, 2016) It is well known that certain *E. coli* amino acid auxotrophs, when paired together in co-cultures, are able to grow in minimal media(Wintermute and Silver, 2010). Thus far, it had been commonly assumed that these strains are able to grow together by cross-feeding amino acids (Antoniewicz, 2020). However, an alternative explanation is that instead of amino acids, metabolic pathway intermediates could be exchanged. If true, then this would require significant revision of our models to describe metabolic interactions in such communities. To date, however, this hypothesis has not been fully explored.

In this study, we therefore investigated if pathway intermediates could be exchanged and how widespread such cross-feeding interactions are for auxotrophic *E. coli* strains. Specifically, we selected 25 *E. coli* single knockout strains that were auxotrophic for five different amino acids: arginine, histidine, isoleucine, proline, and tryptophan. Strains that shared the same amino

acid auxotrophy were paired in co-cultures and growth was monitored. Assuming only amino acids could be exchanged, we expected to observe no growth in any of these co-cultures. However, if growth would be observed, then this would indicate that exchange of metabolic pathway intermediates had occurred. Indeed, we found that nearly half of the co-cultures showed significant growth in minimal medium. To provide additional support for these results, follow up experiments were performed using media supplemented with specific metabolites that were identified as likely to be exchanged. Growth of auxotrophs was recovered as predicted. Taken together, results from this study demonstrate that cross-feeding of metabolic pathway intermediates is common in co-cultures of *E. coli* auxotrophs and that these interactions must be explicitly considered when constructing metabolic interaction models of microbial communities, or when interpreting results from studies involving these auxotrophic strains.

4.4 Methods

4.4.1 Strains and materials

All auxotrophic *E. coli* strains were obtained from the Keio knockout collection (GE Healthcare Dharmacon), which were generated by one-step gene inactivation in *E. coli* K-12 BW25113. Chemicals and M9 minimal medium were purchased from Sigma-Aldrich (St. Louis, MO). The following metabolic pathway intermediates were used: N-acetyl-L-ornithine (Cat# A3626), L-ornithine (Cat# W419001), L-citrulline (Cat# PHR3191), N-acetyl-L-glutamate (Cat# 855642), L-arginino-succinate (Cat# 73097), histidinol (Cat# H6647), keto-isoleucine (Cat# 198978), 2-oxobutanoate (Cat# K0875), and anthranilate (Cat# 10680). All media and stock solutions were sterilized by filtration.

4.4.2 Culture condition

Pre-cultures were grown overnight in M9 medium with 3% LB, 1 mM glucose and 50 μg/L kanamycin at 37°C, and then used to inoculate the experimental cultures. Growth medium for co-cultures and monocultures was M9 medium with 10 mM glucose and 50 μg/L kanamycin. For medium supplementation experiments, additional metabolites were added at 0.1 mM final concentration. All growth experiments were performed in 96-well plates with 200 μL of medium at 37°C and 800 rpm shaking using the BioTek Cytation 5 incubating plate reader. Growth was monitored by measuring OD_{600} every 30 minutes. Co-cultures and monocultures were inoculated with 1 μL of the overnight pre-cultures into 200 μL medium.

4.5 Results

4.5.1 Arginine auxotroph

The Keio *E. coli* knockout collection has six arginine auxotrophs: Δ*argA,* Δ*argB,* Δ*argC,* Δ*argE,* Δ*argG* and Δ*argH* (Fig. 4.1B). All six strains were used in this study for co-culture experiments. There are three other knockout strains in the arginine biosynthesis pathway, Δ*argD,* Δ*argF,* and Δ*argI*, however, these strains are not auxotrophic for arginine and were therefore not used. All 15 pairs of the six auxotrophic strains were co-cultured in duplicate in M9 medium with glucose as the only carbon source. As negative controls, the strains were also inoculated as monocultures. We observed significant growth in 11 out of the 15 co-culture pairs, while no growth was observed in the negative controls. Fig. 4.1A shows the maximum OD_{600} measured during 4-day cultures. The data on the diagonal corresponds to the monoculture controls.

Results from these co-cultures suggested that multiple pathway intermediates must have been exchanged. For example, the fact that Δ*argE* grew in co-cultures with Δ*argA,* Δ*argB* and Δ*argC* suggests that Δ*argE* secreted N-acetyl-L-glutamate-5-semialdehyde and/or N-acetyl-L-

ornithine (highlighted blue in Fig. 4.1B), and that Δ*argA,* Δ*argB* and Δ*argC* secreted either ornithine, citrulline, arginino-succinate or arginine. Since the strain Δ*argG* also grew in co-cultures with Δ*argA,* Δ*argB* and Δ*argC*, suggests that Δ*argG* likely secreted L-ornithine and/or L-citrulline (highlighted yellow in Fig. 1B). This was also supported by the fact that growth was observed in the co-culture between Δ*argE* and Δ*argG*. The strain Δ*argH* grew with all arginine auxotrophic strains except Δ*argG*, indicating that L-arginino-succinate was not likely exchanged between the strains. Moreover, no growth was observed in co-cultures between Δ*argA,* Δ*argB* and Δ*argC*, suggesting that neither N-acetyl-L-glutamate, nor N-acetyl-glutamyl 5-phosphate were exchanged. Taken together, these data suggest that two to four metabolic pathway intermediates must have been exchanged between the *E. coli* arginine auxotrophs.

A

	ΔargA	*ΔargB*	*ΔargC*	*ΔargE*	*ΔargG*	*ΔargH*
ΔargA	0.02	0.02	0.02	0.11	0.19	0.08
ΔargB	0.02	0.04	0.03	0.12	0.15	0.05
ΔargC	0.01	0.02	0.02	0.12	0.17	0.04
ΔargE	0.29	0.22	0.23	0.02	0.16	0.09
ΔargG	0.21	0.17	0.14	0.16	0.01	0.02
ΔargH	0.12	0.12	0.05	0.07	0.02	0.01

B

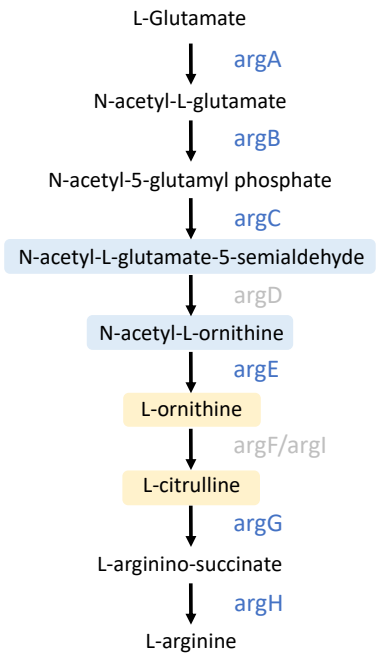

Figure 4.1 Growth of arginine auxotrophic co-culture and arginine biosynthetic pathway. (**A**) Growth of arginine auxotrophic strains in co-cultures in minimal medium. The maximum OD_{600} measured in 96-well plates are shown. The values on the diagonal correspond to maximum OD_{600} measured in monoculture controls. (**B**) Diagram of the arginine biosynthetic pathway. *E. coli* knockout strains Δ*argD,* Δ*argF* and Δ*argI* (genes highlighted in gray font) are not auxotrophic and were not investigated. The most likely metabolic pathway intermediates that were exchanged in co-cultures are highlighted in blue and yellow.

To provide additional support for these results, the auxotrophic strains were next grown in medium containing glucose and specific pathway intermediates. For these experiments, five commercially available pathway intermediates were used, three intermediates that were identified above as likely to be exchanged: N-acetyl-L-ornithine, L-ornithine, and L-citrulline; and two intermediates that were identified above as unlikely to be exchanged: N-acetyl-L-glutamate and L-arginino-succinate. As positive controls, the strains were also grown in medium supplemented with arginine. The results from these experiments are summarized in Fig. 4.2. As expected, N-acetyl-L-ornithine supported the growth of Δ*argA,* Δ*argB* and Δ*argC*; and L-ornithine and L-citrulline supported the growth of Δ*argA,* Δ*argB,* Δ*argC*, and Δ*argE*. Furthermore, neither N-acetyl-L-glutamate, nor L-arginino-succinate supported the growth of any arginine auxotroph, while all strains grew when supplemented with arginine. Taken together, these results confirm that the co-culture experiments correctly identified the specific metabolic pathway intermediates that were exchanged.

	N-acetyl-L-glutamate	N-acetyl-L-ornithine	L-ornithine	L-citrulline	L-arginine-succinate	Arginine
Δ*argA*	0.00	0.28	0.20	0.29	0.03	0.28
Δ*argB*	0.00	0.25	0.18	0.25	0.01	0.26
Δ*argC*	0.00	0.27	0.16	0.26	0.00	0.20
Δ*argE*	0.00	0.00	0.19	0.27	0.02	0.21
Δ*argG*	0.00	0.00	0.02	0.00	0.03	0.24
Δ*argH*	0.00	0.00	0.00	0.00	0.00	0.23

Figure 4.2 Growth of the arginine auxotrophic strains on arginine biosynthesis pathway intermediates. Growth of arginine auxotrophic strains in minimal medium supplemented with one of six different metabolites at 0.1 mM. The maximum OD_{600} measured in 96-well plates cultures are shown.

4.5.2 Histidine auxotroph

Next, seven histidine auxotrophs were investigated: Δ*hisG,* Δ*hisI,* Δ*hisA,* Δ*hisF,* Δ*hisB,* Δ*hisC* and Δ*hisD*. All 21 possible paired combination of co-cultures were performed, as well as monoculture controls, in minimal medium with glucose as the only carbon source. We observed that the only co-cultures that showed significant growth were the ones with Δ*hisD* as the co-culture partner (Fig. 4.3A). HisD is the last enzyme in the histidine biosynthesis pathway that converts histidinol to histidine in two steps (Fig. 4.3B). This result suggests that the most likely metabolic intermediate in the histidine pathway that was exchanged was histidinol (highlighted with blue in Fig. 4.3B).

A

	Δ*hisG*	Δ*hisI*	Δ*hisA*	Δ*hisF*	Δ*hisB*	Δ*hisC*	Δ*hisD*
Δ*hisG*	0.01	0.02	0.02	0.02	0.02	0.02	0.45
Δ*hisI*	0.02	0.01	0.02	0.01	0.01	0.02	0.42
Δ*hisA*	0.02	0.02	0.01	0.01	0.01	0.01	0.53
Δ*hisF*	0.02	0.01	0.01	0.02	0.02	0.02	0.46
Δ*hisB*	0.02	0.01	0.01	0.01	0.01	0.02	0.47
Δ*hisC*	0.01	0.02	0.01	0.01	0.01	0.02	0.60
Δ*hisD*	0.44	0.49	0.52	0.57	0.45	0.60	0.02

B

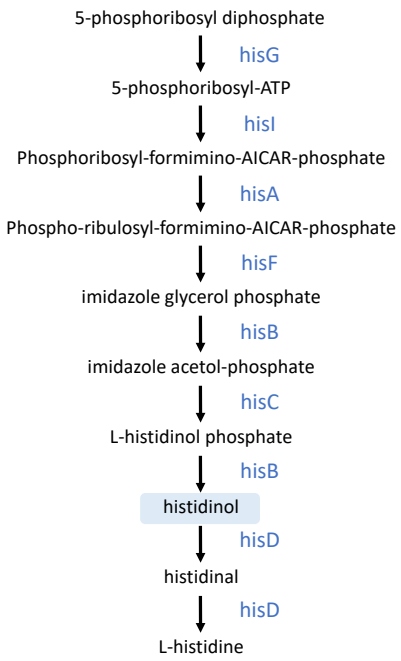

Figure 4.3 Growth of histidine auxotrophic co-culture and histidine biosynthetic pathway. (**A**) Growth of histidine auxotrophic strains in co-cultures in minimal medium. The maximum OD_{600} measured in 96-well plates are shown. The values on the diagonal correspond to maximum OD_{600} measured in monoculture controls. (**B**) Diagram of the histidine biosynthetic pathway. The most likely metabolic pathway intermediate that was exchanged in co-cultures, histidinol, is highlighted in blue.

To provide further support for this result, all seven histidine auxotrophic strains were then grown in medium containing glucose and either histidinol or histidine. As expected, histidinol supported the growth of Δ*hisG,* Δ*hisI,* Δ*hisA,* Δ*hisF,* Δ*hisB,* and Δ*hisC*, but not Δ*hisD*, while histidine supported the growth of all histidine auxotrophs (Fig. 4.4). Because no other metabolites from the histidine biosynthesis pathway were commercially available, we could not determine if other pathway intermediates could also have supported the growth of histidine auxotrophs. Regardless, our results clearly demonstrate that at least one pathway intermediate (i.e. histidinol) was exchanged between histidine auxotrophs.

	Histidinol	Histidine
Δ*hisG*	0.60	0.61
Δ*hisI*	0.57	0.57
Δ*hisA*	0.58	0.58
Δ*hisF*	0.56	0.58
Δ*hisB*	0.55	0.61
Δ*hisC*	0.59	0.61
Δ*hisD*	0.02	0.63

Figure 4.4 Growth of the histidine auxotrophic strains on histidine biosynthesis pathway intermediates. Growth of histidine auxotrophic strains in minimal medium supplemented with either histidinol or histidine at 0.1 mM. The maximum OD_{600} measured in 96-well plates cultures are shown.

4.5.3 Isoleucine and proline auxotrophs

Experiments performed with isoleucine auxotrophs Δ*ilvA*, Δ*ilvC*, Δ*ilvD*, and Δ*ilvE*, and proline auxotrophs Δ*proB*, Δ*proA*, and Δ*proC*, produced similar results as we observed for histidine auxotrophs. Specifically, strains with the knockout at the last gene in the biosynthesis

pathway, i.e., Δ*ilvE* for isoleucine and Δ*proC* for proline, grew with all other auxotrophic strains in the same pathway, while no other co-culture pairs showed significant growth (Fig. 4.5A and 4.5B). These results therefore suggest that for both pathways the last metabolic pathway intermediate was likely exchanged, i.e., keto-isoleucine for isoleucine auxotrophs and glutamate-semialdehyde for proline auxotrophs (Fig. 4.5C and 4.5D).

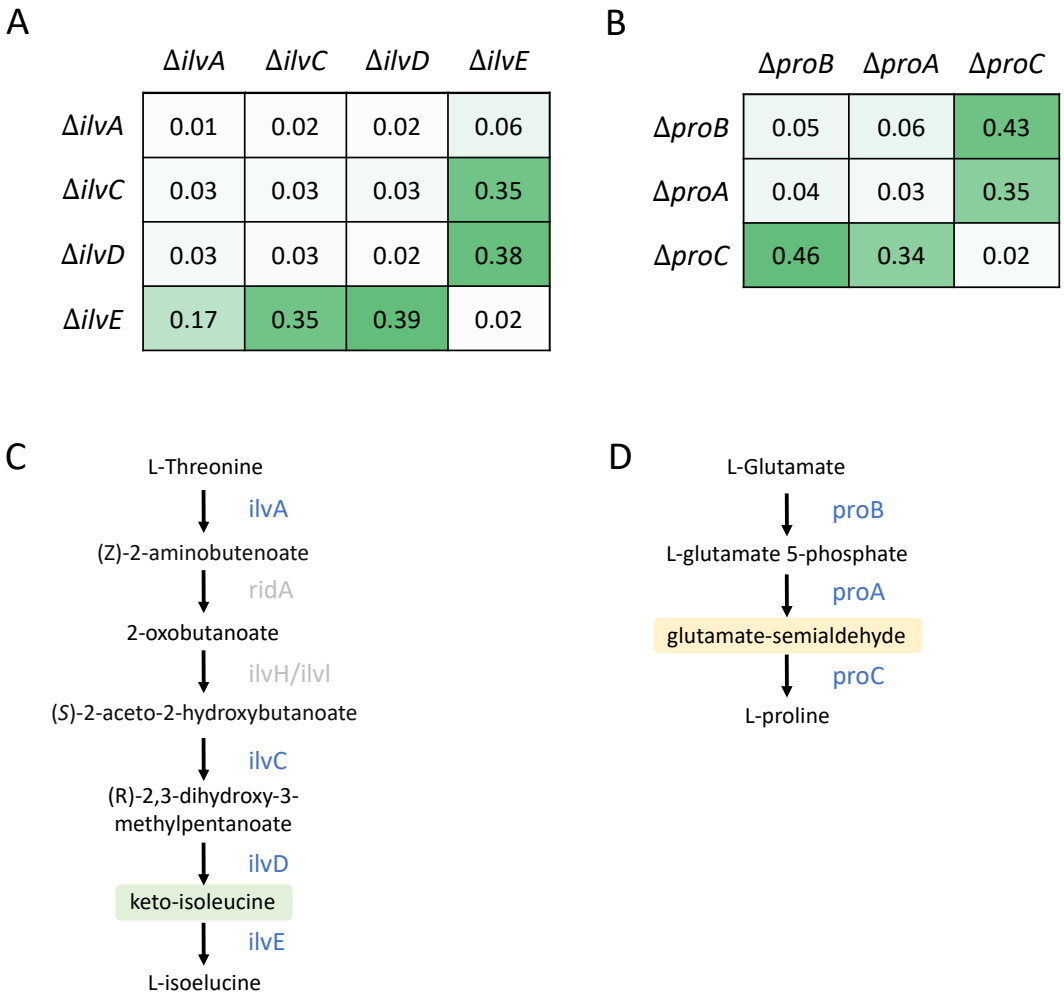

Figure 4.5 Growth of isoleucine auxotrophic co-culture proline auxotrophic co-culture and their biosynthetic pathway. Growth of isoleucine auxotrophic strains (**A**) and proline auxotrophic strains (**B**) in co-cultures in minimal medium. The maximum OD_{600} measured in 96-well plates are shown. The values on the diagonal correspond to maximum OD_{600} measured in monoculture controls. (**C, D**) Diagrams of the isoleucine and proline biosynthetic pathways. *E. coli* knockout strains Δ*ridA,* Δ*ilvH* and Δ*ilvI* (genes highlighted in gray font) are not auxotrophic and were not investigated. The most likely metabolic pathway intermediates that were exchanged in co-cultures, i.e., keto-isoleucine and glutamate-semialdehyde, are highlighted in green and yellow, respectively.

To provide support for the exchange of keto-isoleucine, all four isoleucine auxotrophs were grown in medium containing glucose supplemented with either keto-isoleucine, 2-oxobutanoate (a commercially available intermediate in this pathway), or isoleucine. Growth of the strain Δ*ilvA* was recovered with all three metabolites, while Δ*ilvE* only grew in the presence of isoleucine (Fig. 4.6). Interestingly, no growth was observed for Δ*ilvC* and Δ*ilvD* with any of the three metabolites added. It is known that these two knockout strains are auxotrophic for both leucine and isoleucine. Taken together, these results suggest that in the co-culture experiments where growth was observed (Fig. 4.5A), an additional metabolite from the leucine pathway must also have been exchanged. None of the pathway intermediates in the proline pathway were commercially available, as such, exchange of metabolic intermediates in this pathway could not be further verified.

	2-oxobutanoate	Keto-isoleucine	Isoleucine
Δ*ilvA*	0.17	0.19	0.35
Δ*ilvC*	0.00	0.00	0.00
Δ*ilvD*	0.00	0.00	0.00
Δ*ilvE*	0.00	0.00	0.25

Figure 4.6 Growth of the isoleucine auxotrophic strains on isoleucine biosynthesis pathway intermediates. Growth of isoleucine auxotrophic strains in minimal medium supplemented with either 2-oxobutanoate, keto-isoleucine, or isoleucine at 0.1 mM. The maximum OD_{600} measured in 96-well plates cultures are shown.

4.5.4 Tryptophan auxotroph

Finally, five tryptophan auxotrophic strains were investigated: Δ*trpE,* Δ*trpD,* Δ*trpC,* Δ*trpA* and Δ*trpB*. In this case, growth was observed only in one out of 10 co-cultures,

specifically, the in co-culture between Δ*trpE* and Δ*trpC* (Fig 4.7A). Given that no growth was observed in the co-culture between Δ*trpE* and Δ*trpD* suggests that the most likely pathway intermediate that was exchanged was anthranilate (highlighted in blue in Fig 4.7B). To verify this, all five tryptophan auxotrophs were grown in medium containing glucose supplemented with either anthranilate or tryptophan. As expected, anthranilate supplementation supported the growth of Δ*trpE* and all tryptophan auxotrophs grew when supplemented with tryptophan (Fig. 4.8).

A

	ΔtrpE	*ΔtrpD*	*ΔtrpC*	*ΔtrpA*	*ΔtrpB*
ΔtrpE	0.02	0.06	0.55	0.02	0.02
ΔtrpD	0.07	0.03	0.05	0.02	0.05
ΔtrpC	0.51	0.02	0.01	0.02	0.01
ΔtrpA	0.02	0.05	0.04	0.01	0.05
ΔtrpB	0.01	0.02	0.01	0.01	0.01

B

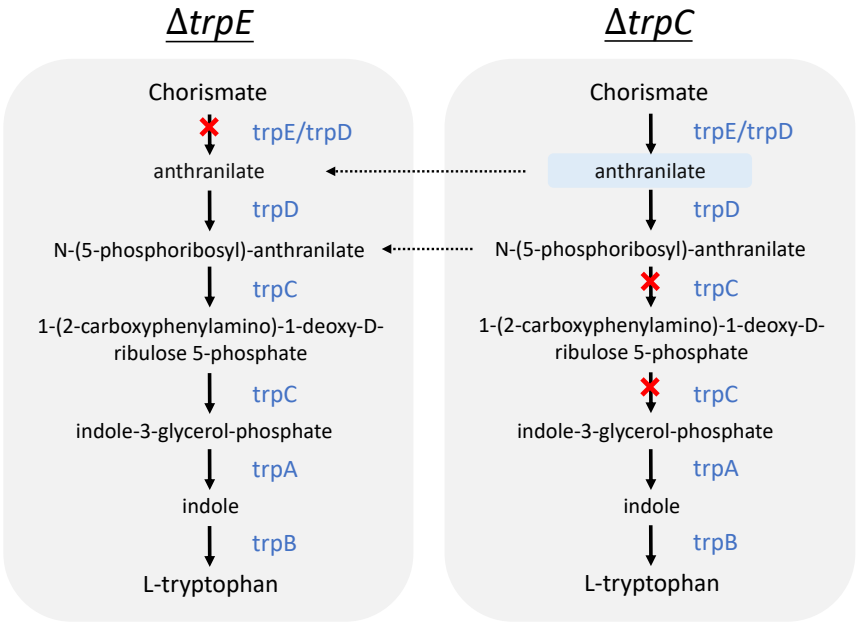

Figure 4.7 Growth of tryptophan auxotrophic co-culture and tryptophan biosynthetic pathway. (**A**) Growth of histidine auxotrophic strains in co-cultures in minimal medium. The maximum OD_{600} measured in 96-well plates are shown. The values on the diagonal correspond to maximum OD_{600} measured in monoculture controls. (**B**) Diagram of the histidine biosynthetic pathway. The most likely metabolic pathway intermediate that was exchanged in co-cultures, histidinol, is highlighted in blue.

Figure 4.8 Growth of the tryptophan auxotrophic strains on tryptophan biosynthesis pathway intermediates. Growth of tryptophan auxotrophic strains in minimal medium supplemented with either anthranilate or tryptophan at 0.1 mM. The maximum OD_{600} measured in 96-well plates cultures are shown.

4.6 Discussion

Rational design of microbial communities for metabolic engineering and medical applications will require a fundamental understanding how interactions between community members give rise to complex community behaviors such as population dynamics, stability, resistance to invasion and other emergent properties (Zhang *et al.*, 2015; Liu *et al.*, 2018; Lawson *et al.*, 2019; Müller *et al.*, 2023). Interactions between community members can involve both cell signaling interactions and exchange of metabolites. Thus far, it has proven challenging to construct predictive models of microbial communities that formally consider metabolite cross-feeding interactions, even for simple co-cultures consisting of two microbial strains (Antoniewicz, 2020). Instead, most computational models used to simulate population dynamics use empirical so-called cooperation parameters that are supposed to capture the net effect of all interactions (Wintermute and Silver, 2010; Mee *et al.*, 2014). One important reason for the lack of more mechanistic models based on metabolite cross-feeding interactions is the fact that it is experimentally difficult to identify which metabolites are exchanged between strains (Shoaie *et*

al., 2013; Kumar *et al.*, 2019). Moreover, tools for measuring the rates of these cross-feeding fluxes are underdeveloped (Gebreselassie and Antoniewicz, 2015; Wolfsberg, Long and Antoniewicz, 2018; Antoniewicz, 2020).

In many studies, auxotrophic strains have been used to construct synthetic communities where community members rely on each other to supply the missing nutrient. *E. coli* amino acid auxotrophs, in particular, have been widely used in the past, since it is well known that some of these strains can support each other's growth (Wintermute and Silver, 2010). The basic assumption has been that the strains complement each other by exchanging amino acids. However, several important questions remain unanswered. For example, it is still unknown why only certain combinations of auxotrophic strains can support each other's growth (Wintermute and Silver, 2010). If amino acid exchange is indeed so common, then many more combinations of auxotrophic strains would be expected to grow in minimal media. One possible explanation is that other metabolites are primarily exchanged. In this study, we tested if metabolic intermediates of amino acid biosynthesis pathways could be exchanged between *E. coli* auxotrophic strains. For this, we selected 25 amino acid knockout strains that were auxotrophic for five different amino acids. By pairing strains that shared the same amino acid auxotrophy and observing growth we clearly demonstrated that metabolites other than amino acids must be exchanged. We observed growth in nearly half of the co-cultures (i.e. 23 out of 55). These experiments also allowed us to pinpoint the most likely metabolic pathway intermediates that were exchanged. To verify these predictions, additional experiments were conducted using media supplemented with the identified intermediates (if commercially available). In total, we identified eight metabolic pathway intermediates that were likely exchanged between *E. coli* strains and verified six of these using follow-up experiments.

Many questions still remain that should be investigated in future work. For example, it would be valuable to identify how metabolic intermediates are transferred between strains. Given that these are large and charged molecules, transport via membrane diffusion is unlikely. It is possible that amino acid transporters are involved in the transport of some of these metabolites. For example, L-ornithine has been reported to share the same transporter as arginine and lysine (Wissenbach *et al.*, 1995) , although specific transporters for pathway intermediates have also been identified (Zhang *et al.*, 2015). Second, future investigation should determine how many of these metabolic intermediates are cross-fed in other microbial communities (Harcombe *et al.*, 2014). In this study, we used auxotrophic *E. coli* knockout strains since these are easily available through the Keio knockout collection and many studies have used *E. coli* knockout strains in the past (Long and Antoniewicz, 2014a, 2019b). It is possible that the metabolite cross-feeding interactions uncovered here are specific to the *E. coli* knockout strains. While many strains in natural communities are also amino acid auxotrophs, their metabolism has co-evolved for thousands, or millions of years (Long and Antoniewicz, 2018), and it is possible that other, perhaps more efficient, cross-feeding interactions have emerged in the process. To test this, it would be, for example, interesting to co-evolve *E. coli* auxotrophs and investigate if additional cross-feeding interactions emerge through evolution.

In summary, in this work we have demonstrated that exchange of metabolic pathway intermediates is more common than has been assumed so far. We argue that in future work these metabolite exchanges must be explicitly considered when constructing models of cross-feeding interactions and interpreting results from microbiome studies involving auxotrophic strains.

Chapter 5 Overexpression of Fluorescent Proteins in *Escherichia Coli* Has Negligible Impact on Cell Physiology and Metabolism

5.1 Abstract

Fluorescent proteins are widely used in metabolic engineering for a range of applications, including as visual reporters to provide easily measured data for strain selection. In microbiome studies, fluorescent proteins are also used to track growth of multiple strains and quantify population compositions. Despite the broad usage of fluorescent proteins, overexpression of heterologous proteins could add a metabolic burden on the host cell and alter cell physiology and metabolism. Until now, few studies have focused on quantifying this effect. To address this knowledge gap, in this study, we characterized the metabolic burden of fluorescent protein overexpression in *E. coli*. Specifically, we selected five common fluorescent proteins that were then overexpressed in wild-type *Escherichia coli*: CFP, Crimson, GFP, Tomato and YFP. To quantify metabolic burden, we measured cell growth physiology, biomass composition, and metabolic flux phenotypes and compared them to wild-type *E. coli*. Overall, we found only slight decreases in growth rates for most strains overexpressing fluorescent proteins. Biomass composition analysis showed negligible impact on macromolecular composition, and little or no impact on amino acid and fatty acid distributions. Finally, using ^{13}C metabolic flux analysis we quantified precise metabolic fluxes for all strains. Our results indicated that there was no significant flux rewiring compared to wild-type *E. coli*. Taken together, this study demonstrates that overexpression of fluorescent proteins in *E. coli* has negligible impact on cell physiology and metabolism.

5.2 Introduction

Fluorescent proteins have emerged as pivotal tools since the first discovery of green fluorescent protein (GFP) in 1962 by Shimomura et al. (Shimomura, Johnson and Saiga, 1962), followed by the heterologous expression of GFP in cells 30 years later (Chalfie *et al.*, 1994). One of the major applications of fluorescent proteins is as a reporter to study gene expression or as a fusion protein to locate targeted protein (Feilmeier *et al.*, 2000; Soboleski, Oaks and Halford, 2005). Another popular application in ecology is as a marker to track microbial populations (Leff and Leff, 1996; Scott *et al.*, 1998; Gandhi *et al.*, 2001). Over the past decades, fluorescent proteins have become an invaluable tool for visualizing and tracking various biological processes within living cells and organisms.

Despite board applications of fluorescent proteins, the expression of foreign proteins can impose metabolic stress on the host cell (Glick, 1995; Mattanovich *et al.*, 2004). The production of heterologous proteins can divert resources and energy from normal cellular processes, thereby impacting cell physiology. Several studies have found that recombinant protein production can altered cell physiology and metabolism such as decreased growth rate, lower biomass yield and redirected metabolic fluxes (Silva, Queiroz and Domingues, 2012; Carneiro, Ferreira and Rocha, 2013). Factors attributing to these negative effects include competition of translational and transcriptional resources, toxicity of heterologous proteins, overaccumulation of metabolite intermediates due to host cell lacking immediate regulatory mechanisms for recombinant protein (Chou, 2007; Cardinale and Arkin, 2012; Borkowski *et al.*, 2016). Many of these studies, however, have focused on the recombinant proteins related to desired industrial product production. To date, only a few studies investigated the potential metabolic burden imposed by fluorescent proteins.

In previous studies, it has been shown that GFP plasmid has insignificant impact on cell growth on bacteria such as *Escherichia coli* and *Salmonella* (Bloemberg *et al.*, 1997; Dandie, Thomas and McClure, 2001; Ma, Zhang and Doyle, 2011). In a more recent study, the metabolic burden of GFP overexpression in four different *Escherichia coli* strains was investigated (Matsuyama *et al.*, 2024). Metabolomic analysis reveals that the GFP overexpression led to shortages of nucleic acids and amino acids. The study further indicated that the impact was strain-dependent, with the BL21star-GFP strain, which had the highest level of GFP expression, exhibiting the most significant changes in its metabolomic profile. In this chapter, we aim to investigate several commonly used fluorescent proteins and apply ^{13}C metabolic flux analysis to assess the metabolic state of the recombinant cells.

To this end, we choose five common fluorescent proteins created by M. Barbier et al. (Barbier and Damron, 2016) and use wild type *E. coli* as host cell. The chosen fluorescent proteins cover a board spectrum including eCFP, E2-Crimson, GFPmut3, tdTomato and eYFP. Cell physiology, including growth rate, acetate secretion and biomass yield, with or without plasmid were analyzed. Moreover, we measured metabolic fluxes of each strain in order to obtain the metabolic response. Metabolic Flux Analysis (MFA) can provide the detailed information such as the distribution of resources in the cell (Wu *et al.*, 2016), enzyme activity in various metabolic pathway and the overall metabolic state (Stephanopoulos, 1999). MFA has been applied in similar studies that analyzed the metabolic burden projected to engineered strains (Rozkov *et al.*, 2004; Wang *et al.*, 2006). In this study, we applied ^{13}C Metabolic Flux Analysis (^{13}C MFA) to precisely quantify fluxes in the living cell. Overall, we aim to provide complementary analysis of fluorescence cells metabolism and expand our understanding for future research.

5.3 Methods

5.3.1 Cell strains and plasmid

Wild type *Escherichia coli* was used for this study. The five fluorescence plasmids we chose were sourced from a set of rainbow plasmids created by M. Barbier et al. (Barbier and Damron, 2016). The plasmids that were used include pUCP20T-eCFP, pUCP20T-E2Crimson, pUCP20T-gfpmut3, pUCP20T-tdTomato and PUCP20T-eYFP. pUCP20T plasmids have antibiotic resistance to ampicillin and is a high copy plasmid (West *et al.*, 1994).

For the rest of this article, WT refers to the original wild type *E. coli* strain that does not carry fluorescence plasmid; and CFP, Crimson, GFP, Tomato and YFP represents the wild type *E. coli* strain harboring corresponding fluorescence plasmids.

5.3.2 Competent cell preparation

Cells were pre-cultured overnight before preparing competent cells. 250µL of the pre culture was inoculated to 50mL of fresh medium and grown for 2-3 hours until OD reached 0.5. Centrifuge the 50mL of the culture at maximum speed for 10 minutes and discard the supernatant. Keep everything on ice or below 4°C after the previous step. Resuspend the cells in 15mL of $CaCl_2$ by pipetting. $CaCl_2$ solution is prepared by dissolving 1.1g of $CaCl_2$ in 100mL of DI water. Leave the resuspended cells on ice for at least 4 hours. Centrifuge the cell and discard the supernatant. Resuspend the cells in 4mL of $CaCl_2$ solution with 15% of glycerol. The prepared competent cells can be used immediately or stored in -80°C.

5.3.3 Plasmid transformation

Plasmid transformation was done by using heat shock method. In short, we mix 20µL of competent *E. coli* with 2µL of fluorescence plasmid solution by gently flicking the Eppendorf

tube. The mixture was left on ice for 10 minutes and placed at 42°C for 45 seconds. After the heat shock step, the cells were left on ice for another 2 minutes and recovered by incubating at 37°C for 1 hour with 200μL of LB. Strains with successful plasmid transformation were selected by plating the culture on agar plates with carbenicillin.

5.3.4 Growth condition

All strains were cultured in minimal medium (M9) with 10mM of glucose as carbon source. Strains with fluorescence plasmids were cultured with additional 50μg/L carbenicillin. OD 600 measured by spectrophotometer was used to calculate the specific growth rate. For the labeling experiments, [1,2-^{13}C] glucose or [1,6-^{13}C] glucose was used in parallel instead of unlabeled glucose. Cells pellets were collected in mid-exponential growth phase for GC-MS analysis.

5.3.5 Fluorescent measurement

Cell growth and fluorescence signal for WT *E. coli* with/without plasmid were monitored by BioTek Cytation 5. The 6 strains were cultured in the medium described above, placed in 96 well plate and shake under the highest speed of the instrument. Excitation and emission wavelengths were setup based on the sourced paper (Barbier and Damron, 2016). OD 600 and the five fluorescence signals were measured every 30 minutes.

5.3.6 Gas chromatography-mass spectrometry

Cell pellets collected from the labeling experiments were derivatized as described in previous paper (Long and Antoniewicz, 2019a). In short, samples are prepared in three ways for different metabolites: hydrolysis of protein and TBDMS derivatization for amino acid, methyl ester derivatization for fatty acid, hydrolysis of glycogen and RNA followed by propionic

anhydride derivatization for glucose and ribose. We integrated peaks of measured metabolites and their isotopomers by mstool to obtain mass isotopomers distribution, and corrected for natural isotope abundances (Fernandez *et al.*, 1996).

5.3.7 ^{13}C metabolic flux analysis

The metabolic model for ^{13}C MFA is listed in Appendix A.1. Reactions include central carbon metabolism, lumped amino acid biosynthesis and biomass formation. Flux analysis was calculated by software Metran which is based on elementary metabolites framework (EMU) framework developed in 2007 (Antoniewicz, Kelleher and Stephanopoulos, 2007b). For each run performed by metran, fluxes were estimated by minimizing the sum of squared residuals (SSR) between the measured and stimulated mass isotopomer distributions and external rate, i.e., acetate production rate. We start the first run with random initial value, and reiterate at least 20 times based on the estimated fluxes from pervious run until there is no improvement in SSR. This cycle was repeated for at least 10 times to obtain global minimal SSR. For the result that gave the lowest SSR, we calculated 95% confidence interval for each flux by evaluating the sensitivities of the minimized SSR to flux variation. The results were subjected to χ^2 statistical analysis for goodness-of-fit, as described in previous literature (Antoniewicz, Kelleher and Stephanopoulos, 2006).

5.3.8 Biomass composition

The methods for determining biomass composition are described in previous paper (Long and Antoniewicz, 2014b). Briefly, cell pellets collected from labeling experiment were mixed 1:1 with the standard biomass. Here, standard biomass was generated by growing cells in fully labeled glucose. Cells were collected to create identical aliquot (1mL, OD_{600} = 1.0) as standard.

The mixtures of sample and standard were derivatized following the steps described above for amino acids, fatty acids, glycogen and RNA. Mass isotopomer distributions measured by GC-MS corresponds to the ratio of our samples to standard, and can be used to calculate sample biomass composition. The composition of the fully labeled standard was measured with chemical standard. Here, we used the data from pervious paper (Long *et al.*, 2016).

For amino acid distribution, 16 amino acids were quantified by the method described above. Arginine, cysteine and tryptophan degrade during the hydrolysis process and histidine fragment has low ion count for providing reliable calculation, therefore the four amino acids were eliminated in the calculation. When calculating the total protein composition, the four amino acids content were estimated from previous literature (Long *et al.*, 2016). We combined the pool of asparagine and aspartate (represent as Asx) and glutamine and glutamate (represent as Glx) due to the deamination of asparagine and glutamine to aspartate and glutamate, respectively, during the hydrolysis of biomass

5.4 Results

5.4.1 Cell growth and fluorescence

Growth and fluorescence signal of wild type (WT) *E. coli* and five fluorescent strains were monitored by BioTek Cytation 5. The fluorescence strains CFP, Crimson, GFP, Tomato and YFP are compared with WT in Fig. 5.1. The left column shows the growth in units of OD600, and the middle column presents the growth on a logarithmic scale. The right column shows the fluorescence signal detected by our instrument. The fluorescence signal is measured with respective excitation/emission wavelengths reported by sourcing literature (Barbier and Damron, 2016).

WT was fully grown in shorter time due to slightly higher inoculation. All fluorescence strains were able to grow with antibiotic added, indicating successful plasmid transformation. The fluorescence signal of fluorescent strains increased with the growth of the cells, while WT only had background noise under all excitation/emission settings. We noticed that the fluorescence signal continued to increase after the cells entered stationary phase. This phenomenon, where cells can still overexpress recombinant protein during stationary phase, had been reported by previous literature (Ou *et al.*, 2004).

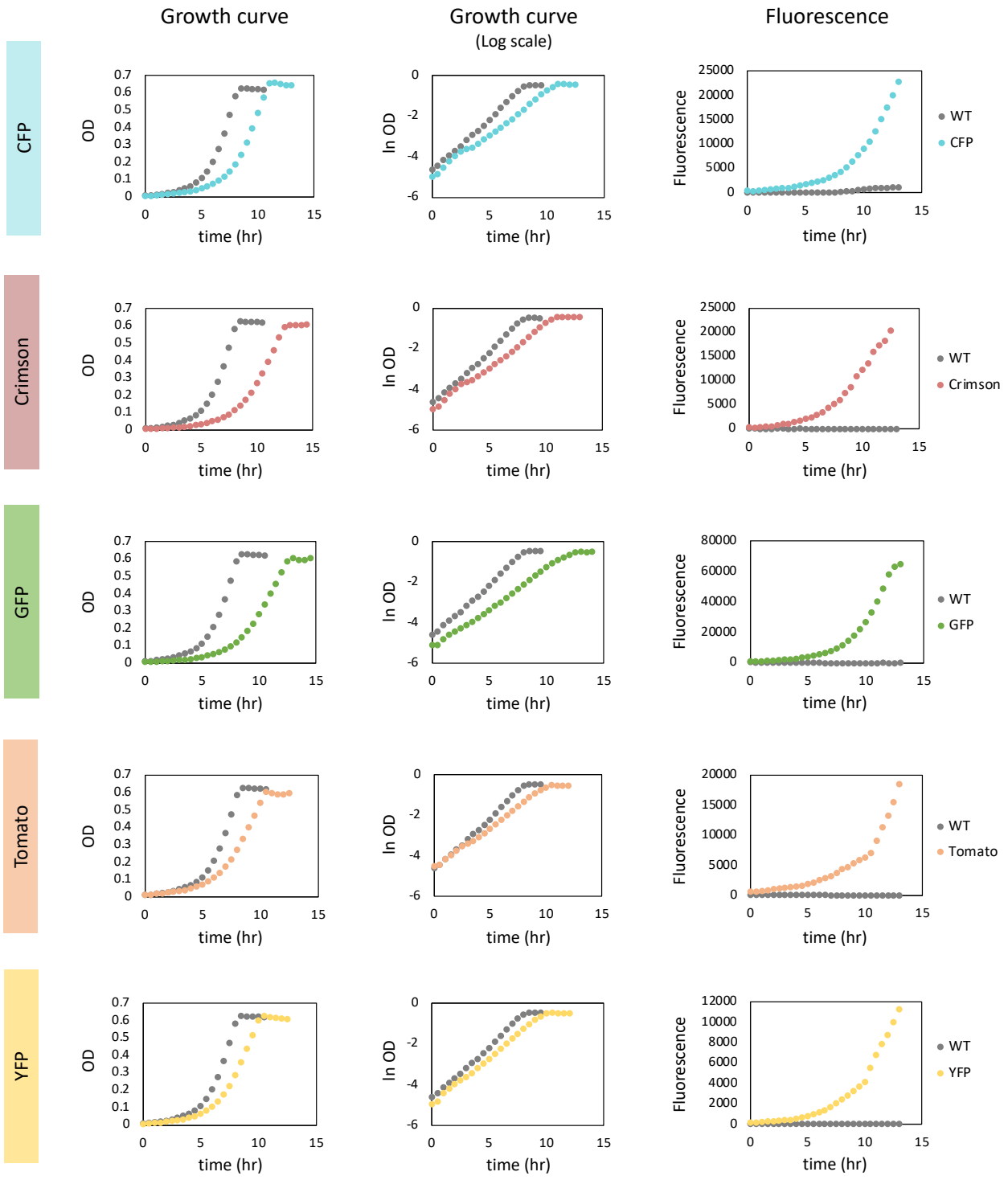

Figure 5.1 The growth and fluorescence signal of wild type and fluorescent strains CFP, Crimson, GFP, Tomato and YFP. The growth and fluorescent signal are monitored by BioTek Cytation 5. The left column is the growth curve with the units of OD600. The middle column is shown with logarithmic scale. The right column shows the fluorescence signal overtime. The grey dots represent the wild type *E. coli* and color dots represent the fluorescent strains.

Growth rate was calculated by taking natural logarithm of the OD_{600} measurement. Fig. 5.2 shows the growth rate for WT *E. coli* and the fluorescence strains. Each strain has two bars with the left one representing the 96 well plate culture and the right one representing flask culture. In either type of culture, most of the fluorescence strains displayed lower growth rates compared to the WT strain. We observed -13% to -28% change in growth rate in the 96 well plate culture and 5% to -22% in flask culture. In both cultures, YFP was the least effected strain and Crimson was the most effected strain, which showed over 20% decrease in growth rate in both cultures.

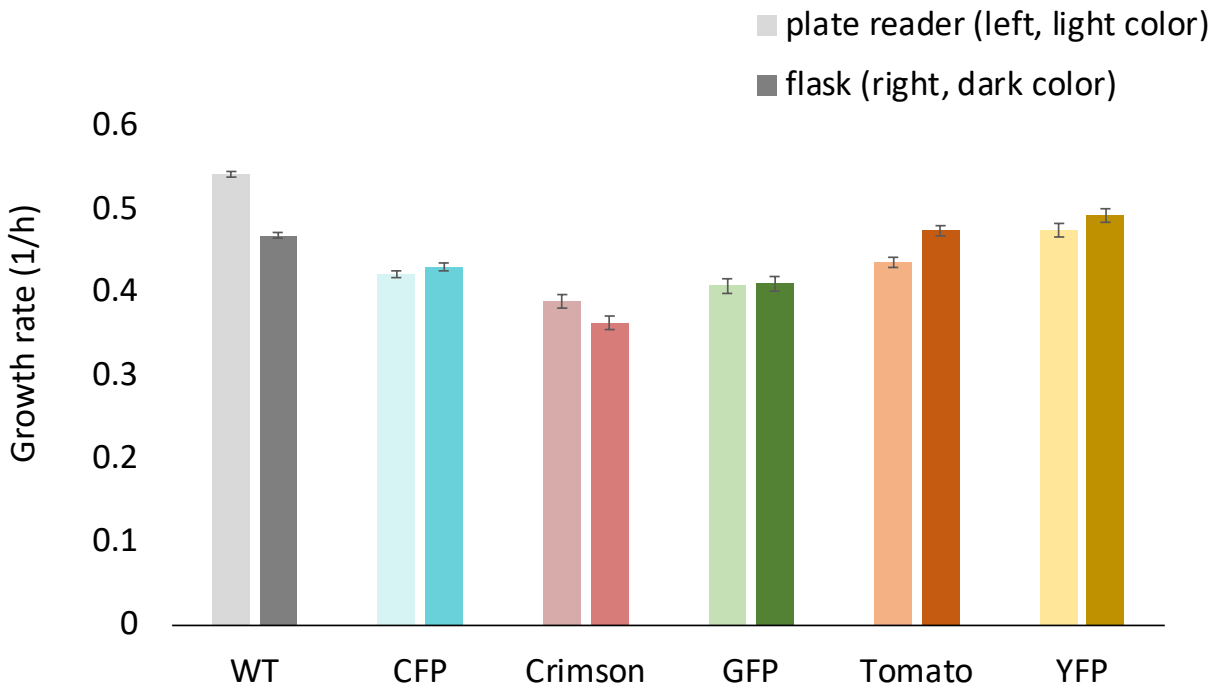

Figure 5.2 Growth rate of wild type and fluorescent strains CFP, Crimson, GFP, Tomato and YFP. Here we show the growth rate of all strains. Each strain has two bars representing the growth rate measured by plate reader from 96 well plate cultures (left, light color) or by photometer from flask cultures (right, dark color). Growth rates are consistent between the two methods. WT has slightly higher growth rate compared to most of the strains. Crimson strain has the most decrease of all the fluorescence strains. Error bar for plate reader represents the standard deviation of the measured growth rate (n=3) and for flask represents the highest and lowest value of the measured growth rate (n=2).

5.4.2 Biomass composition

Biomass composition for all strains is shown in Fig. 5.3. We measured 4 major biomass components including protein, lipid, RNA and glycogen. Protein content did not vary much between WT and the fluorescence strains and between the five fluorescence strains. On the other hand, the Crimson and YFP strain had slightly higher lipid content compared to WT (1.2% and 1.1% difference, respectively). For RNA and glycogen content, CFP and Crimson strain had lower RNA content comparing to WT strain (1.3% and 2.2% difference, respectively) while having higher glycogen content (0.9% and 1.1% difference, respectively). Overall, there were no major differences between WT and the fluorescence strains in biomass composition.

Figure 5.3 The contents of four major macromolecules: protein, lipid, RNA and glycogen of wild type and fluorescent strains. The four major biomass contents were measured and shown in % dry weight. The biomass composition does not vary much (less than 2% difference for all four biomass contents) with or without fluorescence plasmid overexpressing in the cell. Error bar represents the highest and lowest value of the measured biomass composition (n=2).

Amino acid distribution for each strain is shown in Fig. 5.4. The distribution is normalized to mmol/g protein. We did not observe significant differences in amino acid distribution between WT and fluorescence strains. Fig. 5.5. shows the fatty acid distribution. C14:0 and C18:0 fatty acid content was consistent between all strains. Fluorescent strains appeared to have a slightly higher C16:1 fatty acid content and a lower C18:1 fatty acid content compared to the wild-type strain. Previous studies characterizing the physiological responses of *E. coli* knockout strains have reported a positive correlation between C18:1 content and cell growth (Long *et al.*, 2016). This finding is consistent with our observation that the fluorescent strains, which exhibited a lower growth rate, also showed a reduced C18:1 content. For C16:0, only Crimson and GFP were slightly lower comparing to WT, while other fluorescence strains had similar level as WT. Altogether, the detailed biomass contents, i.e., amino acid and fatty acid distributions, did not vary much whether there was fluorescence plasmid or not.

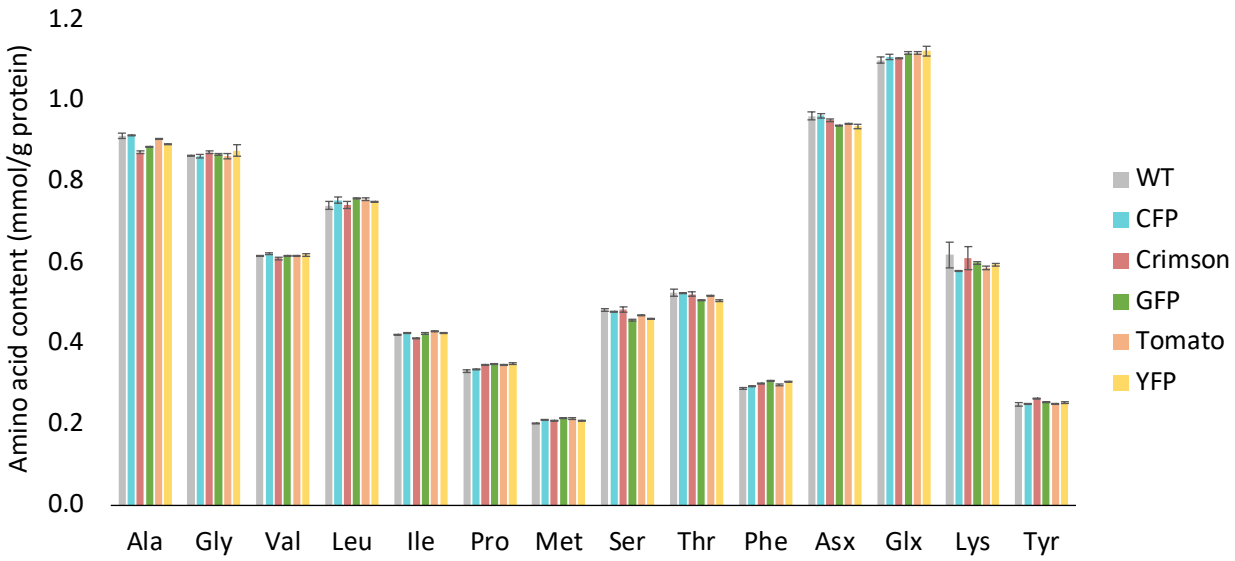

Figure 5.4 Amino acid distribution of wild type and fluorescent strains. Amino acid contents are normalized to mmol/g protein. Asx represents the combined pool of asparagine and aspartate. Glx represents the combined pool of glutamine and glutamate. Arginine, cysteine, tryptophan and histidine are not shown due to measurement limitation. Overall, the amino acid distribution is consistent between all strain. Error bar represents the highest and lowest value of the amino acid content (n=2).

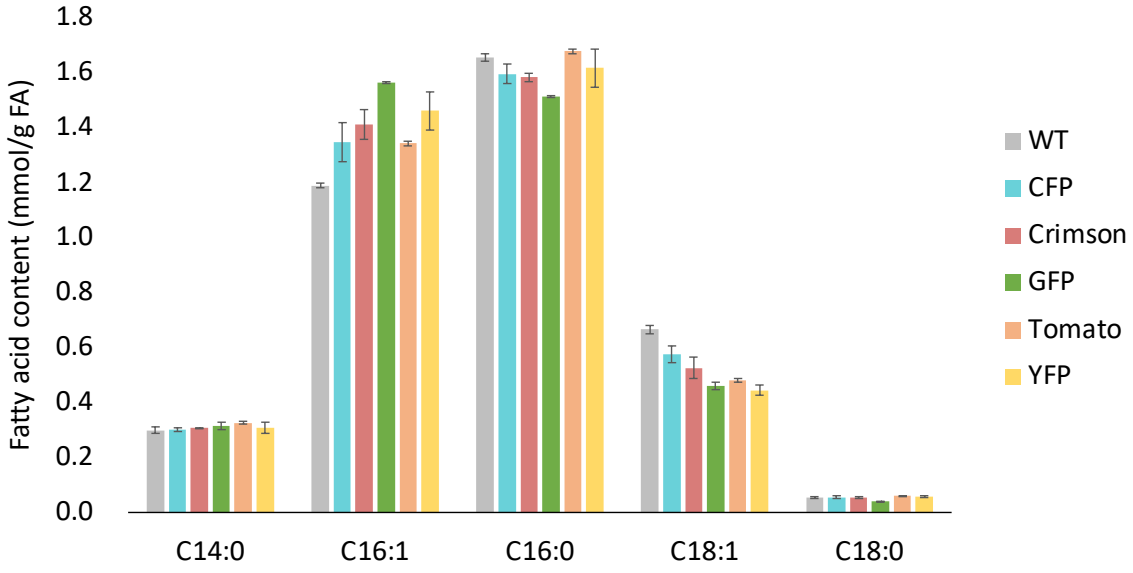

Figure 5.5 Fatty acid distribution of wild type and fluorescent strains. Fatty acid contents are normalized to mmol/g fatty acid. Fluorescence strain has slightly higher C16:1 fatty acid content while slightly lower in C18:1 fatty acid. Other fatty acids stay consistent with or without fluorescence plasmid. Error bar represents the highest and lowest value of the fatty acid content (n=2).

5.4.3 ^{13}C metabolic flux analysis

We further investigated the metabolic state of each strain by performing ^{13}C Metabolic Flux Analysis. Fig. 5.6 shows the independent fluxes in central metabolism including glycolysis, Entner-Doudoroff Pathway, pentose phosphate pathway, TCA cycle, the main anaplerotic reaction and glyoxylate shunt. Fluxes were normalized to 100 glucose uptake. The wild type *E. coli* fluxes distribution agreed with previous study (Long and Antoniewicz, 2019b). The fluorescence strains had similar fluxes as WT strain even though the growth rate appeared to be

lower in some strains. Overall, we did not observe significant flux rewiring between WT strain and fluorescence strains.

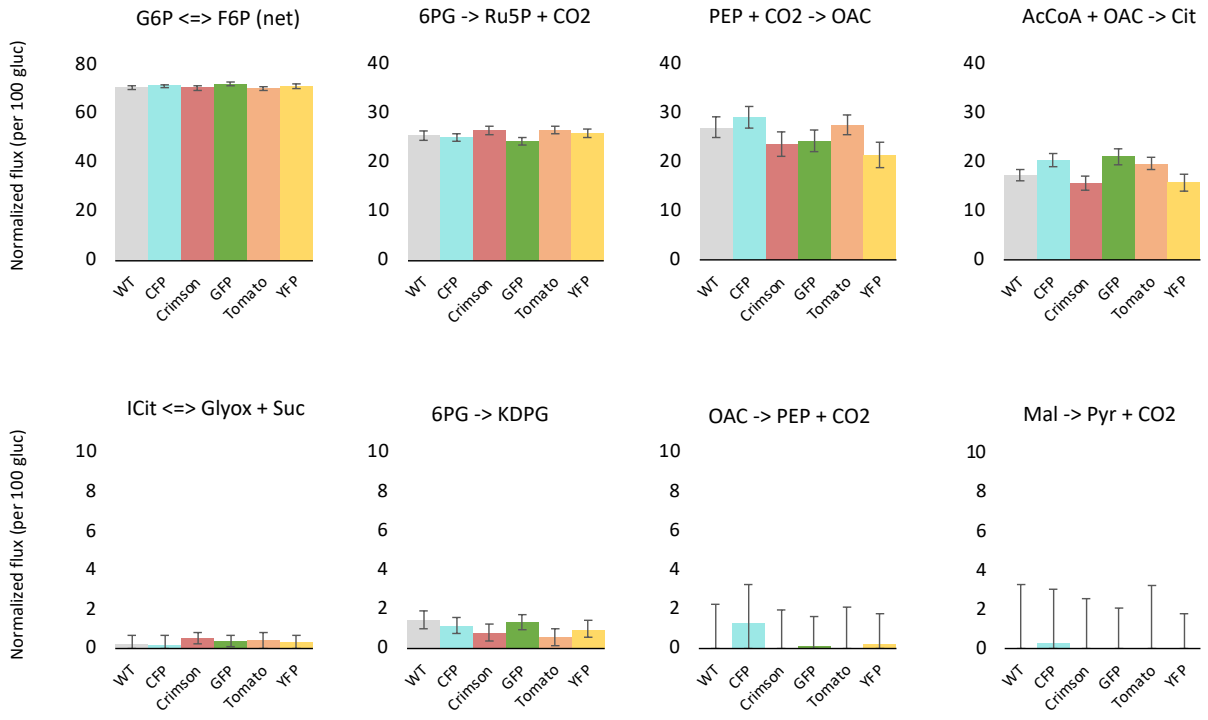

Figure 5.6 Central carbon metabolism of wild type and fluorescent strains. Independent fluxes in central carbon metabolism were shown in this figure. The fluxes are normalized to 100 unit glucose uptake. Fluxes distributions are similar between all strain. Error bar in all figures represent 95% confidence interval.

External rate including glucose uptake and acetate secretion were estimated by ^{13}C Metabolic Flux Analysis as well, shown in Fig. 5.7. The trend of glucose uptake rate of all strains was roughly similar to growth rate, with Crimson being slightly lower and YFP higher compared to the WT. Acetate secretion rate shown in Fig. 5.7 was normalized to 100 glucose uptake to demonstrate the carbon source distribution. YFP had slightly higher acetate secretion compared to WT while other fluorescence strains remain consistent with WT. Overall, the distribution of fluxes of the cell did not alter much when the fluorescence plasmid was expressed.

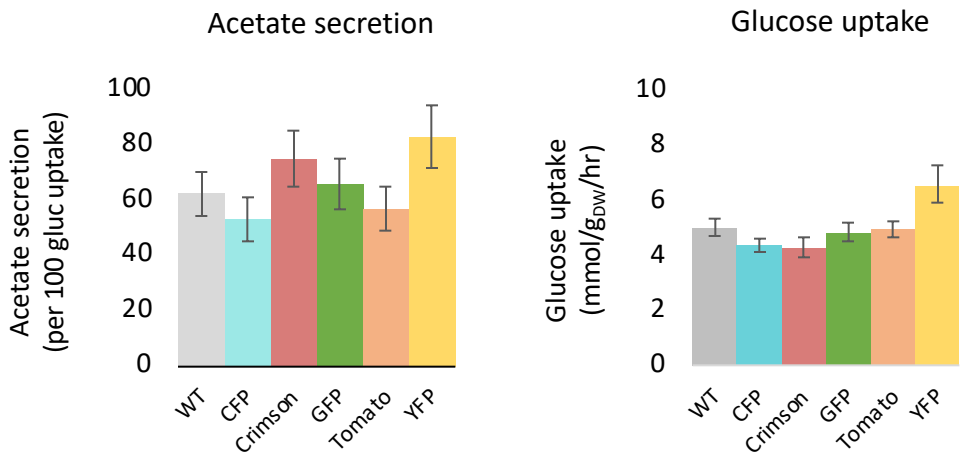

Figure 5.7 Acetate secretion and glucose uptake of wild type and fluorescent strains. External fluxes acetate secretion and glucose uptake are shown. Acetate secretions are normalized to 100 unit glucose uptake, which do not alter much between each strain. Glucose uptakes (unit mmol/g_{DW}/hr) are obtained by the estimate biomass yield from ^{13}C Metabolic Flux Analysis and growth rate measured in the labeling experiment. YFP has higher glucose uptake compared to WT while other fluorescence strains have similar to WT. Error bar in both figures represent 95% confidence interval.

5.5 Discussion

In this chapter, we provide a comprehensive characterization of the potential metabolic burden in *E. coli* caused by overexpression of fluorescent proteins. Five commonly utilized fluorescent proteins CFP, Crimson, GFP, Tomato and YFP were selected. We studied the cell physiology including cell growth and biomass composition. Furthermore, we quantify the metabolic state by performing ^{13}C metabolic flux analysis. We observed growth reduction in the fluorescent strains but overall, no significant changes in biomass composition and metabolic state. Our result suggests that the metabolic burden imposed by fluorescent protein overexpression can be negligible in *E. coli*.

In the past, the metabolic burden caused by GFP in *E. coli* has been studied. Ma et al. investigated the stability of GFP and the plasmid's effect on cell growth (Ma, Zhang and Doyle, 2011). They concluded that the GFP plasmid had insignificant impact on *E. coli*. In a more recent study, 4 different *E. coli* strains with GFP overexpression were investigated (Matsuyama

et al., 2024). It was reported that GFP overexpression did not impact the specific growth rate of all 4 strains. However, in our study, we observed growth rate reduction in the fluorescent strains. In the following paragraph, we will discuss the potential reason for these differing observations.

In our study, after plasmid transformation, the cultures were plated on antibiotic containing LB agar plates for clone selection. We selected four colonies from the GFP plasmid-transformed cultures for growth testing. The growth curves and growth rates of the wild-type and the four GFP strains are shown in Fig. 5.8. We found that GFP 1 and GFP 2 had growth rates comparable to the wild type but exhibited significantly longer lag phases. In contrast, GFP 3 and GFP 4 showed more substantial growth reductions, with GFP 4 exhibiting an approximate 27% decrease in growth rate. The distinct growth behavior between these strains demonstrates that strain selection can cause differing observations.

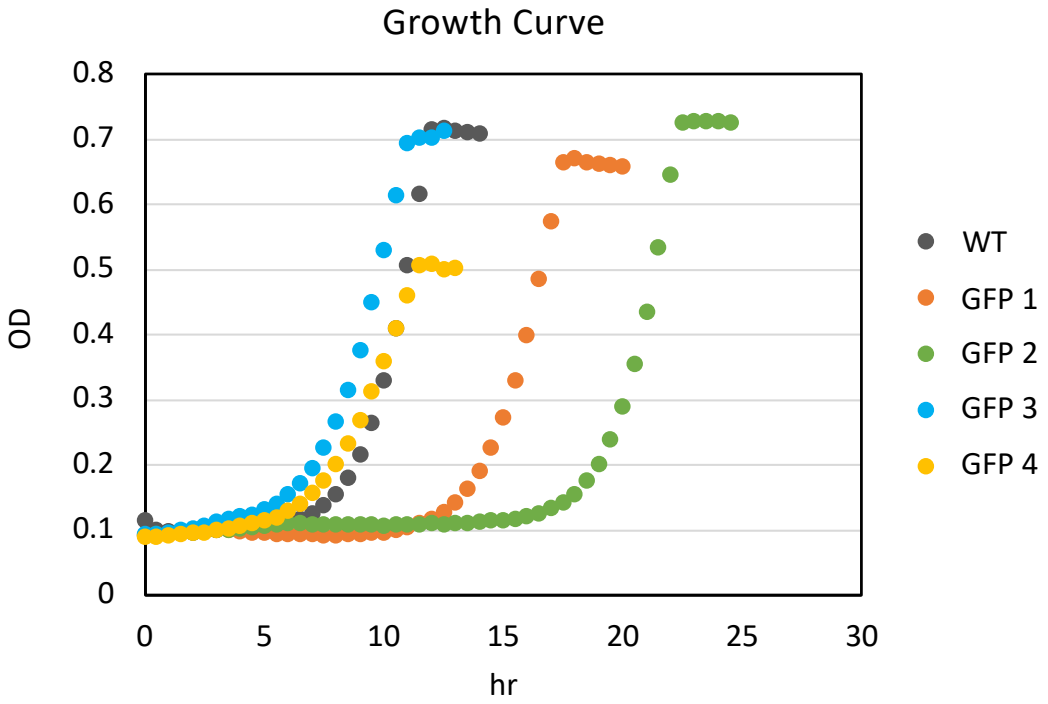

Growth rate (1/h)				
WT	GFP 1	GFP 2	GFP 3	GFP 4
0.60	0.59	0.53	0.47	0.44

Figure 5.8 The growth curve and growth rate of wild type and four GFP strains. The growth of wild type and 4 GFP colony from the same transformation culture were monitored by Biotek Cytation 5. The growth rate of each culture is shown in the bottom table.

During the cell growth, the fluorescent signal was measured as well, as shown in Fig. 5.9. Interestingly, the fluorescence signal intensity varied among the different strains. We observed an inverse correlation between growth rate and fluorescence signal intensity. GFP 1 and GFP 2, which had growth rates similar to the wild type, exhibited much lower fluorescence signals compared to the other two strains. In contrast, GFP 3 and GFP 4, which showed significant growth reductions, displayed strong fluorescence signals. It is likely that these "highly fluorescent strains" allocate more energy or resources to fluorescent protein production, resulting

in a more pronounced impact on cell growth. In this study, GFP 3 was selected to investigate the metabolic burden. GFP 3 had stronger fluorescence signal but slower growth rate, which is likely the reason why we had different observation in growth rate compared to previous literature.

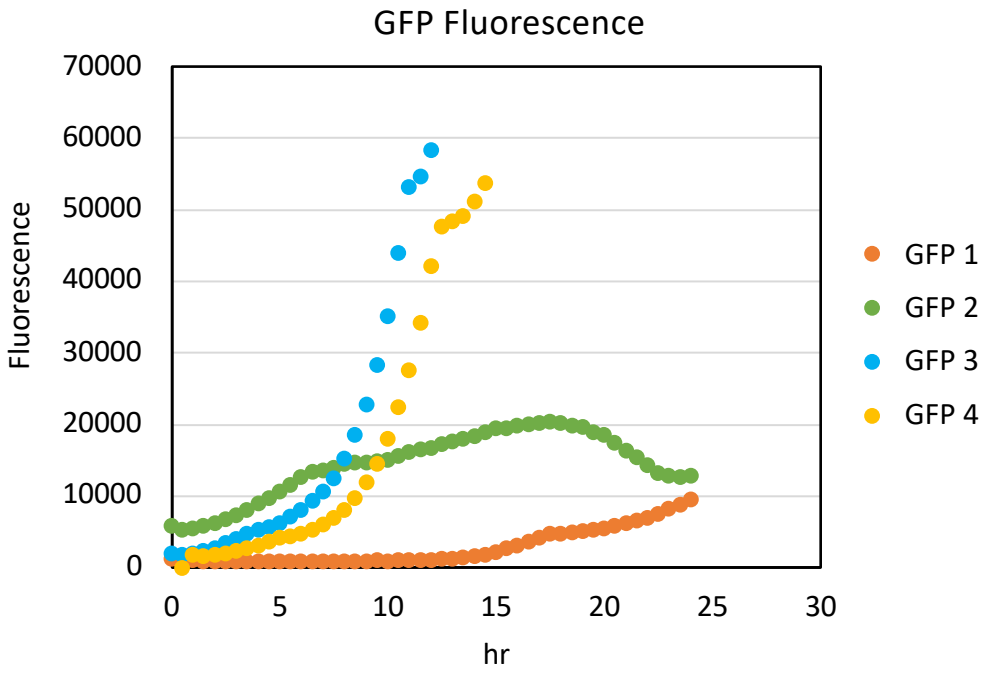

Figure 5.9 The GFP fluorescent signal of four GFP strains during cell growth. The GFP fluorescent signal of four GFP strains were measured by Biotek Cytation 5. The wild type has signal below 1000 throughout the entire growth, which is not shown in this figure.

In our characterization, we provided a detailed distribution of macromolecules in biomass and amino acids in protein. Our results suggest that the cells did not utilize an excessive amount of carbon sources to synthesize fluorescent proteins, as we did not observe significant changes in protein content (Fig. 5.3) or amino acid distribution (Fig. 5.4). One could argue that, although the overall protein content remains the same, the cells are producing fluorescent protein instead of biomass. However, if that were the case, we should see some differences in amino acid distribution between each strain. In Fig. 5.10, we compare the amino acid distribution of wild-type *E. coli* biomass and fluorescent proteins. The wild-type *E. coli* biomass was obtained

through our experiment. The amino acid distribution of the fluorescent proteins was calculated based on their sequences and converted into mmol per gram protein. Several amino acids differ significantly when comparing the fluorescent protein to the cell biomass. For example, wild-type biomass had much more alanine but less lysine, histidine, and tyrosine. Differences were also observed between different fluorescent proteins. If fluorescent protein production diverted a significant amount of carbon from biomass production, we would expect to see a distinct distribution between the wild-type strain and the fluorescent strains. Our result, however, suggest that there is no excessive carbon being directed to fluorescent protein production, which agrees with our flux analysis result that not significant flux rewiring was observed.

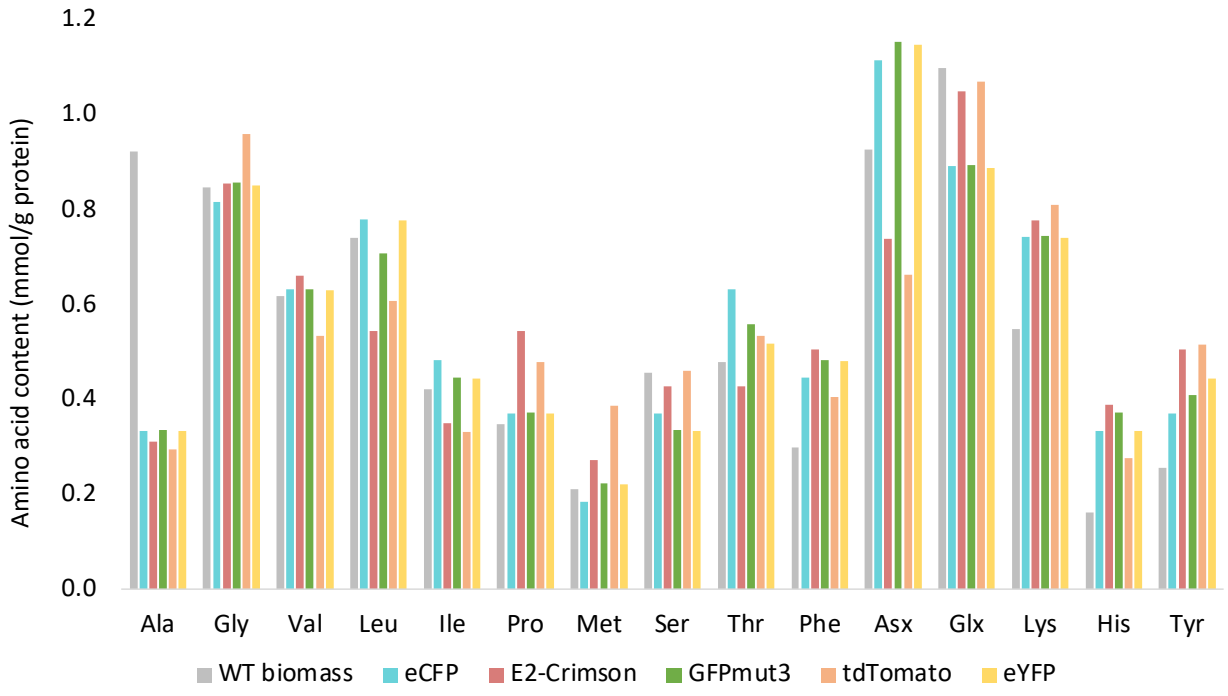

Figure 5.10 Amino acid distribution of wild type *E. coli* biomass and fluorescent protein. The amino acid content of wild type *E. coli* biomass and fluorescent protein is shown in mmol per gram protein for comparison. The amino acid distribution of wild type biomass is obtained through experiment and the fluorescent protein is calculated from the protein sequence.

In summary, we characterized the impact of five fluorescent protein overexpression in wild type *E. coli* in this chapter. Although we observed growth reduction in the fluorescent

strains, we did not find changes in biomass composition or metabolic state. In previous literature, it has been reported that overexpression of protein containing less abundant amino acids (His, Trp, Tyr, Phe and Met) in *E. coli* can result in less efficient translation (Bonomo and Gill, 2005), which could potentially explain what we observed. More advanced genome scale modeling can also provide insights into the resource allocation in the recombinant cells (Oftadeh and Hatzimanikatis, 2024). Overall, we provide a comprehensive characterization of cell physiology and metabolism for cells that overexpress fluorescent protein, which could serve as a solid foundation for future studies that apply fluorescent proteins.

5.6 Supplementary experiment

5.6.1 IPTG induction

The fluorescent plasmids we purchased are isopropyl-β-d-thiogalactoside (IPTG) inducible plasmids (Barbier and Damron, 2016). After transformation, all fluorescent strains were tested with different concentrations of IPTG from 0.01mM to 0.5mM. We noticed that the addition of IPTG did not impact cell growth and fluorescence intensity, as shown in Fig. 5.11. Therefore, for the experiments we conducted in this chapter, we did not add any IPTG into the culture.

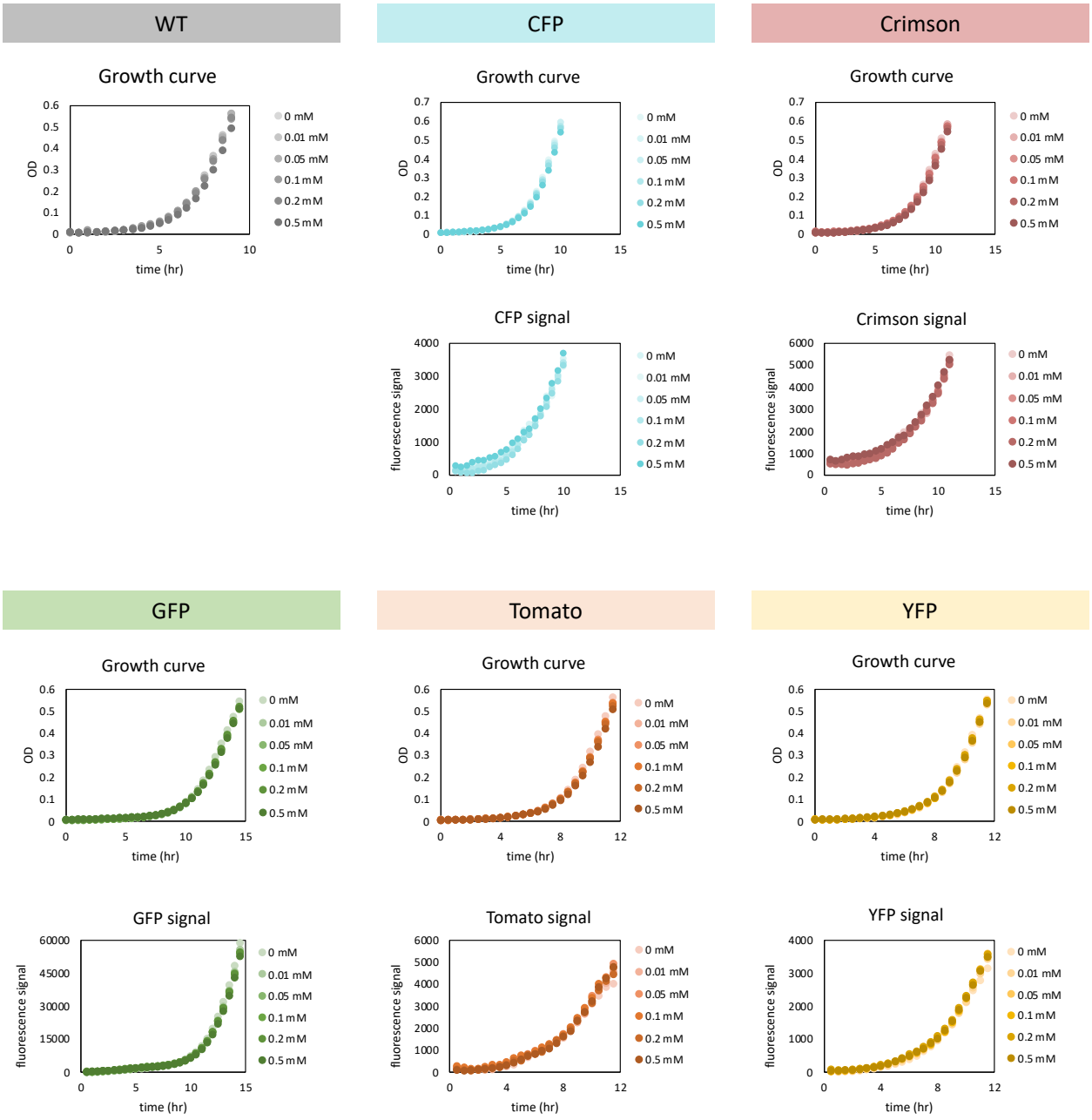

Figure 5.11 The growth and fluorescence signal with inducer IPTG. The growth and fluorescence signal with different concentration from 0 to 0.5mM of IPTG are monitored by BioTek Cytation 5.

Chapter 6 The Future and Challenge for Co-culture ^{13}C Metabolic Flux Analysis

In this chapter, we first discuss a new application of ^{13}C metabolic flux analysis (^{13}C MFA) on a fluorescent syntrophic co-culture consisting Δ*ilvC*-Crimson/Δ*icd*-CFP. Following this, we conclude by highlighting some of the challenges of applying ^{13}C MFA on a co-culture system and propose new directions for future studies.

6.1 Case study for fluorescent co-culture by applying ^{13}C metabolic flux analysis

6.1.1 Cell strain and growth

Fluorescent proteins, as described in the previous chapter, can serve as a tool to track population composition in co-culture. After confirming they have negligible impact on cell physiology and metabolism, we overexpressed two selected fluorescent proteins, Crimson and CFP, in *E. coli* auxotrophic strains Δ*ilvC* and Δ*icd*, respectively. Cells overexpressing fluorescent proteins were easily visible under fluorescent microscopy using the BioTek Cytation 5 cell imaging reader, as shown in Fig. 6.1A. By utilizing the built-in software, we were able to determine the population composition by counting individual cells based on their color, as shown in Fig 6.1A and B.

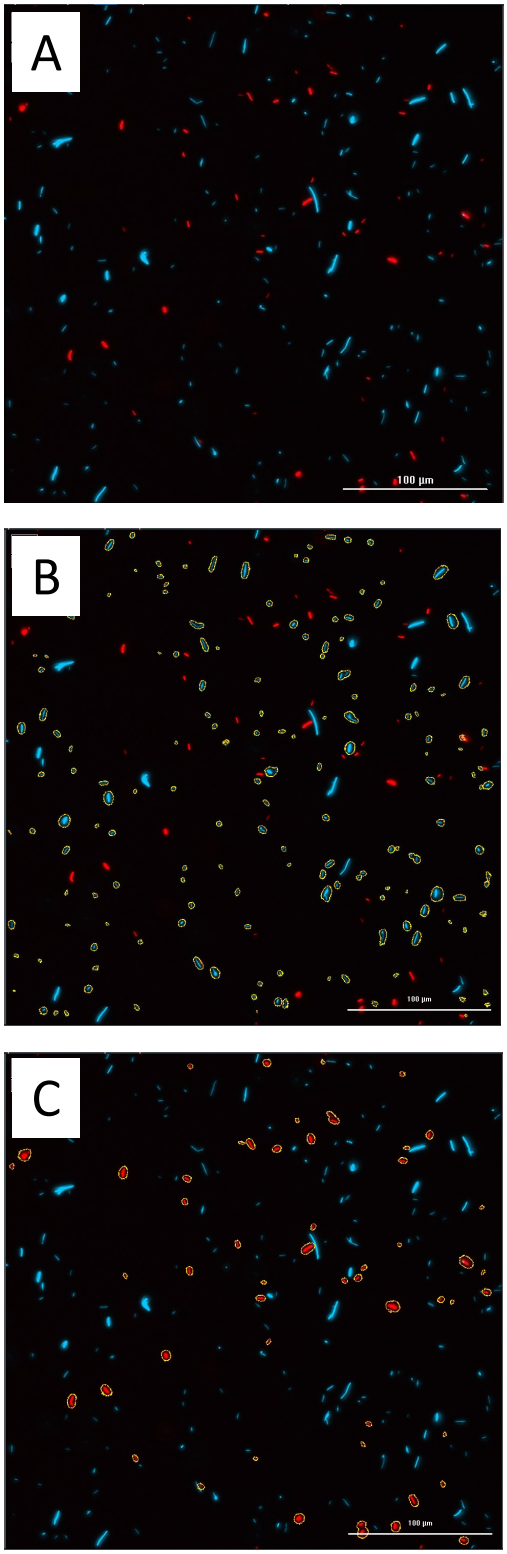

Figure 6.1 Δ*ilvC*-Crimson and Δ*icd*-CFP co-culture under fluorescent microscopy. The picture was capture by BioTek Cytation 5 cell imaging reader. CFP fluorescent proteins are cyan and Crimson fluorescent proteins are red. The scale car shows 100µm. A): the picture of the co-culture. B): Cell with CFP fluorescent protein overexpression is counted by the software. C): Cell with Crimson fluorescent protein overexpression is counted by the software.

By employing fluorescent proteins, we were able to track the population dynamics in the Δ*ilvC*-Crimson and Δ*icd*-CFP co-culture. The growth and population composition of the co-culture over time are shown in Fig. 6.2. The fluorescent syntrophic co-culture, has a growth rate around 0.09 1/h, which is slightly higher than the non-fluorescent syntrophic co-culture. We also noticed that the population composition seems to be more unbalanced, where the regular co-culture is around 40%: 60% and the fluorescent co-culture is 30%: 70%. In the next part, we will first apply ^{13}C MFA assuming both strains have the same glucose uptake.

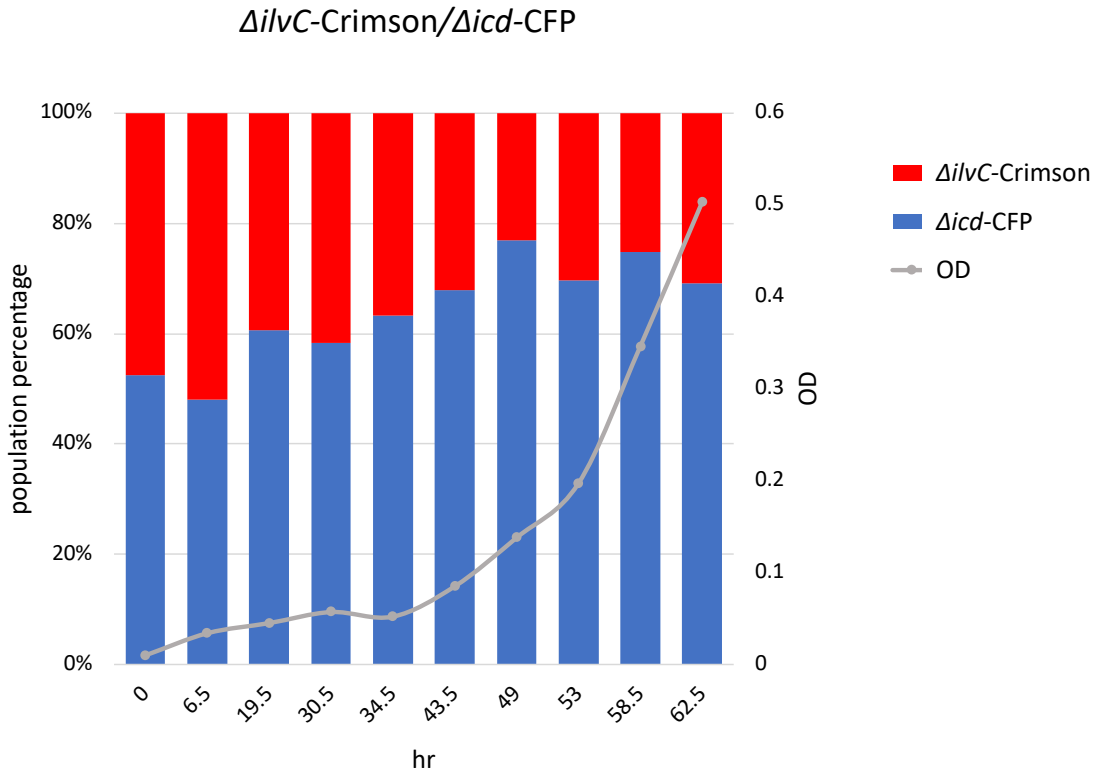

Figure 6.2 Growth and population dynamic of Δ*ilvC*-Crimson and Δ*icd*-CFP co-culture. The bar graph demonstrates the population composition as different time points, measured by BioTek Cytation 5. The red represents Δ*ilvC*-Crimson strain and the blue represents Δ*icd*-CFP strain. The growth of the co-culture is also shown in this graph. Noted that the time points are not evenly distributed.

6.1.2 ^{13}C metabolic flux analysis

Since it was uncertain whether fluorescent protein overexpression would impact the syntrophic interaction between the two strains, we followed the same procedure as outlined in

chapter 3 to determine the cross-feeding metabolites. Fig. 6.3 demonstrates the SSR when exchange fluxes were included into the metabolic model. We started with adding the required amino acids, glutamate, valine and isoleucine, for the auxotrophic strains, which resulted in an unacceptable fit, as shown in the first bar. Additional leucine, aspartate and threonine exchange fluxes improved the fit significantly but remained statistically unacceptable, as shown in the second bar. When we further included the intermediates acetolactate and 2-hydroxybutanoate into the model, the SSR dropped significantly to 56.1, which indicated that we might be overfitting our model.

During flux analysis, the results were subjected to a χ^2 statistical test at 95% confidence level to determine the goodness of fit. The acceptable SSR value should fall between ${\chi^2}_{\alpha/2}(n-p)$ and ${\chi^2}_{1-\alpha/2}(n-p)$, where α is a chosen threshold value 0.05 for 95% confidence level and (n-p) represents the degree of freedom with n being the number of fitted measurement and p being the estimated independent parameter (Antoniewicz, Kelleher and Stephanopoulos, 2006). In our co-culture MFA, the acceptable SSR value fell between 130 to 210. Therefore, SSR value lower than 130 suggests potential overfitting.

Here we argue that, in some cases, the addition of metabolite exchange fluxes may lead to overfitting. In other words, the model becomes overly complex, and insufficient experimental data is available to serve as a constraint. Generally, to address overfitting, either the model must be simplified, or additional constraints must be incorporated. In our case, we are elucidating metabolite cross-feeding by adding exchange fluxes to the model. Thus, simplification is not an option, as the expanded model is what we are evaluating. In the future, we would recommend conducting three or four parallel labeling experiments to provide additional constrains for conducting co-culture MFA.

In Fig. 6.4, the exchange flux map of the co-culture, with all exchange fluxes included, is shown. We further continued our analysis by systematically removing exchange fluxes from the metabolic model and evaluating the impact on the SSR. Threonine and leucine exchange fluxes were removed first, as they were predicted to be relatively insignificant in Fig. 6.4. The SSR remained roughly the same after the removal of these two exchange fluxes, as shown in the fourth and fifth bar in Fig. 6.3. Interestingly, removing the 2-aceto-hydroxybutanoate exchange flux instead of the leucine exchange flux from the metabolic model resulted in a significant increase in SSR. This fit suggested that the exchange of 2-aceto-hydroxybutanoate was critical, unlike the observations discussed in Chapter 3, where its removal did not significantly impact the SSR (Fig. 3.8, fourth bar). Notably, in another fluorescent syntrophic co-culture consisting of Δ*ilvC*-CFP and Δ*icd*-Crimson, the exchange of 2-aceto-hydroxybutanoate was also critical, with the SSR exceeding 2000 when it was excluded. At this point, we are unable to confirm whether this is due to the overexpression of fluorescent proteins altering the dependency between the two auxotrophic strains or a measurement issue.

If we removed the aspartate exchange flux from the model instead of leucine, the SSR increased and became statistically acceptable without overfitting. This suggests that the inclusion of aspartate exchange flux is likely causing the overfitting. Determining whether aspartate is being exchanged is challenging with the current data. Although the model predicted that aspartate was exchanged at a significant rate, as shown in Fig. 6.4, the accuracy of this prediction is uncertain due to the potential overfitting. In our case, we decided to not include aspartate exchange in the final model as we were unsure if we could trust the result. The final model also excluded leucine exchange flux as it did not impact the fit, as shown in the last bar in Fig. 6.3.

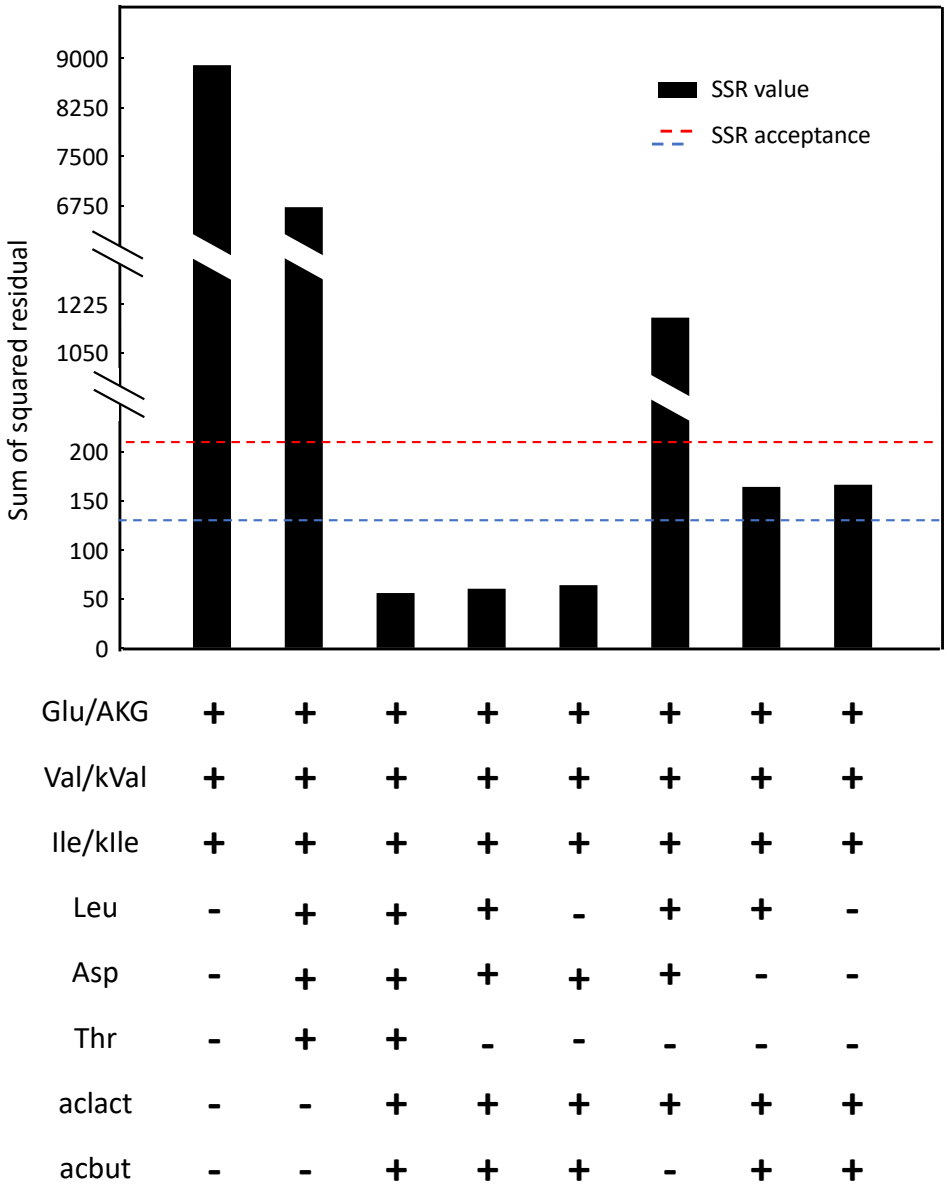

Figure 6.3 Sum of square residual (SSR) of co-culture model with different exchange metabolites combination for the fluorescent co-culture Δ*ilvC*-Crimson/ Δ*icd*-CFP. The bars represent the SSR values of each metabolic model, with the red and blue dashed line indicating the range for acceptable SSR. The chart below the bar graph displays the metabolite exchange fluxes included in the metabolic network model for each fit. Glu/AKG: glutamate/alpha-ketoglutarate; Val/kVal: valine/keto-valine; Ile/kIle: isoleucine/keto-isoleucine; Leu: leucine; Asp: aspartate; Thr: threonine; aclact: acetolactate; acbut: 2-aceto-hydroxybutanoate.

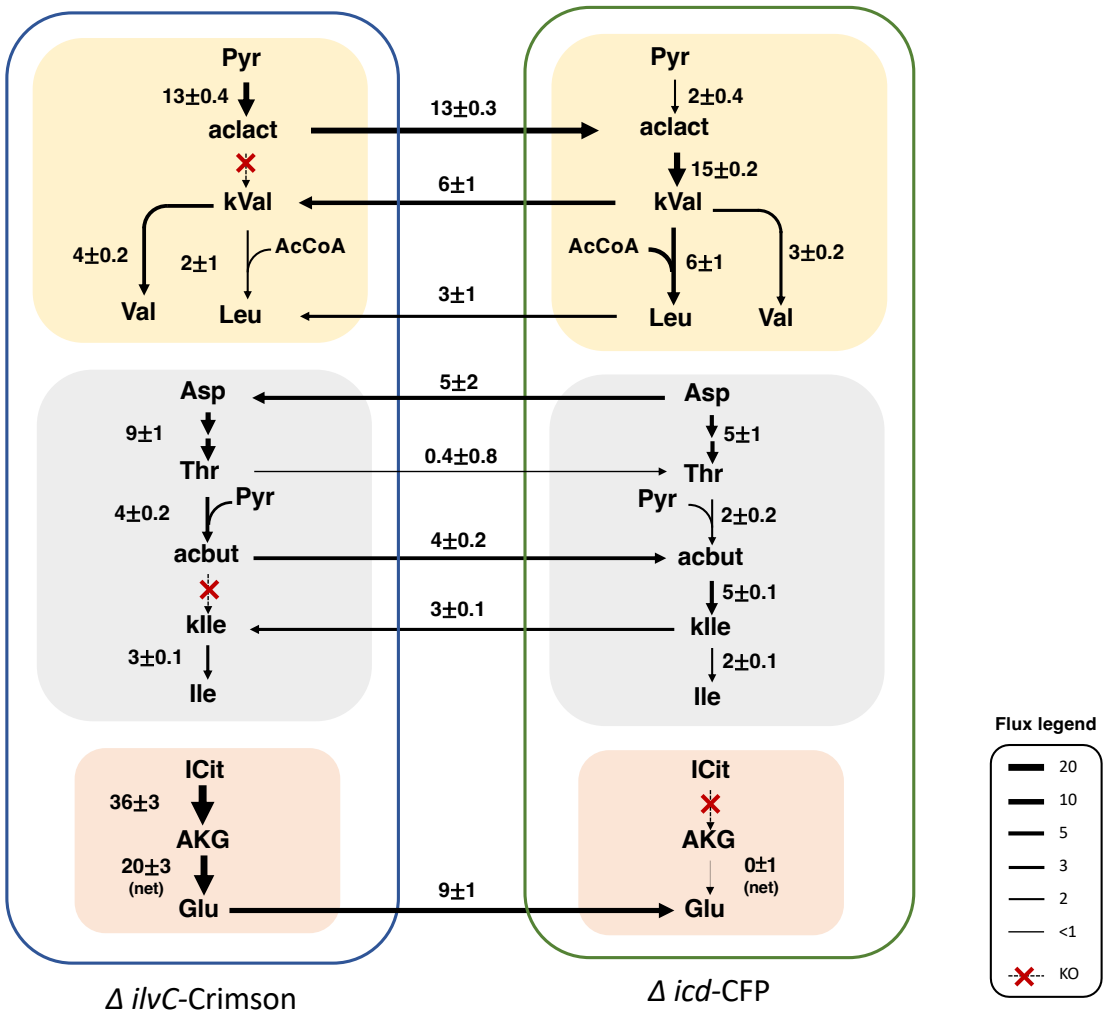

Figure 6.4 Exchange flux map of co-culture model that include all possible exchanges. The exchange flux map when all exchange fluxes are included in the model. Fluxes values are shown with standard deviation. Yellow box (top): Valine/Leucine biosynthesis pathway. Gray box (middle): Isoleucine biosynthesis pathway. Orange box (bottom): Glutamate biosynthesis pathway.

The final exchange flux map is shown in Fig 6.5. Note that we were unable to compare the exchange fluxes with those in the previous co-culture consisting Δ*ilvC* and Δ*icd* since they used different metabolic model. However, this result also demonstrates the importance of intermediate exchange, as we concluded in the previous chapter. Most importantly, in this example, we want to highlight the potential challenge of overfitting due to the increasingly model complexity.

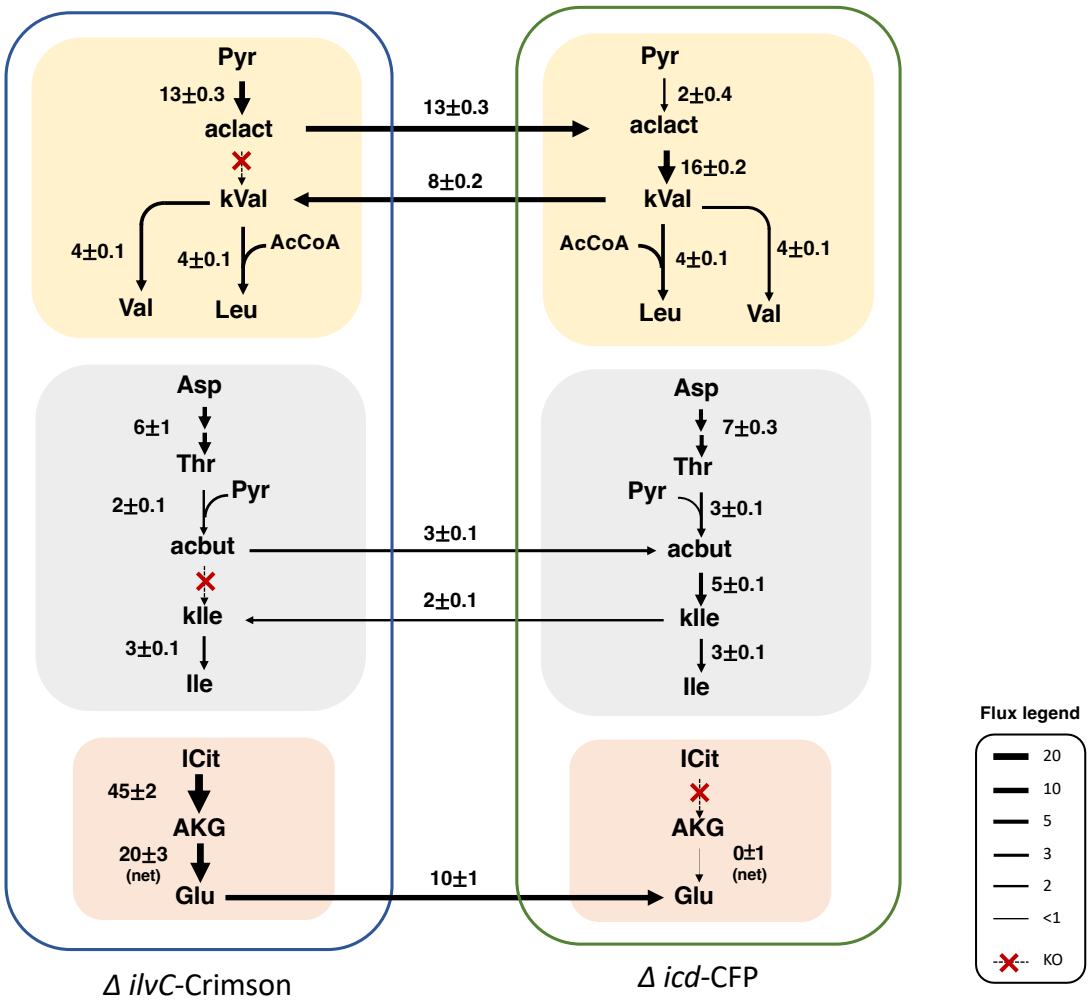

Figure 6.5 Exchange flux map of Δ*ilvC*-Crimson and Δ*icd*-CFP co-culture. The final exchange flux map for the Δ*ilvC*-Crimson and Δ*icd*-CFP co-culture. Fluxes values are shown with standard deviation. Yellow box (top): Valine/Leucine biosynthesis pathway. Gray box (middle): Isoleucine biosynthesis pathway. Orange box (bottom): Glutamate biosynthesis pathway.

6.1.3 ^{13}C metabolic flux analysis for different glucose uptake

In Chapter 3, we discuss how population composition can potentially impact the accuracy of flux analysis. In brief, in our co-culture model, the two sets of metabolic networks are both normalized to 100 units of glucose uptake. When we included exchange fluxes between the two strains, their metabolic networks were linked by the exchange fluxes. Therefore, the inherent assumption in this case was that the two strains have the same glucose uptake. The glucose uptake here refers to the entire uptake of a single strain, which is the glucose uptake per single

cell multiplied by its population size. In chapter 3, we assumed both strains had the same glucose uptake since there was no mutation related to glucose uptake and the population of the two strains was roughly 50%: 50%. However, in the fluorescent co-culture described in this chapter, the population composition of Δ*ilvC*-Crimson: Δ*icd*-CFP is about 30%: 70% (Fig. 6.2), which is more skewed than the co-culture in chapter 3. Therefore, we modified the glucose uptake of Δ*ilvC*-Crimson, which is strains 1 in the model, and performed flux analysis. Since the population ratio is roughly 1: 2.33, the glucose uptake of strain 1 was set to 40 and strain 2 remained 100 to achieve a glucose uptake ratio of 1: 2.5, as shown in Fig. 6.6.

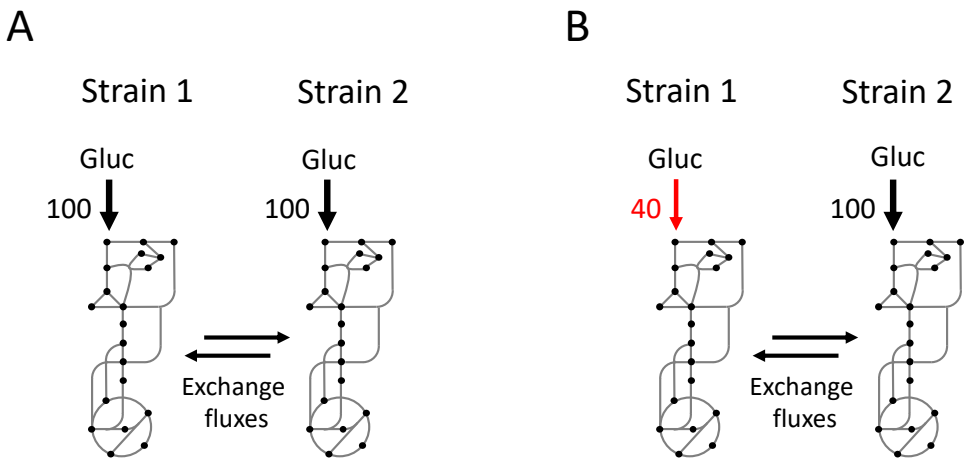

Figure 6.6 Metabolic model for different glucose uptake. (A) In the case where the two strains had similar population size, the glucose uptake was set to 100 for both strains. (B) In the fluorescent, the population sizes were not equal between the two strains, the glucose uptake were manually edited. In our case, Δ*ilvC*-Crimson: Δ*icd*-CFP is 30%: 70%, which is roughly 1: 2.3. We adjusted the glucose uptake for strain 1 to 40 so that the uptake ratio between the two strains is 1:2.5.

With the glucose uptake adjusted, the exchange between the two strains is shown in Fig. 6.7. For easier comparison to Fig. 6.5, we normalized Δ*ilvC*-Crimson back to 100 glucose uptake, which is why the exchange flux values differed between the two strains. Overall, the fluxes of Δ*icd*-CFP were similar between equal glucose uptake (Fig. 6.5) and different glucose uptake (Fig. 6.7). On the other hand, Δ*ilvC*-Crimson was cross-feeding more acetolactate and glutamate to Δ*icd*-CFP, but gaining less valine/keto-valine and isoleucine/keto-isoleucine when

the glucose uptake was different. Interestingly, although there were differences in exchange fluxes, the two models fit equally well (SSR for equal uptake: 166.3; SSR for different uptake: 169.4). When we compared central carbon metabolism, both strains had similar flux distribution between the equal glucose uptake model and the different glucose uptake model. As this point, we do not have a strong argument regarding which model is more correct. However, our results suggested that the population differences did not impact the fitting as much as we concerned.

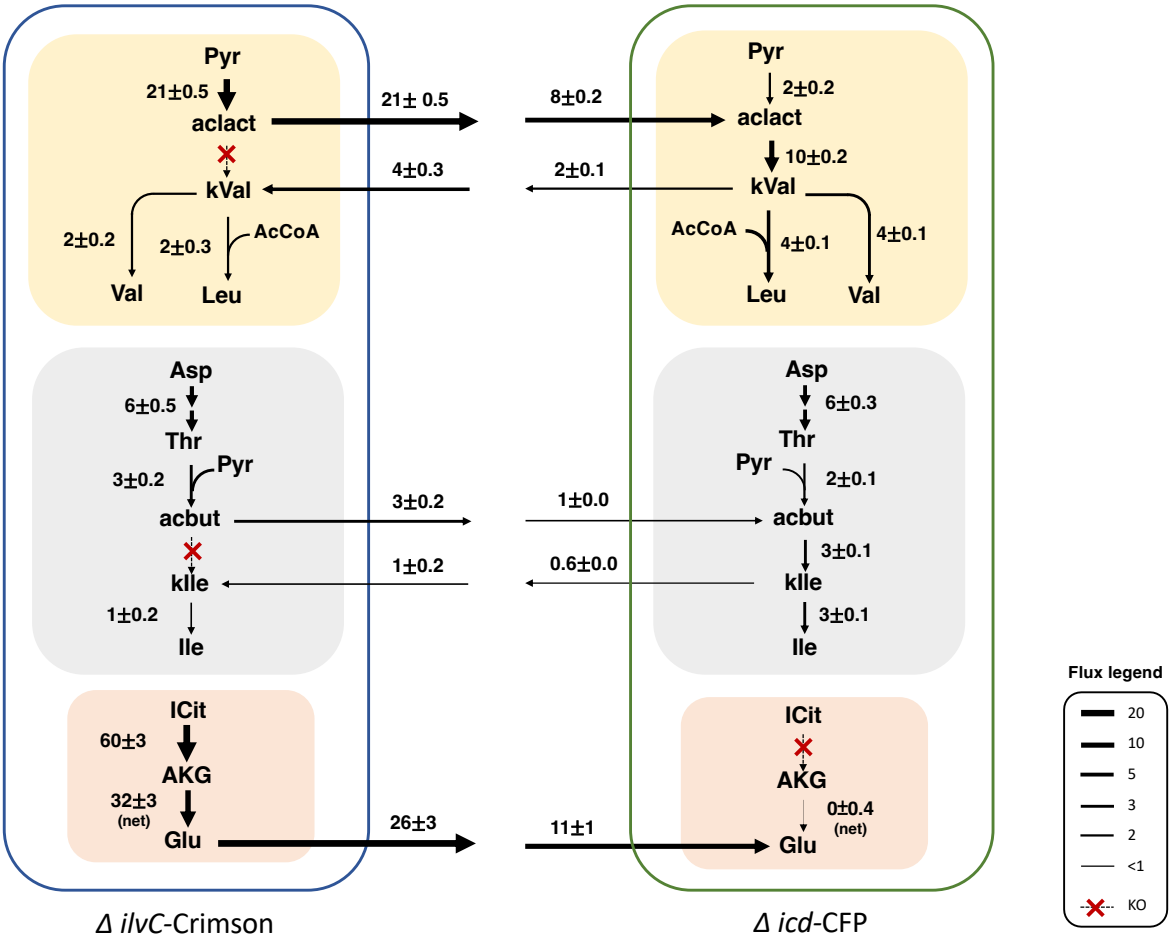

Figure 6.7 Exchange flux map of Δ*ilvC*-Crimson and Δ*icd*-CFP co-culture for different glucose uptake. The exchange flux map for the Δ*ilvC*-Crimson and Δ*icd*-CFP co-culture when the glucose uptake of Δ*ilvC*-Crimson is set to 40 in the model. The flux of Δ*ilvC*-Crimson was adjusted back to per 100 glucose uptake for easier comparison to Fig. 6.5. Fluxes values are shown with standard deviation. Yellow box (top): Valine/Leucine biosynthesis pathway. Gray box (middle): Isoleucine biosynthesis pathway. Orange box (bottom): Glutamate biosynthesis pathway.

6.2 Challenges for ^{13}C metabolic flux analysis

In this thesis, ^{13}C MFA was applied for the first time on syntrophic co-cultures that consisted of two strains exchanging metabolites. In this section, we will discuss potential challenges of applying ^{13}C MFA to co-culture systems.

In Chapter 3, we demonstrated our ability to elucidate exchanging metabolites by constructing metabolic models with increasing complexity and evaluating their performance through statistical analysis. Specifically, the calculated sum of square residuals (SSR) was used to represent how well the metabolic models fit the experimental measurements. However, SSR only reflects the overall performance of the model. We found that, in some cases, different combinations of exchange fluxes can yield statistically acceptable fits. Specifically, exchange fluxes that improve the SSR by 50 or less can be substituted by other fluxes. Thus, we were unable to provide a strong statistical argument to confirm or refute the existence of specific metabolite exchanges solely based on flux analysis. These non-critical metabolite exchanges will require further investigation to confirm their presence. Nevertheless, we demonstrated that ^{13}C MFA could provide solid evidence when critical metabolites were being exchanged such as the required amino acid and their pathway intermediates.

Another challenge, as mentioned in this chapter, is that including exchange fluxes in the model can sometimes lead to overfitting. This overfitting can obscure the identification of actual exchanging metabolites, as it becomes unclear whether the fluxes are real or simply artifacts of fitting measurement errors or noise. A potential solution is to provide additional measurements to the model as constraints. Conducting three or four parallel experiments could be valuable to test if this resolves the overfitting issue.

While utilizing different tracers can provide more measurements, which may help resolve interactions in more complex systems, we will eventually be constrained by the exponentially increasing number of possible exchanging metabolites between strains. In a more complex system that contains four or more strain, the possible interactions between each strain can increase rapidly. This would result in an overwhelming number of metabolic models with different exchange scenarios to test, ultimately becoming inefficient.

Nevertheless, although there remain challenges for ^{13}C MFA, it is important to keep in mind that currently there are only limited methods to elucidate the exchanging metabolites.

6.3 Future direction

In this work, we focused on studying the syntrophic interactions between auxotrophic strains. In Chapter 2, we investigated how these strains restored their growth when the missing amino acids were supplemented. Our findings revealed that the glutamate-deficient strain Δ*icd*, with a gene knockout in the TCA cycle, undergoes a more complex flux rewiring rather than simply restoring the TCA cycle when supplemented with glutamate. In the future, a comprehensive study on how various auxotrophic strains restore their growth could provide valuable insights into how other strains rewire metabolism when required resources are available. Besides amino acid auxotrophic strains, other knockout strains could also be studied. Previous research has explored metabolic responses to the deletion of 20 core enzymes in the upper central carbon metabolism using ^{13}C MFA (Long and Antoniewicz, 2019b). It would also be interesting to examine how these knockout strains respond when the deficient metabolites are supplied in the medium.

In chapter 3, ^{13}C MFA was applied to a syntrophic co-culture. When different metabolic network models were tested, we observed a significant improvement from the mono-culture

model to the co-culture model. This is likely due to the distinct central carbon metabolism between the two auxotrophic strains we used. Δ*ilvC* exhibited similar flux distribution to wild type while Δ*icd* showed more active pentose phosphate pathway and glyoxylate shunt. In another syntrophic pair consisting of Δ*argE* and Δ*tyrA*, both of which had gene knockouts located away from central carbon metabolism, we noticed that the mono-culture model was able to fit comparably to the co-culture model without exchange fluxes. Future studies could investigate how much difference in central carbon metabolic fluxes is required for the co-culture model to fit better than the mono-culture model. In Fig. 6.8, we demonstrate how this can be achieved by running simulations to generate labeling data from two sets of metabolic fluxes with different distributions. We will start with identical flux distribution for the two strains and increase the differences in the flux distribution. The resulting labeling data can be fitted with mono-culture and co-culture models and analyzed statistically. We should expect the group with identical flux distribution to fit equally well with the mono-culture model and co-culture model. As the difference in the flux distribution increases, mono culture should no longer be sufficient to fit the generated labeling data and. Therefore, we should start observing higher SSR in mono culture model compared to a co-culture model. This analysis will help us understand how differences in metabolic fluxes impact the fitting performance between mono-culture and co-culture models. Additionally, we can study flux differences in various pathways. For instance, instead of altering fluxes in glycolysis and the pentose phosphate pathway, we could adjust the flux in the TCA cycle to evaluate the model's sensitivity to changes in different pathways. Overall, this analysis can provide valuable insights for future applications of ^{13}C MFA on co-culture.

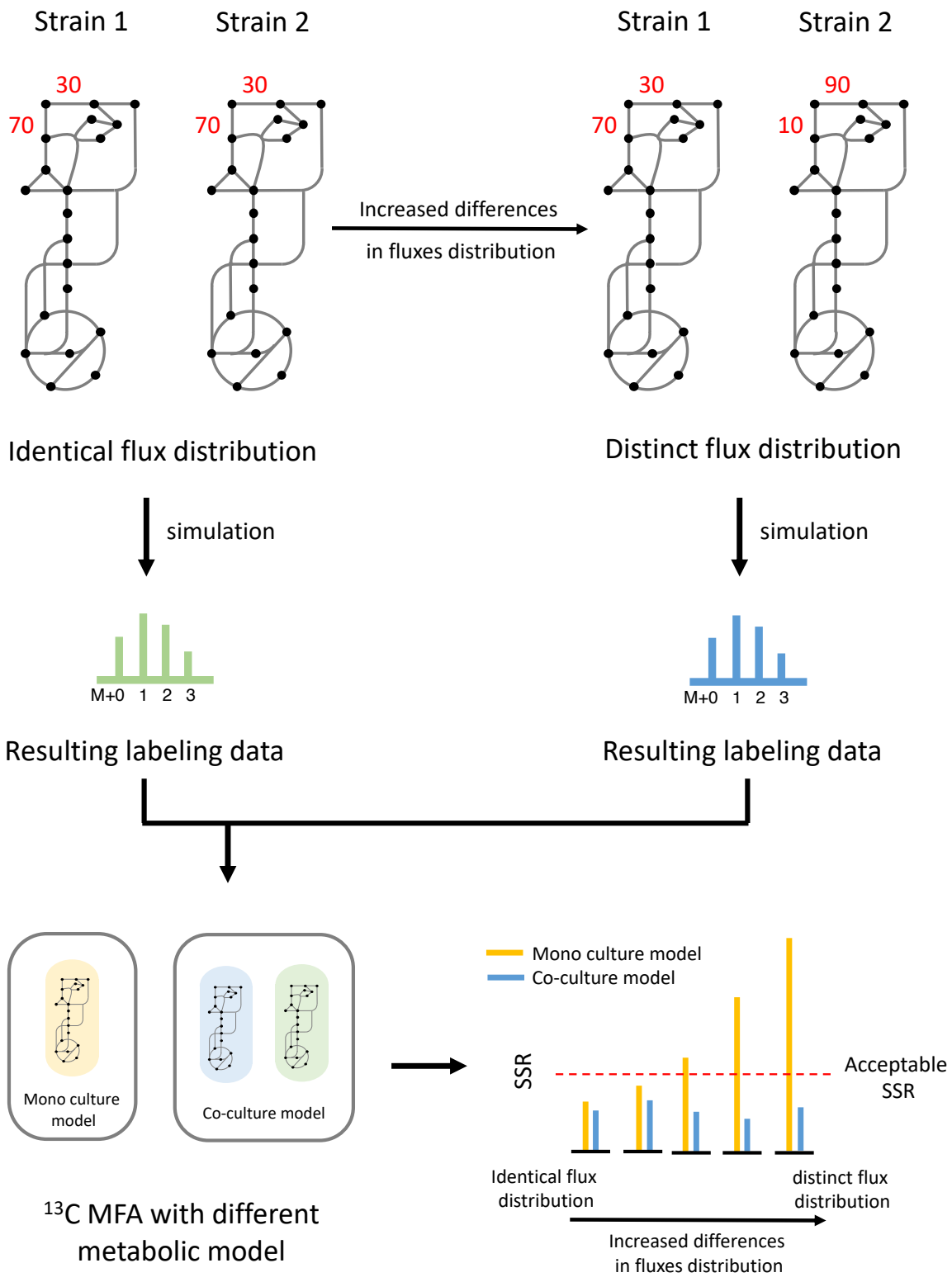

Figure 6.8 Workflow for evaluating how flux differences in two strains impact the mono-culture model and co-culture model performance. For the simulation, we will generate labeling data from designed flux distribution. As shown in top, the metabolic flux distribution of the two strains starts from being identical to having huge

difference. We can create several sets of distribution for more detailed analysis. The resulting labeling data from these flux distributions will then be tested the mono culture model and co-culture model. In the figure at bottom right the yellow bars represent the SSR for mono culture model and the blue bars represent co-culture model. Each group of yellow and blue bar represent on pair of flux distribution. As shown on the plot, we should expect as the flux difference increase, the performance of mono culture model will become worse.

In syntrophic co-cultures, growth is likely constrained by the exchange of metabolites. Such constraints may arise from factors including the concentration of metabolites in the medium, the rate at which transporters uptake the metabolites, and the number of available transporters. To gain a more detailed understanding, experiments could be designed to measure the K_m value for metabolite uptake. If growth is limited by substrate uptake, the growth rate should be proportional to the rate of substrate uptake. Consequently, the K_m value can be determined by supplementing the auxotrophic strain with varying concentrations of metabolite and measuring the corresponding growth rate. The K_m value is the metabolite concentration at which the growth rate is half of the maximum growth rate. This parameter is crucial for constructing mathematical models to predict co-culture growth. Future work could involve developing more robust models for syntrophic co-cultures by incorporating growth-limiting factors into the model. Another promising avenue for research is to investigate whether cells alter their transporter expression levels in a co-culture to enhance growth. To conduct transcriptomic analysis of individual strains within the co-culture, a transwell system can be employed, wherein the strains are physically separated by a membrane that permits metabolite diffusion. This setup allows for comparison of transporter expression levels between syntrophic co-cultures and mono-cultures. Taken together, we present several future directions that could be further investigated to better understand syntrophic interactions.

Besides the Δ*ilvC* and Δ*icd* co-culture mentioned in this thesis, more syntrophic pairs could also be investigated in the future. Specifically, auxotrophic *E. coli* pairs that could grow together have been reported in previous literature (Wintermute and Silver, 2010). These

syntrophic pairs can be analyzed through the method developed in this thesis. Furthermore, it would be valuable to test if we could apply the new information that we learn from the co-culture to design or elucidate a more complex system. For example, if we uncover the interaction between strain A and B, strain B and C, strain A and C, are they going to interact the same way in a tri-culture system? As mentioned earlier, ^{13}C MFA has enough redundancy to solve a tri-culture system. Therefore, it is possible to answer the above question with our current tool.

In this thesis, we demonstrate the application of ^{13}C metabolic flux analysis (^{13}C MFA) on syntrophic co-cultures. ^{13}C MFA can provide compelling evidence for the exchange of critical metabolites through rigorous statistical analysis. We discovered that the exchange of metabolic pathway intermediates is also crucial between auxotrophic strains. This finding was further supported by investigating 55 pairs of *E. coli* that shared the same amino acid deficiency. We hope that in the future, this method can be applied to different strain combinations to broaden our understanding of microbial interactions.

Appendix

A.1 Mono-culture Metabolic Network Model

Glycolysis

Gluc.ext + PEP -> G6P + Pyr

G6P <=> F6P (net)

G6P <=> F6P (exch)

F6P + ATP -> FBP + ADP

FBP <=> DHAP + GAP (net)

FBP <=> DHAP + GAP (exch)

DHAP <=> GAP (net)

DHAP <=> GAP (exch)

GAP + NAD + ADP + Pi <=> 3PG + ATP + NADH (net)

GAP + NAD + ADP + Pi <=> 3PG + ATP + NADH (exch)

3PG <=> PEP (net)

3PG <=> PEP (exch)

PEP + ADP <=> Pyr + ATP (net)

PEP + ADP <=> Pyr + ATP (exch)

Pentose Phosphate Pathway

G6P + NADP -> 6PG + NADPH

6PG + NADP -> Ru5P + CO2 + NADPH

Ru5P <=> X5P (net)

Ru5P <=> X5P (exch)

Ru5P <=> R5P (net)

Ru5P <=> R5P (exch)

X5P <=> GAP + E-C2 (net)

X5P <=> GAP + E-C2 (exch)

F6P <=> E4P + E-C2 (net)

F6P <=> E4P + E-C2 (exch)

S7P <=> R5P + E-C2 (net)

S7P <=> R5P + E-C2 (exch)

F6P <=> GAP + E-C3 (net)

F6P <=> GAP + E-C3 (exch)

S7P <=> E4P + E-C3 (net)

S7P <=> E4P + E-C3 (exch)

ED Pathway

6PG -> KDPG

KDPG -> GAP + Pyr

TCA Cycle

Pyr + NAD -> AcCoA + CO2 + NADH

AcCoA + OAC -> Cit

Cit <=> ICit (net)

Cit <=> ICit (exch)

ICit + NADP <=> AKG + CO2 + NADPH (net)

ICit + NADP <=> AKG + CO2 + NADPH (exch)

AKG + NAD <=> SucCoA + CO2 + NADH (net)

AKG + NAD <=> SucCoA + CO2 + NADH (exch)

SucCoA + ADP + Pi <=> Suc + ATP (net)

SucCoA + ADP + Pi <=> Suc + ATP (exch)

Suc + FAD <=> Fum + FADH2 (net)

Suc + FAD <=> Fum + FADH2 (exch)

Fum <=> Mal (net)

Fum <=> Mal (exch)

Mal + NAD <=> OAC + NADH (net)

Mal + NAD <=> OAC + NADH (exch)

Glyoxylate Shunt

ICit <=> Glyox + Suc (net)

ICit <=> Glyox + Suc (exch)

AcCoA + Glyox -> Mal

Amphibolic Reactions

Mal + NADP -> Pyr + CO2 + NADPH

Mal + NAD -> Pyr + CO2 + NADH

PEP + CO2 -> OAC + Pi

OAC + ATP -> PEP + CO2 + ADP

Acetate Production

AcCoA + ADP + Pi <=> Ac + ATP (net)

AcCoA + ADP + Pi <=> Ac + ATP (exch)

Amino Acid Biosynthesis

AKG + NADPH + NH3 -> Glu + NADP

Glu + ATP + NH3 -> Gln + ADP + Pi

Glu + 2 NADPH + ATP -> Pro + 2 NADP + ADP + Pi

Glu + CO2 + Gln + NADPH + Asp + AcCoA + 5 ATP -> Arg + AKG + NADP + Fum + Ac + 5ADP + 5Pi

OAC + Glu -> Asp + AKG

Asp + NH3 + 2 ATP -> Asn + 2 ADP + 2 Pi

Pyr + Glu -> Ala + AKG

3PG + Glu + NAD -> Ser + NADH + AKG + Pi

Ser + THF <=> Gly + MEETHF (net)

Ser + THF <=> Gly + MEETHF (exch)

Gly + THF + NAD <=> CO2 + MEETHF + NH3 + NADH (net)

Gly + THF + NAD <=> CO2 + MEETHF + NH3 + NADH (exch)

Thr + NAD -> Gly + AcCoA + NADH

Ser + AcCoA + SO4 + 3 ATP + 4 NADPH -> Cys + Ac + 4 NADP + 3 ADP + 3 Pi

Asp + Pyr + Glu + 2 NADPH + ATP + SucCoA -> LL-DAP + AKG + 2 NADP + ADP + Pi + Suc

LL-DAP -> Lys + CO2

Asp + 2 NADPH + 2 ATP -> Thr + 2 NADP + 2 ADP + 2 Pi

Asp + METHF + Cys + 2 NADPH + ATP + SucCoA -> Met + Pyr + 2 NADP + ADP + Pi

2 Pyr + NADPH + Glu -> Val + CO2 + NADP + AKG

2 Pyr + AcCoA + Glu + NADPH + NAD -> Leu + 2 CO2 + AKG + NADP + NADH

Thr + Pyr + Glu + NADPH -> Ile + CO2 + AKG + NADP + NH3

E4P + 2 PEP + Glu + NADPH + ATP -> Phe + CO2 + AKG + NADP + ADP + 4 Pi

E4P + 2 PEP + Glu + NADPH + NAD + ATP -> Tyr + CO2 + AKG + NADP + NADH + ADP + 4Pi

E4P + 2 PEP + R5P + Ser + Gln + NADPH + 3 ATP -> Trp + CO2 + Pyr + GAP + Glu + NADP + 3ADP + 6Pi

R5P + FTHF + Gln + Asp + 5 ATP + 2 NAD -> His + 2 NADH + AKG + Fum + 5 ADP + 6Pi + THF

One Carbon Metabolism

MEETHF + NADH -> METHF + NAD

MEETHF + NADP -> FTHF + NADPH

Oxidative Phosphorylation

NADH + 0.5 O2 + 1.5 ADP + 1.5 Pi -> NAD + 1.5 ATP

FADH2 + 0.5 O2 + 0.5 ADP + 0.5 Pi -> FAD + 0.5 ATP

Transhydrogenation

NADH + NADP <=> NADPH + NAD (net)

NADH + NADP <=> NADPH + NAD (exch)

ATP Hydrolysis

ATP -> ADP + Pi

Transport

Ac -> Ac.ext

CO2 -> CO2.ext

O2.ext -> O2

NH3.ext -> NH3

SO4.ext -> SO4

Pi.ext -> Pi

CO2.atm + CO2 -> CO2 + CO2.snk

Biomass Formation

0.488 Ala + 0.281 Arg + 0.229 Asn + 0.229 Asp + 0.087 Cys + 0.25 Glu + 0.25 Gln + 0.582 Gly + 0.09 His + 0.276 Ile + 0.428 Leu + 0.326 Lys + 0.146 Met + 0.176 Phe + 0.21 Pro + 0.205 Ser + 0.241 Thr + 0.131 Tyr + 0.402 Val + 0.205 G6P + 0.071 F6P + 0.129 GAP + 0.619 3PG + 0.083 Pyr + 2.51 AcCoA + 0.087 AKG + 0.34 OAC + 0.054 Trp + 0.754 R5P + 0.051 PEP + 33.247 ATP + 5.363 NADPH + 0.443 MEETHF + 1.455 NAD -> 39.683 Biomass + 1.455 NADH + 33.247 ADP + 33.247 Pi + 5.363 NADP + 0.443 THF

A.2 Co-Culture Metabolic Network Model

Glycolysis

PEP.1 + 2 Gluc.Ext + PEP.2 -> G6P.1 + Pyr.1 + G6P.2 + Pyr.2 + X-glc1 + X-glc2

G6P.1 <=> F6P.1 (net)

G6P.1 <=> F6P.1 (exch)

G6P.2 <=> F6P.2 (net)

G6P.2 <=> F6P.2 (exch)

F6P.1 + ATP.1 -> FBP.1 + ADP.1

F6P.2 + ATP.2 -> FBP.2 + ADP.2

FBP.1 <=> DHAP.1 + GAP.1 (net)

FBP.1 <=> DHAP.1 + GAP.1 (exch)

FBP.2 <=> DHAP.2 + GAP.2 (net)

FBP.2 <=> DHAP.2 + GAP.2 (exch)

DHAP.1 <=> GAP.1 (net)

DHAP.1 <=> GAP.1 (exch)

DHAP.2 <=> GAP.2 (net)

DHAP.2 <=> GAP.2 (exch)

GAP.1 + NAD.1 + ADP.1 + Pi.1 <=> 3PG.1 + ATP.1 + NADH.1 (net)

GAP.1 + NAD.1 + ADP.1 + Pi.1 <=> 3PG.1 + ATP.1 + NADH.1 (exch)

GAP.2 + NAD.2 + ADP.2 + Pi.2 <=> 3PG.2 + ATP.2 + NADH.2 (net)

GAP.2 + NAD.2 + ADP.2 + Pi.2 <=> 3PG.2 + ATP.2 + NADH.2 (exch)

3PG.1 <=> PEP.1 (net)

3PG.1 <=> PEP.1 (exch)

3PG.2 <=> PEP.2 (net)

3PG.2 <=> PEP.2 (exch)

PEP.1 + ADP.1 <=> Pyr.1 + ATP.1 (net)

PEP.1 + ADP.1 <=> Pyr.1 + ATP.1 (exch)

PEP.2 + ADP.2 <=> Pyr.2 + ATP.2 (net)

PEP.2 + ADP.2 <=> Pyr.2 + ATP.2 (exch)

Pentose Phosphate Pathway

G6P.1 + NADP.1 -> 6PG.1 + NADPH.1

G6P.2 + NADP.2 -> 6PG.2 + NADPH.2

6PG.1 + NADP.1 -> Ru5P.1 + CO2.1 + NADPH.1

6PG.2 + NADP.2 -> Ru5P.2 + CO2.2 + NADPH.2

Ru5P.1 <=> X5P.1 (net)

Ru5P.1 <=> X5P.1 (exch)

Ru5P.2 <=> X5P.2 (net)

Ru5P.2 <=> X5P.2 (exch)

Ru5P.1 <=> R5P.1 (net)

Ru5P.1 <=> R5P.1 (exch)

Ru5P.2 <=> R5P.2 (net)

Ru5P.2 <=> R5P.2 (exch)

X5P.1 <=> GAP.1 + E-C2.1 (net)

X5P.1 <=> GAP.1 + E-C2.1 (exch)

X5P.2 <=> GAP.2 + E-C2.2 (net)

X5P.2 <=> GAP.2 + E-C2.2 (exch)

F6P.1 <=> E4P.1 + E-C2.1 (net)

F6P.1 <=> E4P.1 + E-C2.1 (exch)

F6P.2 <=> E4P.2 + E-C2.2 (net)

F6P.2 <=> E4P.2 + E-C2.2 (exch)

S7P.1 <=> R5P.1 + E-C2.1 (net)

S7P.1 <=> R5P.1 + E-C2.1 (exch)

S7P.2 <=> R5P.2 + E-C2.2 (net)

S7P.2 <=> R5P.2 + E-C2.2 (exch)

F6P.1 <=> GAP.1 + E-C3.1 (net)

F6P.1 <=> GAP.1 + E-C3.1 (exch)

F6P.2 <=> GAP.2 + E-C3.2 (net)

F6P.2 <=> GAP.2 + E-C3.2 (exch)

S7P.1 <=> E4P.1 + E-C3.1 (net)

S7P.1 <=> E4P.1 + E-C3.1 (exch)

S7P.2 <=> E4P.2 + E-C3.2 (net)

S7P.2 <=> E4P.2 + E-C3.2 (exch)

ED Pathway

6PG.1 -> KDPG.1

6PG.2 -> KDPG.2

KDPG.1 -> GAP.1 + Pyr.1

KDPG.2 -> GAP.2 + Pyr.2

TCA Cycle

Pyr.1 + NAD.1 -> AcCoA.1 + CO2.1 + NADH.1

Pyr.2 + NAD.2 -> AcCoA.2 + CO2.2 + NADH.2

AcCoA.1 + OAC.1 -> Cit.1

AcCoA.2 + OAC.2 -> Cit.2

Cit.1 <=> ICit.1 (net)

Cit.1 <=> ICit.1 (exch)

Cit.2 <=> ICit.2 (net)

Cit.2 <=> ICit.2 (exch)

ICit.1 + NADP.1 <=> AKG.1 + CO2.1 + NADPH.1 (net)

ICit.1 + NADP.1 <=> AKG.1 + CO2.1 + NADPH.1 (exch)

AKG.1 + NAD.1 -> SucCoA.1 + CO2.1 + NADH.1

AKG.2 + NAD.2 -> SucCoA.2 + CO2.2 + NADH.2

SucCoA.1 + ADP.1 + Pi.1 <=> Suc.1 + ATP.1 (net)

SucCoA.1 + ADP.1 + Pi.1 <=> Suc.1 + ATP.1 (exch)

SucCoA.2 + ADP.2 + Pi.2 <=> Suc.2 + ATP.2 (net)

SucCoA.2 + ADP.2 + Pi.2 <=> Suc.2 + ATP.2 (exch)

Suc.1 + FAD.1 <=> Fum.1 + FADH2.1 (net)

Suc.1 + FAD.1 <=> Fum.1 + FADH2.1 (exch)

Suc.2 + FAD.2 <=> Fum.2 + FADH2.2 (net)

Suc.2 + FAD.2 <=> Fum.2 + FADH2.2 (exch)

Fum.1 <=> Mal.1 (net)

Fum.1 <=> Mal.1 (exch)

Fum.2 <=> Mal.2 (net)

Fum.2 <=> Mal.2 (exch)

Mal.1 + NAD.1 <=> OAC.1 + NADH.1 (net)

Mal.1 + NAD.1 <=> OAC.1 + NADH.1 (exch)

Mal.2 + NAD.2 <=> OAC.2 + NADH.2 (net)

Mal.2 + NAD.2 <=> OAC.2 + NADH.2 (exch)

Glyoxylate Shunt

ICit.1 <=> Glyox.1 + Suc.1 (net)

ICit.1 <=> Glyox.1 + Suc.1 (exch)

ICit.2 <=> Glyox.2 + Suc.2 (net)

ICit.2 <=> Glyox.2 + Suc.2 (exch)

AcCoA.1 + Glyox.1 -> Mal.1

AcCoA.2 + Glyox.2 -> Mal.2

Amphibolic Reactions

Mal.1 + NADP.1 -> Pyr.1 + CO2.1 + NADPH.1

Mal.2 + NADP.2 -> Pyr.2 + CO2.2 + NADPH.2

PEP.1 + CO2.1 -> OAC.1 + Pi.1

PEP.2 + CO2.2 -> OAC.2 + Pi.2

OAC.1 + ATP.1 -> PEP.1 + CO2.1 + ADP.1

OAC.2 + ATP.2 -> PEP.2 + CO2.2 + ADP.2

Acetate Production

AcCoA.1 + ADP.1 + Pi.1 <=> Ac.1 + ATP.1 (net)

AcCoA.1 + ADP.1 + Pi.1 <=> Ac.1 + ATP.1 (exch)

AcCoA.2 + ADP.2 + Pi.2 <=> Ac.2 + ATP.2 (net)

AcCoA.2 + ADP.2 + Pi.2 <=> Ac.2 + ATP.2 (exch)

Amino Acid Biosynthesis

AKG.1 + NADPH.1 + NH3.1 -> Glu.1 + NADP.1

AKG.2 + NADPH.2 + NH3.2 -> Glu.2 + NADP.2

Glu.1 + ATP.1 + NH3.1 -> Gln.1 + ADP.1 + Pi.1

Glu.2 + ATP.2 + NH3.2 -> Gln.2 + ADP.2 + Pi.2

Glu.1 + 2 NADPH.1 + ATP.1 -> Pro.1 + 2 NADP.1 + ADP.1 + Pi.1

Glu.2 + 2 NADPH.2 + ATP.2 -> Pro.2 + 2 NADP.2 + Pi.2 + ADP.2

Glu.1 + CO2.1 + Gln.1 + NADPH.1 + Asp.1 + AcCoA.1 + 5 ATP.1 -> Arg.1 + AKG.1 + NADP.1 + Fum.1 + Ac.1 + 5 ADP.1 + 5 Pi.1

Glu.2 + CO2.2 + Gln.2 + NADPH.2 + Asp.2 + AcCoA.2 + 5 ATP.2 -> Arg.2 + AKG.2 + NADP.2 + Fum.2 + Ac.2 + 5 ADP.2 + 5 Pi.2

OAC.1 + Glu.1 -> Asp.1 + AKG.1

OAC.2 + Glu.2 -> Asp.2 + AKG.2

Asp.1 + NH3.1 + 2 ATP.1 -> Asn.1 + 2 ADP.1 + 2 Pi.1

Asp.2 + NH3.2 + 2 ATP.2 -> Asn.2 + 2 ADP.2 + 2 Pi.2

Pyr.1 + Glu.1 -> Ala.1 + AKG.1

Pyr.2 + Glu.2 -> Ala.2 + AKG.2

3PG.1 + Glu.1 + NAD.1 -> Ser.1 + NADH.1 + AKG.1 + Pi.1

3PG.2 + Glu.2 + NAD.2 -> Ser.2 + NADH.2 + AKG.2 + Pi.2

Ser.1 + THF.1 <=> Gly.1 + MEETHF.1 (net)

Ser.1 + THF.1 <=> Gly.1 + MEETHF.1 (exch)

Ser.2 + THF.2 <=> Gly.2 + MEETHF.2 (net)

Ser.2 + THF.2 <=> Gly.2 + MEETHF.2 (exch)

Gly.1 + THF.1 + NAD.1 <=> CO2.1 + MEETHF.1 + NH3.1 + NADH.1 (net)

Gly.1 + THF.1 + NAD.1 <=> CO2.1 + MEETHF.1 + NH3.1 + NADH.1 (exch)

Gly.2 + THF.2 + NAD.2 <=> CO2.2 + MEETHF.2 + NH3.2 + NADH.2 (net)

Gly.2 + THF.2 + NAD.2 <=> CO2.2 + MEETHF.2 + NH3.2 + NADH.2 (exch)

Thr.1 + NAD.1 -> Gly.1 + AcCoA.1 + NADH.1

Thr.2 + NAD.2 -> Gly.2 + AcCoA.2 + NADH.2

Ser.1 + AcCoA.1 + SO4.1 + 3 ATP.1 + 4 NADPH.1 -> Cys.1 + Ac.1 + 4 NADP.1 + 3 ADP.1 + 3 Pi.1

Ser.2 + AcCoA.2 + SO4.2 + 3 ATP.2 + 4 NADPH.2 -> Cys.2 + Ac.2 + 4 NADP.2 + 3 ADP.2 + 3 Pi.2

Asp.1 + Pyr.1 + Glu.1 + 2 NADPH.1 + ATP.1 + SucCoA.1 -> LL-DAP.1 + AKG.1 + 2 NADP.1 + ADP.1 + Pi.1 + Suc.1

Asp.2 + Pyr.2 + Glu.2 + 2 NADPH.2 + ATP.2 + SucCoA.2 -> LL-DAP.2 + AKG.2 + 2 NADP.2 + ADP.2 + Pi.2 + Suc.2

LL-DAP.1 -> Lys.1 + CO2.1

LL-DAP.2 -> Lys.2 + CO2.2

Asp.1 + 2 NADPH.1 + 2 ATP.1 -> Thr.1 + 2 NADP.1 + 2 ADP.1 + 2 Pi.1

Asp.2 + 2 NADPH.2 + 2 ATP.2 -> Thr.2 + 2 NADP.2 + 2 ADP.2 + 2 Pi.2

Asp.1 + METHF.1 + Cys.1 + 2 NADPH.1 + ATP.1 + SucCoA.1 -> Met.1 + Pyr.1 + 2 NADP.1 + ADP.1 + Pi.1 + Suc.1 + NH3.1 + THF.1

Asp.2 + METHF.2 + Cys.2 + 2 NADPH.2 + ATP.2 + SucCoA.2 -> Met.2 + Pyr.2 + 2 NADP.2 + ADP.2 + Pi.2 + Suc.2 + NH3.2 + THF.2

E4P.1 + 2 PEP.1 + Glu.1 + NADPH.1 + ATP.1 -> Phe.1 + CO2.1 + AKG.1 + NADP.1

E4P.2 + 2 PEP.2 + Glu.2 + NADPH.2 + ATP.2 -> Phe.2 + CO2.2 + AKG.2 + NADP.2

E4P.1 + 2 PEP.1 + Glu.1 + NADPH.1 + NAD.1 + ATP.1 -> Tyr.1 + CO2.1 + AKG.1 + NADP.1 + NADH.1 + ADP.1 + 4 Pi.1

E4P.2 + 2 PEP.2 + Glu.2 + NADPH.2 + NAD.2 + ATP.2 -> Tyr.2 + CO2.2 + AKG.2 + NADP.2 + NADH.2 + ADP.2 + 4 Pi.2

E4P.1 + 2 PEP.1 + R5P.1 + Ser.1 + Gln.1 + NADPH.1 + 3 ATP.1 -> Trp.1 + CO2.1 + Pyr.1 + GAP.1 + Glu.1 + NADP.1 + 3 ADP.1 + 6 Pi.1

E4P.2 + 2 PEP.2 + R5P.2 + Ser.2 + Gln.2 + NADPH.2 + 3 ATP.2 -> Trp.2 + CO2.2 + Pyr.2 + GAP.2 + Glu.2 + NADP.2 + 3 ADP.2 + 6 Pi.2

R5P.1 + FTHF.1 + Gln.1 + Asp.1 + 5 ATP.1 + 2 NAD.1 -> His.1 + 2 NADH.1 + AKG.1 + Fum.1 + 5 ADP.1 + 6 Pi.1 + THF.1

R5P.2 + FTHF.2 + Gln.2 + Asp.2 + 5 ATP.2 + 2 NAD.2 -> His.2 + 2 NADH.2 + AKG.2 + Fum.2 + 5 ADP.2 + 6 Pi.2 + THF.2

kVal.1 + Glu.1 <=> Val.1 + AKG.1 (net)

kVal.1 + Glu.1 <=> Val.1 + AKG.1 (exch)

kVal.2 + Glu.2 <=> Val.2 + AKG.2 (net)

kVal.2 + Glu.2 <=> Val.2 + AKG.2 (exch)

kVal.1 + AcCoA.1 + NAD.1 + Glu.1 -> Leu.1 + CO2.1 + NADH.1 + AKG.1

kVal.2 + AcCoA.2 + NAD.2 + Glu.2 -> Leu.2 + CO2.2 + NADH.2 + AKG.2

2 Pyr.1 -> aclact.1 + CO2.1

2 Pyr.2 -> aclact.2 + CO2.2

aclact.2 + NADPH.2 -> kVal.2 + NADP.2

Thr.1 + Pyr.1 -> acbut.1 + CO2.1

Thr.2 + Pyr.2 -> acbut.2 + CO2.2

acbut.2 + NADPH.2 -> kIle.2 + NADP.2

kIle.1 + Glu.1 -> Ile.1 + AKG.1

kIle.2 + Glu.2 -> Ile.2 + AKG.2

One Carbon Metabolism

MEETHF.1 + NADH.1 -> METHF.1 + NAD.1

MEETHF.2 + NADH.2 -> METHF.2 + NAD.2

MEETHF.1 + NADP.1 -> FTHF.1 + NADPH.1

MEETHF.2 + NADP.2 -> FTHF.2 + NADPH.2

Oxidative Phosphorylation

NADH.1 + 0.5 O2.1 + 2 ADP.1 + 2 Pi.1 -> NAD.1 + 2 ATP.1

NADH.2 + 0.5 O2.2 + 2 ADP.2 + 2 Pi.2 -> NAD.2 + 2 ATP.2

FADH2.1 + 0.5 O2.1 + ADP.1 + Pi.1 -> FAD.1 + ATP.1

FADH2.2 + 0.5 O2.2 + ADP.2 + Pi.2 -> FAD.2 + ATP.2

Transhydrogenation

NADH.1 + NADP.1 <=> NADPH.1 + NAD.1 (net)

NADH.1 + NADP.1 <=> NADPH.1 + NAD.1 (exch)

NADH.2 + NADP.2 <=> NADPH.2 + NAD.2 (net)

NADH.2 + NADP.2 <=> NADPH.2 + NAD.2 (exch)

ATP Hydrolysis

ATP.1 -> ADP.1 + Pi.1

ATP.2 -> ADP.2 + Pi.2

Transport

Ac.1 -> Ac.Ext + X-ac1

Ac.2 -> Ac.Ext + X-ac2

CO2.1 -> CO2.Ext

CO2.2 -> CO2.Ext

O2.Ext -> O2.1

O2.Ext -> O2.2

NH3.Ext -> NH3.1

NH3.Ext -> NH3.2

SO4.Ext -> SO4.1

SO4.Ext -> SO4.2

CO2.M0 + CO2.1 -> CO2.1 + CO2.snk

CO2.M0 + CO2.2 -> CO2.2 + CO2.snk

Pi.Ext -> Pi.1

Pi.Ext -> Pi.2

Biomass Formation

0.488 Ala.1 + 0.281 Arg.1 + 0.229 Asn.1 + 0.229 Asp.1 + 0.087 Cys.1 + 0.25 Glu.1 + 0.25 Gln.1 + 0.582 Gly.1 + 0.02 His.1 + 0.276 Ile.1 + 0.428 Leu.1 + 0.326 Lys.1 + 0.146 Met.1 + 0.176 Phe.1 + 0.21 Pro.1 + 0.205 Ser.1 + 0.241 Thr.1 + 0.131 Tyr.1 + 0.402 Val.1 + 0.205 G6P.1 + 0.071 F6P.1 + 0.129 GAP.1 + 0.619 3PG.1 + 0.083 Pyr.1 + 2.51 AcCoA.1 + 0.087 AKG.1 + 0.34 OAC.1 + 0.054 Trp.1 + 0.754 R5P.1 + 0.051 PEP.1 + 33.247 ATP.1 + 5.363 NADPH.1 + 0.443 MEETHF.1 + 1.455 NAD.1 -> 1.455 NADH.1 + 33.247 ADP.1 + 33.247 Pi.1 + 0.443 THF.1 + 5.363 NADP.1 + 39.683 Biomass.1

0.488 Ala.2 + 0.281 Arg.2 + 0.229 Asn.2 + 0.229 Asp.2 + 0.087 Cys.2 + 0.25 Glu.2 + 0.25 Gln.2 + 0.582 Gly.2 + 0.02 His.2 + 0.276 Ile.2 + 0.428 Leu.2 + 0.326 Lys.2 + 0.146 Met.2 + 0.176 Phe.2 + 0.21 Pro.2 + 0.205 Ser.2 + 0.241 Thr.2 + 0.131 Tyr.2 + 0.402 Val.2 + 0.205 G6P.2 + 0.071 F6P.2 + 0.129 GAP.2 + 0.619 3PG.2 + 0.083 Pyr.2 + 2.51 AcCoA.2 + 0.087 AKG.2 + 0.34 OAC.2 + 0.054 Trp.2 + 0.754 R5P.2 + 0.051 PEP.2 + 33.247 ATP.2 + 5.363 NADPH.2 + 0.443 MEETHF.2 + 1.455 NAD.2 -> 1.455 NADH.2 + 33.247 ADP.2 + 33.247 Pi.2 + 0.443 THF.2 + 5.363 NADP.2 + 39.683 Biomass.2

8 AcCoA.1 <=> C16:0.1 (net)

8 AcCoA.1 <=> C16:0.1 (exch)

8 AcCoA.2 <=> C16:0.2 (net)

8 AcCoA.2 <=> C16:0.2 (exch)

Co-culture Exchange Fluxes

Leu.1 <=> Leu.2 (net)

Leu.1 <=> Leu.2 (exch)

Thr.1 <=> Thr.2 (net)

Thr.1 <=> Thr.2 (exch)

Asp.1 <=> Asp.2 (net)

Asp.1 <=> Asp.2 (exch)

Glu.1 <=> Glu.2 (net)

Glu.1 <=> Glu.2 (exch)

kVal.1 <=> kVal.2 (net)

kVal.1 <=> kVal.2 (exch)

aclact.1 <=> aclact.2 (net)

aclact.1 <=> aclact.2 (exch)

acbut.1 <=> acbut.2 (net)

acbut.1 <=> acbut.2 (exch)

kIle.1 <=> kIle.2 (net)

kIle.1 <=> kIle.2 (exch)

Pyr.1 <=> Pyr.2 (net)

Pyr.1 <=> Pyr.2 (exch)

Co-culture reaction

Ala.s1 + Gly.s1 + Val.s1 + Leu.s1 + Ile.s1 + Pro.s1 + Met.s1 + Ser.s1 + Thr.s1 + Phe.s1 + Asp.s1 + Glu.s1 + Lys.s1 + His.s1 + Tyr.s1 -> X-s1

Ala.s2 + Gly.s2 + Val.s2 + Leu.s2 + Ile.s2 + Pro.s2 + Met.s2 + Ser.s2 + Thr.s2 + Phe.s2 + Asp.s2 + Glu.s2 + Lys.s2 + His.s2 + Tyr.s2 -> X-s2

Ala.1 + Gly.1 + Val.1 + Leu.1 + Ile.1 + Pro.1 + Met.1 + Ser.1 + Thr.1 + Phe.1 + Asp.1 + Glu.1 + Lys.1 + His.1 + Tyr.1 -> Ala.s1 + Gly.s1 + Val.s1 + Leu.s1 + Ile.s1 + Pro.s1 + Met.s1 + Ser.s1 + Thr.s1 + Phe.s1 + Asp.s1 + Glu.s1 + Lys.s1 + His.s1 + Tyr.s1 + Ala.1 + Gly.1 + Val.1 + Leu.1 + Ile.1 + Pro.1 + Met.1 + Ser.1 + Thr.1 + Phe.1 + Asp.1 + Glu.1 + Lys.1 + His.1 + Tyr.1

Ala.1 + Gly.1 + Val.1 + Leu.1 + Ile.1 + Pro.1 + Met.1 + Ser.1 + Thr.1 + Phe.1 + Asp.1 + Glu.1 + Lys.1 + His.1 + Tyr.1 -> Ala.s2 + Gly.s2 + Val.s2 + Leu.s2 + Ile.s2 + Pro.s2 + Met.s2 + Ser.s2 + Thr.s2 + Phe.s2 + Asp.s2 + Glu.s2 + Lys.s2 + His.s2 + Tyr.s2 + Ala.1 + Gly.1 + Val.1 + Leu.1 + Ile.1 + Pro.1 + Met.1 + Ser.1 + Thr.1 + Phe.1 + Asp.1 + Glu.1 + Lys.1 + His.1 + Tyr.1

Ala.2 + Gly.2 + Val.2 + Leu.2 + Ile.2 + Pro.2 + Met.2 + Ser.2 + Thr.2 + Phe.2 + Asp.2 + Glu.2 + Lys.2 + His.2 + Tyr.2 -> Ala.s1 + Gly.s1 + Val.s1 + Leu.s1 + Ile.s1 + Pro.s1 + Met.s1 + Ser.s1 + Thr.s1 + Phe.s1 + Asp.s1 + Glu.s1 + Lys.s1 + His.s1 + Tyr.s1 + Ala.2 + Gly.2 + Val.2 + Leu.2 + Ile.2 + Pro.2 + Met.2 + Ser.2 + Thr.2 + Phe.2 + Asp.2 + Glu.2 + Lys.2 + His.2 + Tyr.2

Ala.2 + Gly.2 + Val.2 + Leu.2 + Ile.2 + Pro.2 + Met.2 + Ser.2 + Thr.2 + Phe.2 + Asp.2 + Glu.2 + Lys.2 + His.2 + Tyr.2 -> Ala.s2 + Gly.s2 + Val.s2 + Leu.s2 + Ile.s2 + Pro.s2 + Met.s2 + Ser.s2 + Thr.s2 + Phe.s2 + Asp.s2 + Glu.s2 + Lys.s2 + His.s2 + Tyr.s2 + Ala.2 + Gly.2 + Val.2 + Leu.2 + Ile.2 + Pro.2 + Met.2 + Ser.2 + Thr.2 + Phe.2 + Asp.2 + Glu.2 + Lys.2 + His.2 + Tyr.2

C16:0.1 -> C16:0.s1 + C16:0.1 + F-s1

C16:0.1 -> C16:0.s2 + C16:0.1 + F-s2

C16:0.2 -> C16:0.s1 + C16:0.2 + F-s1

C16:0.2 -> C16:0.s2 + C16:0.2 + F-s2

Bibliography

Akashi, H. and Gojobori, T. (2002) 'Metabolic efficiency and amino acid composition in the proteomes of Escherichia coli and Bacillus subtilis', *Proceedings of the National Academy of Sciences of the United States of America*, 99(6). doi: 10.1073/pnas.062526999.

Akram, M. (2013) 'Mini-review on glycolysis and cancer', *Journal of Cancer Education*. doi: 10.1007/s13187-013-0486-9.

Amann, R. I., Ludwig, W. and Schleifer, K. H. (1995) 'Phylogenetic identification and in situ detection of individual microbial cells without cultivation', *Microbiological Reviews*. doi: 10.1128/mmbr.59.1.143-169.1995.

Antoniewicz, M. R. (2013) '13C metabolic flux analysis: Optimal design of isotopic labeling experiments', *Current Opinion in Biotechnology*. doi: 10.1016/j.copbio.2013.02.003.

Antoniewicz, M. R. (2015) 'Methods and advances in metabolic flux analysis: a mini-review', *Journal of Industrial Microbiology and Biotechnology*, 42(3). doi: 10.1007/s10295-015-1585-x.

Antoniewicz, M. R. (2018) 'A guide to 13C metabolic flux analysis for the cancer biologist', *Experimental and Molecular Medicine*. doi: 10.1038/s12276-018-0060-y.

Antoniewicz, M. R. (2020) 'A guide to deciphering microbial interactions and metabolic fluxes in microbiome communities', *Current Opinion in Biotechnology*. doi: 10.1016/j.copbio.2020.07.001.

Antoniewicz, M. R. (2021) 'A guide to metabolic flux analysis in metabolic engineering: Methods, tools and applications', *Metabolic Engineering*. doi: 10.1016/j.ymben.2020.11.002.

Antoniewicz, M. R., Kelleher, J. K. and Stephanopoulos, G. (2006) 'Determination of confidence intervals of metabolic fluxes estimated from stable isotope measurements', *Metabolic Engineering*, 8(4). doi: 10.1016/j.ymben.2006.01.004.

Antoniewicz, M. R., Kelleher, J. K. and Stephanopoulos, G. (2007a) 'Accurate assessment of amino acid mass isotopomer distributions for metabolic flux analysis', *Analytical Chemistry*, 79(19). doi: 10.1021/ac0708893.

Antoniewicz, M. R., Kelleher, J. K. and Stephanopoulos, G. (2007b) 'Elementary metabolite units (EMU): A novel framework for modeling isotopic distributions', *Metabolic Engineering*, 9(1). doi: 10.1016/j.ymben.2006.09.001.

Ashworth, J. M. and Kornberg, H. L. (1966) 'The anaplerotic fixation of carbon dioxide by Escherichia coli.', *Proceedings of the Royal Society of London. Series B, Containing papers of a Biological character. Royal Society (Great Britain)*, 165(999). doi: 10.1098/rspb.1966.0063.

Bailey, J. E. (1991) 'Toward a science of metabolic engineering', *Science*, 252(5013). doi: 10.1126/science.2047876.

Barbier, M. and Damron, F. H. (2016) 'Rainbow vectors for broad-range bacterial fluorescence labeling', *PLoS ONE*, 11(3). doi: 10.1371/journal.pone.0146827.

Basan, M. *et al.* (2015) 'Overflow metabolism in Escherichia coli results from efficient proteome allocation', *Nature*, 528(7580). doi: 10.1038/nature15765.

Basile, A. *et al.* (2020) 'Revealing metabolic mechanisms of interaction in the anaerobic digestion microbiome by flux balance analysis', *Metabolic Engineering*, 62. doi: 10.1016/j.ymben.2020.08.013.

Bertels, F., Merker, H. and Kost, C. (2012) 'Design and characterization of auxotrophy-based amino acid biosensors', *PLoS ONE*, 7(7). doi: 10.1371/journal.pone.0041349.

Bloemberg, G. V. *et al.* (1997) 'Green fluorescent protein as a marker for Pseudomonas spp.', *Applied and Environmental Microbiology*, 63(11). doi: 10.1128/aem.63.11.4543-4551.1997.

Bonomo, J. and Gill, R. T. (2005) 'Amino acid content of recombinant proteins influences the metabolic burden response', *Biotechnology and Bioengineering*, 90(1). doi: 10.1002/bit.20436.

Borkowski, O. *et al.* (2016) 'Overloaded and stressed: whole-cell considerations for bacterial synthetic biology', *Current Opinion in Microbiology*. doi: 10.1016/j.mib.2016.07.009.

Bowman, E. K. and Alper, H. S. (2020) 'Microdroplet-Assisted Screening of Biomolecule Production for Metabolic Engineering Applications', *Trends in Biotechnology*. doi: 10.1016/j.tibtech.2019.11.002.

Burgin, A. J. *et al.* (2011) 'Beyond carbon and nitrogen: How the microbial energy economy couples elemental cycles in diverse ecosystems', in *Frontiers in Ecology and the Environment*. doi: 10.1890/090227.

Cardinale, S. and Arkin, A. P. (2012) 'Contextualizing context for synthetic biology - identifying causes of failure of synthetic biological systems', *Biotechnology Journal*. doi: 10.1002/biot.201200085.

Carneiro, S., Ferreira, E. C. and Rocha, I. (2013) 'Metabolic responses to recombinant bioprocesses in Escherichia coli', *Journal of Biotechnology*, 164(3). doi: 10.1016/j.jbiotec.2012.08.026.

Chalfie, M. *et al.* (1994) 'Green fluorescent protein as a marker for gene expression', *Science*, 263(5148). doi: 10.1126/science.8303295.

Chang, D. E. *et al.* (2004) 'Carbon nutrition of Escherichia coli in the mouse intestine', *Proceedings of the National Academy of Sciences of the United States of America*, 101(19). doi: 10.1073/pnas.0307888101.

Chaudhry, R. and Varacallo, M. (2018) *Biochemistry, Glycolysis*, *StatPearls*.

Che, S. and Men, Y. (2019) 'Synthetic microbial consortia for biosynthesis and biodegradation: promises and challenges', *Journal of Industrial Microbiology and Biotechnology*, 46(9–10). doi: 10.1007/s10295-019-02211-4.

Chou, C. P. (2007) 'Engineering cell physiology to enhance recombinant protein production in Escherichia coli', *Applied Microbiology and Biotechnology*. doi: 10.1007/s00253-007-1039-0.

Conway, T. (1992) 'The Entner-Doudoroff pathway: history, physiology and molecular biology', *FEMS Microbiology Letters*, 103(1). doi: 10.1016/0378-1097(92)90334-K.

Crown, S. B. and Antoniewicz, M. R. (2012) 'Selection of tracers for 13C-Metabolic Flux Analysis using Elementary Metabolite Units (EMU) basis vector methodology', *Metabolic Engineering*, 14(2). doi: 10.1016/j.ymben.2011.12.005.

Crown, S. B. and Antoniewicz, M. R. (2013) 'Parallel labeling experiments and metabolic flux analysis: Past, present and future methodologies', *Metabolic Engineering*. doi: 10.1016/j.ymben.2012.11.010.

Crown, S. B., Long, C. P. and Antoniewicz, M. R. (2016) 'Optimal tracers for parallel labeling experiments and 13C metabolic flux analysis: A new precision and synergy scoring system', *Metabolic Engineering*, 38. doi: 10.1016/j.ymben.2016.06.001.

D'Onofrio, A. *et al.* (2010) 'Siderophores from Neighboring Organisms Promote the Growth of Uncultured Bacteria', *Chemistry and Biology*, 17(3). doi: 10.1016/j.chembiol.2010.02.010.

D'Souza, G. *et al.* (2014) 'Less is more: Selective advantages can explain the prevalent loss of biosynthetic genes in bacteria', *Evolution*. doi: 10.1111/evo.12468.
Dai, Z. and Locasale, J. W. (2017) 'Understanding metabolism with flux analysis: From theory to application', *Metabolic Engineering*. doi: 10.1016/j.ymben.2016.09.005.
Dandie, C. E., Thomas, S. M. and McClure, N. C. (2001) 'Comparison of a range of green fluorescent protein-tagging vectors for monitoring a microbial inoculant in soil', *Letters in Applied Microbiology*, 32(1). doi: 10.1046/j.1472-765X.2001.00848.x.
Dien, L. T. H., Ravel, J. M. and Shive, W. (1954) 'Some inhibitory interrelationships among leucine, isoleucine and valine', *Archives of Biochemistry and Biophysics*, 49(2). doi: 10.1016/0003-9861(54)90199-X.
Dietrich, J. A., McKee, A. E. and Keasling, J. D. (2010) 'High-throughput metabolic engineering: Advances in small-molecule screening and selection', *Annual Review of Biochemistry*. doi: 10.1146/annurev-biochem-062608-095938.
Dolan, S. K. and Welch, M. (2018) 'The Glyoxylate Shunt, 60 Years on', *Annual Review of Microbiology*. doi: 10.1146/annurev-micro-090817-062257.
Embree, M. *et al.* (2015) 'Networks of energetic and metabolic interactions define dynamics in microbial communities', *Proceedings of the National Academy of Sciences of the United States of America*, 112(50). doi: 10.1073/pnas.1506034112.
Farmer, W. R. and Liao, J. C. (1997) 'Reduction of aerobic acetate production by Escherichia coli', *Applied and Environmental Microbiology*, 63(8). doi: 10.1128/aem.63.8.3205-3210.1997.
Faust, K. and Raes, J. (2012) 'Microbial interactions: From networks to models', *Nature Reviews Microbiology*. doi: 10.1038/nrmicro2832.
Feilmeier, B. J. *et al.* (2000) 'Green fluorescent protein functions as a reporter for protein localization in Escherichia coli', *Journal of Bacteriology*, 182(14). doi: 10.1128/JB.182.14.4068-4076.2000.
Feng, X. *et al.* (2012) 'MicrobesFlux: a web platform for drafting metabolic models from the KEGG database', *BMC Systems Biology*, 6. doi: 10.1186/1752-0509-6-94.
Fernandez, C. A. *et al.* (1996) 'Correction of 13C mass isotopomer distributions for natural stable isotope abundance', *Journal of Mass Spectrometry*, 31(3). doi: 10.1002/(SICI)1096-9888(199603)31:3<255::AID-JMS290>3.0.CO;2-3.

Fester, T. *et al.* (2014) 'Plant-microbe interactions as drivers of ecosystem functions relevant for the biodegradation of organic contaminants', *Current Opinion in Biotechnology*. doi: 10.1016/j.copbio.2014.01.017.

Fischer, E. and Sauer, U. (2003) 'Metabolic flux profiling of Escherichia coli mutants in central carbon metabolism using GC-MS', *European Journal of Biochemistry*, 270(5). doi: 10.1046/j.1432-1033.2003.03448.x.

Fritts, R. K., McCully, A. L. and McKinlay, J. B. (2021) 'Extracellular Metabolism Sets the Table for Microbial Cross-Feeding', *Microbiology and Molecular Biology Reviews*, 85(1). doi: 10.1128/mmbr.00135-20.

Gabrielli, N. *et al.* (2023) ' Unravelling metabolic cross-feeding in a yeast–bacteria community using 13 C -based proteomics ', *Molecular Systems Biology*, 19(4). doi: 10.15252/msb.202211501.

Gandhi, M. *et al.* (2001) 'Use of green fluorescent protein expressing Salmonella Stanley to investigate survival, spatial location, and control on alfalfa sprouts', *Journal of Food Protection*, 64(12). doi: 10.4315/0362-028X-64.12.1891.

Garrett, W. S. (2015) 'Cancer and the microbiota', *Science*, 348(6230). doi: 10.1126/science.aaa4972.

Gebreselassie, N. A. and Antoniewicz, M. R. (2015) '13C-metabolic flux analysis of co-cultures: A novel approach', *Metabolic Engineering*. doi: 10.1016/j.ymben.2015.07.005.

Gerdes, H. H. and Kaether, C. (1996) 'Green fluorescent protein: Applications in cell biology', in *FEBS Letters*. doi: 10.1016/0014-5793(96)00586-8.

Germerodt, S. *et al.* (2016) 'Pervasive Selection for Cooperative Cross-Feeding in Bacterial Communities', *PLoS Computational Biology*, 12(6). doi: 10.1371/journal.pcbi.1004986.

Ghosh, A. *et al.* (2014) 'A Peptide-Based Method for 13C Metabolic Flux Analysis in Microbial Communities', *PLoS Computational Biology*, 10(9). doi: 10.1371/journal.pcbi.1003827.

Glick, B. R. (1995) 'Metabolic load and heterologous gene expression', *Biotechnology Advances*. doi: 10.1016/0734-9750(95)00004-A.

Gopalakrishnan, S. and Maranas, C. D. (2015) '13C metabolic flux analysis at a genome-scale', *Metabolic Engineering*, 32. doi: 10.1016/j.ymben.2015.08.006.

Gottstein, W. *et al.* (2016) 'Constraint-based stoichiometric modelling from single organisms to microbial communities', *Journal of the Royal Society Interface*. doi: 10.1098/rsif.2016.0627.

Goudar, C. *et al.* (2010) 'Metabolic flux analysis of CHO cells in perfusion culture by metabolite balancing and 2D [13C, 1H] COSY NMR spectroscopy', *Metabolic Engineering*, 12(2). doi: 10.1016/j.ymben.2009.10.007.

Guardiola, J. *et al.* (1974) 'Multiplicity of isoleucine, leucine, and valine transport systems in Escherichia coli K 12', *Journal of Bacteriology*, 117(2). doi: 10.1128/jb.117.2.382-392.1974.

Guest, J. R. and Russell, G. C. (1992) 'Complexes and Complexities of the Citric Acid Cycle in Escherichia coli', in *Current Topics in Cellular Regulation*. doi: 10.1016/B978-0-12-152833-1.50018-6.

GUNSALUS, I. C., HORECKER, B. L. and WOOD, W. A. (1955) 'Pathways of carbohydrate metabolism in microorganisms.', *Bacteriological reviews*, 19(2). doi: 10.1128/mmbr.19.2.79-128.1955.

Haddadin, F. T. and Harcum, S. W. (2005) 'Transcriptome profiles for high-cell-density recombinant and wild-type Escherichia coli', *Biotechnology and Bioengineering*, 90(2). doi: 10.1002/bit.20340.

Harcombe, W. R. *et al.* (2014) 'Metabolic resource allocation in individual microbes determines ecosystem interactions and spatial dynamics', *Cell Reports*, 7(4). doi: 10.1016/j.celrep.2014.03.070.

Henson, M. A. and Hanly, T. J. (2014) 'Dynamic flux balance analysis for synthetic microbial communities', *IET Systems Biology*, 8(5). doi: 10.1049/iet-syb.2013.0021.

Hollinshead, W. D. *et al.* (2016) 'Examining Escherichia coli glycolytic pathways, catabolite repression, and metabolite channeling using Δpfk mutants', *Biotechnology for Biofuels*, 9(1). doi: 10.1186/s13068-016-0630-y.

Hugenholtz, P., Goebel, B. M. and Pace, N. R. (1998) 'Impact of culture-independent studies on the emerging phylogenetic view of bacterial diversity', *Journal of Bacteriology*. doi: 10.1128/jb.180.18.4765-4774.1998.

Huttenhower, C. *et al.* (2012) 'Structure, function and diversity of the healthy human microbiome', *Nature*, 486(7402). doi: 10.1038/nature11234.

Jagmann, N. and Philipp, B. (2014) 'Design of synthetic microbial communities for biotechnological production processes', *Journal of Biotechnology*, 184. doi: 10.1016/j.jbiotec.2014.05.019.

Johns, N. I. *et al.* (2016) 'Principles for designing synthetic microbial communities', *Current Opinion in Microbiology*. doi: 10.1016/j.mib.2016.03.010.
Jones, R. G. (1967) 'Ubiquinone deficiency in an auxotroph of Escherichia coli requiring 4-hydroxybenzoic acid.', *The Biochemical journal*. doi: 10.1042/bj1030714.
Judge, A. and Dodd, M. S. (2020) 'Metabolism', *Essays in Biochemistry*, pp. 607–647. doi: 10.1042/EBC20190041.
Jullesson, D. *et al.* (2015) 'Impact of synthetic biology and metabolic engineering on industrial production of fine chemicals', *Biotechnology Advances*. doi: 10.1016/j.biotechadv.2015.02.011.
Kaleta, C. *et al.* (2013) 'Metabolic costs of amino acid and protein production in Escherichia coli', *Biotechnology Journal*, 8(9). doi: 10.1002/biot.201200267.
Kanehisa, M. *et al.* (2012) 'KEGG for integration and interpretation of large-scale molecular data sets', *Nucleic Acids Research*, 40(D1). doi: 10.1093/nar/gkr988.
Khandelwal, R. A. *et al.* (2013) 'Community Flux Balance Analysis for Microbial Consortia at Balanced Growth', *PLoS ONE*, 8(5). doi: 10.1371/journal.pone.0064567.
Klitgord, N. and Segrè, D. (2010) 'Environments that induce synthetic microbial ecosystems', *PLoS Computational Biology*, 6(11). doi: 10.1371/journal.pcbi.1001002.
Kornberg, H. L. (1966) 'The role and control of the glyoxylate cycle in Escherichia coli.', *The Biochemical journal*. doi: 10.1042/bj0990001.
Kouzuma, A., Kato, S. and Watanabe, K. (2015) 'Microbial interspecies interactions: Recent findings in syntrophic consortia', *Frontiers in Microbiology*. doi: 10.3389/fmicb.2015.00477.
Kruger, N. J. and Von Schaewen, A. (2003) 'The oxidative pentose phosphate pathway: Structure and organisation', *Current Opinion in Plant Biology*. doi: 10.1016/S1369-5266(03)00039-6.
Kumar, A. and Chordia, N. (2017) 'Role of Microbes in Human Health', *Applied Microbiology: Open Access*. doi: 10.4172/2471-9315.1000131.
Kumar, M. *et al.* (2019) 'Modelling approaches for studying the microbiome', *Nature Microbiology*. doi: 10.1038/s41564-019-0491-9.
Lane, N. (2015) 'The unseen World: Reflections on Leeuwenhoek (1677) "Concerning little animals"', *Philosophical Transactions of the Royal Society B: Biological Sciences*. doi: 10.1098/rstb.2014.0344.

Lawson, C. E. *et al.* (2019) 'Common principles and best practices for engineering microbiomes', *Nature Reviews Microbiology*. doi: 10.1038/s41579-019-0255-9.
Lee, J. M., Gianchandani, E. P. and Papin, J. A. (2006) 'Flux balance analysis in the era of metabolomics', *Briefings in Bioinformatics*. doi: 10.1093/bib/bbl007.
Leewenhoeck, A. van (1676) 'Concerning little Animals by him observed in Rain- Well- Sea- and Snow-water; as also in water wherein Pepper had lain infused.', *Philosophical transactions*, 12.
Leff, L. G. and Leff, A. A. (1996) 'Use of green fluorescent protein to monitor survival of genetically engineered bacteria in aquatic environments', *Applied and Environmental Microbiology*, 62(9). doi: 10.1128/aem.62.9.3486-3488.1996.
Li, M. *et al.* (2006) 'Effect of lpdA gene knockout on the metabolism in Escherichia coli based on enzyme activities, intracellular metabolite concentrations and metabolic flux analysis by 13C-labeling experiments', *Journal of Biotechnology*, 122(2). doi: 10.1016/j.jbiotec.2005.09.016.
Lin, J. L., Wagner, J. M. and Alper, H. S. (2017) 'Enabling tools for high-throughput detection of metabolites: Metabolic engineering and directed evolution applications', *Biotechnology Advances*. doi: 10.1016/j.biotechadv.2017.07.005.
Liu, X. *et al.* (2018) 'Convergent engineering of syntrophic Escherichia coli coculture for efficient production of glycosides', *Metabolic Engineering*, 47. doi: 10.1016/j.ymben.2018.03.016.
Lloyd-Price, J., Abu-Ali, G. and Huttenhower, C. (2016) 'The healthy human microbiome', *Genome Medicine*. doi: 10.1186/s13073-016-0307-y.
Long, C. P. *et al.* (2016) 'Characterization of physiological responses to 22 gene knockouts in Escherichia coli central carbon metabolism', *Metabolic Engineering*, 37. doi: 10.1016/j.ymben.2016.05.006.
Long, C. P. *et al.* (2017) 'Fast growth phenotype of E. coli K-12 from adaptive laboratory evolution does not require intracellular flux rewiring', *Metabolic Engineering*, 44. doi: 10.1016/j.ymben.2017.09.012.
Long, C. P. *et al.* (2018) 'Dissecting the genetic and metabolic mechanisms of adaptation to the knockout of a major metabolic enzyme in Escherichia coli', *Proceedings of the National Academy of Sciences of the United States of America*, 115(1). doi: 10.1073/pnas.1716056115.

Long, C. P. and Antoniewicz, M. R. (2014a) ‘Metabolic flux analysis of Escherichia coli knockouts: Lessons from the Keio collection and future outlook’, *Current Opinion in Biotechnology*. doi: 10.1016/j.copbio.2014.02.006.
Long, C. P. and Antoniewicz, M. R. (2014b) ‘Quantifying Biomass Composition by Gas Chromatography/Mass Spectrometry’, *Analytical Chemistry*, 86(19). doi: 10.1021/ac502734e.
Long, C. P. and Antoniewicz, M. R. (2018) ‘How adaptive evolution reshapes metabolism to improve fitness: recent advances and future outlook’, *Current Opinion in Chemical Engineering*. doi: 10.1016/j.coche.2018.11.001.
Long, C. P. and Antoniewicz, M. R. (2019a) ‘High-resolution 13C metabolic flux analysis’, *Nature Protocols*. doi: 10.1038/s41596-019-0204-0.
Long, C. P. and Antoniewicz, M. R. (2019b) ‘Metabolic flux responses to deletion of 20 core enzymes reveal flexibility and limits of E. coli metabolism’, *Metabolic Engineering*, 55. doi: 10.1016/j.ymben.2019.08.003.
Ma, L., Zhang, G. and Doyle, M. P. (2011) ‘Green fluorescent protein labeling of Listeria, Salmonella, and Escherichia coli O157:H7 for safety-related studies’, *PLoS ONE*, 6(4). doi: 10.1371/journal.pone.0018083.
March, J. C., Eiteman, M. A. and Altman, E. (2002) ‘Expression of an anaplerotic enzyme, pyruvate carboxylase, improves recombinant protein production in Escherichia coli’, *Applied and Environmental Microbiology*, 68(11). doi: 10.1128/AEM.68.11.5620-5624.2002.
March, J. C., Rao, G. and Bentley, W. E. (2003) ‘Biotechnological applications of green fluorescent protein’, *Applied Microbiology and Biotechnology*. doi: 10.1007/s00253-003-1339-y.
Matsuyama, C. *et al.* (2024) ‘Metabolome analysis of metabolic burden in Escherichia coli caused by overexpression of green fluorescent protein and delta-rhodopsin’, *Journal of Bioscience and Bioengineering*, 137(3). doi: 10.1016/j.jbiosc.2023.12.003.
Mattanovich, D. *et al.* (2004) ‘Stress in recombinant protein producing yeasts’, in *Journal of Biotechnology*. doi: 10.1016/j.jbiotec.2004.04.035.
Mee, M. T. *et al.* (2014) ‘Syntrophic exchange in synthetic microbial communities’, *Proceedings of the National Academy of Sciences of the United States of America*. doi: 10.1073/pnas.1405641111.
Mee, M. T. and Wang, H. H. (2012) ‘Engineering ecosystems and synthetic ecologies’, *Molecular BioSystems*. doi: 10.1039/c2mb25133g.

Mesquita, I. and Rodrigues, F. (2018) 'Cellular Metabolism at a Glance', *Experientia supplementum (2012)*, 109. doi: 10.1007/978-3-319-74932-7_1.
Misteli, T. and Spector, D. L. (1997) 'Applications of The Green Fluorescent Protein In Cell Biology and Biotechnology', *Nature Biotechnology*, 15(10). doi: 10.1038/nbt1097-961.
Morgan, S. A. *et al.* (2016) 'Biofuel metabolic engineering with biosensors', *Current Opinion in Chemical Biology*. doi: 10.1016/j.cbpa.2016.09.020.
Morris, B. E. L. *et al.* (2013) 'Microbial syntrophy: Interaction for the common good', *FEMS Microbiology Reviews*. doi: 10.1111/1574-6976.12019.
Morris, J. J. *et al.* (2008) 'Facilitation of robust growth of Prochlorococcus colonies and dilute liquid cultures by "helper" heterotrophic bacteria', *Applied and Environmental Microbiology*, 74(14). doi: 10.1128/AEM.02479-07.
Müller, T. *et al.* (2023) 'Synthetic mutualism in engineered E. coli mutant strains as functional basis for microbial production consortia', *Engineering in Life Sciences*, 23(1). doi: 10.1002/elsc.202100158.
Muñoz-Elías, E. J. and McKinney, J. D. (2006) 'Carbon metabolism of intracellular bacteria', *Cellular Microbiology*. doi: 10.1111/j.1462-5822.2005.00648.x.
Nemergut, D. R. *et al.* (2013) 'Patterns and Processes of Microbial Community Assembly', *Microbiology and Molecular Biology Reviews*, 77(3). doi: 10.1128/mmbr.00051-12.
Neubauer, P., Lin, H. Y. and Mathiszik, B. (2003) 'Metabolic load of recombinant protein production: Inhibition of cellular capacities for glucose uptake and respiration after induction of a heterologous gene in Escherichia coli', *Biotechnology and Bioengineering*, 83(1). doi: 10.1002/bit.10645.
Nöh, K. *et al.* (2007) 'Metabolic flux analysis at ultra short time scale: Isotopically non-stationary 13C labeling experiments', *Journal of Biotechnology*, 129(2). doi: 10.1016/j.jbiotec.2006.11.015.
Noor, E. *et al.* (2010) 'Central Carbon Metabolism as a Minimal Biochemical Walk between Precursors for Biomass and Energy', *Molecular Cell*, 39(5). doi: 10.1016/j.molcel.2010.08.031.
Noto Guillen, M. *et al.* (2021) 'Assembling stable syntrophic Escherichia coli communities by comprehensively identifying beneficiaries of secreted goods', *Cell Systems*, 12(11). doi: 10.1016/j.cels.2021.08.002.

Oftadeh, O. and Hatzimanikatis, V. (2024) ‘Genome-scale models of metabolism and expression predict the metabolic burden of recombinant protein expression’, *Metabolic Engineering*. Elsevier Inc., 84(May), pp. 109–116. doi: 10.1016/j.ymben.2024.06.005.

Orth, J. D., Thiele, I. and Palsson, B. O. (2010) ‘What is flux balance analysis?’, *Nature Biotechnology*. doi: 10.1038/nbt.1614.

Ou, J. *et al.* (2004) ‘Stationary phase protein overproduction is a fundamental capability of Escherichia coli’, *Biochemical and Biophysical Research Communications*, 314(1). doi: 10.1016/j.bbrc.2003.12.077.

Pande, S. *et al.* (2014) ‘Fitness and stability of obligate cross-feeding interactions that emerge upon gene loss in bacteria’, *ISME Journal*, 8(5). doi: 10.1038/ismej.2013.211.

Pande, S. and Kost, C. (2017) ‘Bacterial Unculturability and the Formation of Intercellular Metabolic Networks’, *Trends in Microbiology*. doi: 10.1016/j.tim.2017.02.015.

Peekhaus, N. and Conway, T. (1998) ‘What’s for dinner?: Entner-Doudoroff metabolism in Escherichia coli’, *Journal of Bacteriology*. doi: 10.1128/jb.180.14.3495-3502.1998.

Peretti, S. W. and Bailey, J. E. (1987) ‘Simulations of host–plasmid interactions in Escherichia coli: Copy number, promoter strength, and ribosome binding site strength effects on metabolic activity and plasmid gene expression’, *Biotechnology and Bioengineering*, 29(3). doi: 10.1002/bit.260290305.

Petersen, C. and Round, J. L. (2014) ‘Defining dysbiosis and its influence on host immunity and disease’, *Cellular Microbiology*. doi: 10.1111/cmi.12308.

Ponomarova, O. and Patil, K. R. (2015) ‘Metabolic interactions in microbial communities: Untangling the Gordian knot’, *Current Opinion in Microbiology*. doi: 10.1016/j.mib.2015.06.014.

Raman, K. and Chandra, N. (2009) ‘Flux balance analysis of biological systems: Applications and challenges’, *Briefings in Bioinformatics*. doi: 10.1093/bib/bbp011.

Rani, N. *et al.* (2019) ‘Microbes: A key player in industrial wastewater treatment’, in *Microbial Wastewater Treatment*. doi: 10.1016/B978-0-12-816809-7.00005-1.

Remington, S. J. (2011) ‘Green fluorescent protein: A perspective’, *Protein Science*. doi: 10.1002/pro.684.

Rodionova, I. A. *et al.* (2015) 'Genomic distribution of B-vitamin auxotrophy and uptake transporters in environmental bacteria from the Chloroflexi phylum', *Environmental Microbiology Reports*. doi: 10.1111/1758-2229.12227.
Rozkov, A. *et al.* (2004) 'Characterization of the metabolic burden on Escherichia coli DH1 cells imposed by the presence of a plasmid containing a gene therapy sequence', *Biotechnology and Bioengineering*, 88(7). doi: 10.1002/bit.20327.
Rühl, M., Hardt, W. D. and Sauer, U. (2011) 'Subpopulation-specific metabolic pathway usage in mixed cultures as revealed by reporter protein-based 13C analysis', *Applied and Environmental Microbiology*. doi: 10.1128/AEM.02696-10.
Sarkar, D. *et al.* (2021) 'Elucidation of trophic interactions in an unusual single-cell nitrogen-fixing symbiosis using metabolic modeling', *PLoS Computational Biology*, 17(5). doi: 10.1371/journal.pcbi.1008983.
Sauer, U. (2006) 'Metabolic networks in motion: 13C-based flux analysis', *Molecular Systems Biology*. doi: 10.1038/msb4100109.
Schmidt, K. *et al.* (1997) 'Modeling isotopomer distributions in biochemical networks using isotopomer mapping matrices', *Biotechnology and Bioengineering*, 55(6). doi: 10.1002/(SICI)1097-0290(19970920)55:6<831::AID-BIT2>3.0.CO;2-H.
Scott, K. P. *et al.* (1998) 'The green fluorescent protein as a visible marker for lactic acid bacteria in complex ecosystems', *FEMS Microbiology Ecology*, 26(3). doi: 10.1016/S0168-6496(98)00037-3.
Shaikh, A. S. *et al.* (2008) 'Isotopomer distributions in amino acids from a highly expressed protein as a proxy for those from total protein', *Analytical Chemistry*. doi: 10.1021/ac071445+.
Shastri, A. A. and Morgan, J. A. (2005) 'Flux balance analysis of photoautotrophic metabolism', *Biotechnology Progress*, 21(6). doi: 10.1021/bp050246d.
Shimomura, O., Johnson, F. H. and Saiga, Y. (1962) 'Extraction, Purification and Properties of Aequorin, a Bioluminescent Protein from the Luminous Hydromedusan,Aequorea', *Journal of Cellular and Comparative Physiology*, 59(3). doi: 10.1002/jcp.1030590302.
Shoaie, S. *et al.* (2013) 'Understanding the interactions between bacteria in the human gut through metabolic modeling', *Scientific Reports*, 3. doi: 10.1038/srep02532.

Shupletsov, M. S. *et al.* (2014) 'OpenFLUX2: 13C-MFA modeling software package adjusted for the comprehensive analysis of single and parallel labeling experiments', *Microbial Cell Factories*, 13(1). doi: 10.1186/s12934-014-0152-x.

Silva, F., Queiroz, J. A. and Domingues, F. C. (2012) 'Evaluating metabolic stress and plasmid stability in plasmid DNA production by Escherichia coli', *Biotechnology Advances*. doi: 10.1016/j.biotechadv.2011.12.005.

Soboleski, M. R., Oaks, J. and Halford, W. P. (2005) 'Green fluorescent protein is a quantitative reporter of gene expression in individual eukaryotic cells', *The FASEB Journal*, 19(3). doi: 10.1096/fj.04-3180fje.

Stephanopoulos, G. (1999) 'Metabolic Fluxes and Metabolic Engineering', *Metabolic Engineering*, 1(1). doi: 10.1006/mben.1998.0101.

Stephanopoulos, G. and Vallino, J. J. (1991) 'Network rigidity and metabolic engineering in metabolite overproduction', *Science*, 252(5013). doi: 10.1126/science.1904627.

Stincone, A. *et al.* (2015) 'The return of metabolism: Biochemistry and physiology of the pentose phosphate pathway', *Biological Reviews*, 90(3). doi: 10.1111/brv.12140.

Tang, X. *et al.* (2010) 'Construction of an artificial microalgal-bacterial consortium that efficiently degrades crude oil', *Journal of Hazardous Materials*, 181(1–3). doi: 10.1016/j.jhazmat.2010.05.033.

Tang, Y. J. *et al.* (2009) 'Advances in analysis of microbial Metabolic fluxes via 13C isotopic labeling', *Mass Spectrometry Reviews*, 28(2). doi: 10.1002/mas.20191.

Torsvik, V., Øvreås, L. and Thingstad, T. F. (2002) 'Prokaryotic diversity - Magnitude, dynamics, and controlling factors', *Science*. doi: 10.1126/science.1071698.

Toya, Y. *et al.* (2010) '13C-Metabolic flux analysis for batch culture of Escherichia coli and its pyk and pgi gene knockout mutants based on mass isotopomer distribution of intracellular metabolites', *Biotechnology Progress*, 26(4). doi: 10.1002/btpr.420.

Toya, Y. and Shimizu, H. (2013) 'Flux analysis and metabolomics for systematic metabolic engineering of microorganisms', *Biotechnology Advances*. doi: 10.1016/j.biotechadv.2013.05.002.

Tracy, B. P., Gaida, S. M. and Papoutsakis, E. T. (2010) 'Flow cytometry for bacteria: Enabling metabolic engineering, synthetic biology and the elucidation of complex phenotypes', *Current Opinion in Biotechnology*. doi: 10.1016/j.copbio.2010.02.006.

Vallino, J. J. and Stephanopoulos, G. (2000) 'Metabolic flux distributions in corynebacterium glutamicum during growth and lysine overproduction', *Biotechnology and Bioengineering*, 67(6). doi: 10.1002/(sici)1097-0290(20000320)67:6<872::aid-bit21>3.0.co;2-x.
Vartoukian, S. R., Palmer, R. M. and Wade, W. G. (2010) 'Strategies for culture of "unculturable" bacteria', *FEMS Microbiology Letters*. doi: 10.1111/j.1574-6968.2010.02000.x.
Vuoristo, K. S. *et al.* (2016) 'Metabolic Engineering of TCA Cycle for Production of Chemicals', *Trends in Biotechnology*. doi: 10.1016/j.tibtech.2015.11.002.
Wang, Z. *et al.* (2006) 'Effects of the presence of ColE1 plasmid DNA in Escherichia coli on the host cell metabolism', *Microbial Cell Factories*. BioMed Central, 5(1), pp. 1–18.
Ward, W. W. (2005) 'Biochemical and physical properties of green fluorescent protein', *Methods of Biochemical Analysis*, 47. doi: 10.1002/0471739499.ch3.
Weiße, A. Y. *et al.* (2015) 'Mechanistic links between cellular trade-offs, gene expression, and growth', *Proceedings of the National Academy of Sciences of the United States of America*, 112(9). doi: 10.1073/pnas.1416533112.
Weitzel, M. *et al.* (2013) '13CFLUX2 - High-performance software suite for 13C-metabolic flux analysis', *Bioinformatics*, 29(1). doi: 10.1093/bioinformatics/bts646.
West, S. E. H. *et al.* (1994) 'Construction of improved Escherichia-Pseudomonas shuttle vectors derived from pUC18/19 and sequence of the region required for their replication in Pseudomonas aeruginosa', *Gene*, 148(1). doi: 10.1016/0378-1119(94)90237-2.
Wiechert, W. *et al.* (1999) 'Bidirectional reaction steps in metabolic networks: III. Explicit solution and analysis of isotopomer labeling systems', *Biotechnology and Bioengineering*, 66(2). doi: 10.1002/(SICI)1097-0290(1999)66:2<69::AID-BIT1>3.0.CO;2-6.
Wintermute, E. H. and Silver, P. A. (2010) 'Emergent cooperation in microbial metabolism', *Molecular Systems Biology*. doi: 10.1038/msb.2010.66.
Wissenbach, U. *et al.* (1995) ' A third periplasmic transport system for l -arginine in Escherichia coli : molecular characterization of the artPIQMJ genes, arginine binding and transport ', *Molecular Microbiology*, 17(4). doi: 10.1111/j.1365-2958.1995.mmi_17040675.x.
Wolfsberg, E., Long, C. P. and Antoniewicz, M. R. (2018) 'Metabolism in dense microbial colonies: 13 C metabolic flux analysis of E. coli grown on agar identifies two distinct cell populations with acetate cross-feeding', *Metabolic Engineering*, 49. doi: 10.1016/j.ymben.2018.08.013.

Wu, G. *et al.* (2016) 'Metabolic Burden: Cornerstones in Synthetic Biology and Metabolic Engineering Applications', *Trends in Biotechnology*. doi: 10.1016/j.tibtech.2016.02.010.
Yang, C., Hua, Q. and Shimizu, K. (2002) 'Metabolic flux analysis in Synechocystis using isotope distribution from 13C-labeled glucose', *Metabolic Engineering*, 4(3). doi: 10.1006/mben.2002.0226.
Yoo, H. *et al.* (2008) 'Quantifying reductive carboxylation flux of glutamine to lipid in a brown adipocyte cell line', *Journal of Biological Chemistry*, 283(30). doi: 10.1074/jbc.M706494200.
Young, J. D. *et al.* (2011) 'Mapping photoautotrophic metabolism with isotopically nonstationary 13C flux analysis', *Metabolic Engineering*, 13(6). doi: 10.1016/j.ymben.2011.08.002.
Young, J. D. (2014) 'INCA: A computational platform for isotopically non-stationary metabolic flux analysis', *Bioinformatics*, 30(9). doi: 10.1093/bioinformatics/btu015.
Zamboni, N. (2011) '13C metabolic flux analysis in complex systems', *Current Opinion in Biotechnology*. doi: 10.1016/j.copbio.2010.08.009.
Zelezniak, A. *et al.* (2015) 'Metabolic dependencies drive species co-occurrence in diverse microbial communities', *Proceedings of the National Academy of Sciences of the United States of America*, 112(20). doi: 10.1073/pnas.1421834112.
Zeng, H. and Yang, A. (2019) 'Quantification of proteomic and metabolic burdens predicts growth retardation and overflow metabolism in recombinant Escherichia coli', *Biotechnology and Bioengineering*, 116(6). doi: 10.1002/bit.26943.
Zengler, K. and Zaramela, L. S. (2018) 'The social network of microorganisms - How auxotrophies shape complex communities', *Nature Reviews Microbiology*. doi: 10.1038/s41579-018-0004-5.
Zhang, H. *et al.* (2015) 'Engineering Escherichia coli coculture systems for the production of biochemical products', *Proceedings of the National Academy of Sciences of the United States of America*, 112(27). doi: 10.1073/pnas.1506781112.
Zhao, J. and Shimizu, K. (2003) 'Metabolic flux analysis of Escherichia coli K12 grown on 13C-labeled acetate and glucose using GC-MS and powerful flux calculation method', *Journal of Biotechnology*, 101(2). doi: 10.1016/S0168-1656(02)00316-4.

Zuñiga, C., Zaramela, L. and Zengler, K. (2017) ‘Elucidation of complexity and prediction of interactions in microbial communities’, *Microbial Biotechnology*. doi: 10.1111/1751-7915.12855.